



Title	BINOL derived chiral photoswitchable catalysts: Design and modulation approach towards Mannich type reaction and Aza-Friedel-Crafts reaction
Author(s)	Krishnan, G Chandu
Citation	大阪大学, 2022, 博士論文
Version Type	
URL	<a href="https://hdl.handle.net/11094/89557">https://hdl.handle.net/11094/89557</a>
rights	
Note	

*The University of Osaka Institutional Knowledge Archive : OUKA*

<https://ir.library.osaka-u.ac.jp/>

The University of Osaka

**BINOL derived chiral photoswitchable catalysts: Design and modulation approach  
towards Mannich type reaction and Aza-Friedel-Crafts reaction**

A Doctoral Thesis  
Submitted to the Department of Chemistry  
Graduate School of Science  
Osaka University

By  
Chandu G Krishnan

Synthetic Organic Chemistry  
SANKEN  
August 2022

## Contents

### Chapter 1: Background

- 1-1. Stimuli-responsive catalyst
- 1-2. Stimuli-responsive catalyst utilizing additives
  - 1-2-1. Metal additives
  - 1-2-2. Acid-base additives
- 1-3. Stimuli-responsive photoswitchable catalyst mediated by Light
- 1-4. Importance of photoswitchable catalyst
- 1-5. Previous approaches towards photoswitchable catalyst
  - 1-5-1. Stilbene -based catalyst
  - 1-5-2. Diarylethene-based catalyst
  - 1-5-3. Azobenzene-based catalyst
  - 1-5-4. Hydrazone-based catalyst
- 1-6. Outline of my research

### Chapter 2: Photoswitchable chiral cation-binding catalyst: Photocontrol of catalytic activity on enantioselective aminal synthesis

- 2-1. Introduction: Crown ether
- 2-2. Photoresponsive crown ether
- 2-3. Crown ether as an asymmetric phase transfer catalyst
- 2-4. Development of chiral photoresponsive crown ethers
- 2-5. OligoEGs as bifunctional promoters
- 2-6. My concept: Azobenzene based photoswitchable cation binding catalyst (ABOEGs)
- 2-7. General procedure for preparation of ABOEGs
- 2-8. Photoisomerization experiments
  - 2-8-1. Isomerization studies of ABOEGs using  $^1\text{H}$  NMR spectroscopy
  - 2-8-2. Isomerization studies of ABOEGs using UV-Vis spectroscopy
- 2-9. ABOEGs catalyzed enantioselective Mannich type reaction.
  - 2-9-1. Optimization of reaction conditions
  - 2-9-2. Coordination experiments
  - 2-9-3. Thermal stability and half-life measurement of (Z)-ABOEGs
  - 2-9-4. Substrate scope
  - 2-9-5. Time course studies
  - 2-9-6. Mass spectra of ABOEGs- $\text{K}^+$  complex
  - 2-9-7. Control experiments
- 2-10. Experimental section
  - 2-10-1. General procedure
  - 2-10-2. Reaction setup
  - 2-10-3. General procedure for preparation of ABOEGs
  - 2-10-4. Typical procedure for the preparation of ABOEGs
  - 2-10-5. General procedure for the ABPEs catalyzed enantioselective Mannich type reaction
  - 2-10-6. NMR and Mass data

**Chapter 3: Photoswitchable dithienylethene based chiral phosphoric acid catalyst:  
Photocontrol of catalytic activity on enantioselective Aza-Friedel-Craft reaction**

- 3-1. Introduction: Dithienylethene photochromic unit
- 3-2. Dithienylethene skeleton towards achiral metal catalysis
- 3-3. Dithienylethene skeleton towards asymmetric metal catalysis
- 3-4. Dithienylethene skeleton towards achiral organo catalysis
- 3-5. This work: Dithienylethene based photoswitchable chiral phosphoric acid catalyst
- 3-6. General procedure for preparation of DTE-BPAs
- 3-7. Photoisomerization experiments
  - 3-7-1. Isomerization studies of DTE-BPAs using  $^1\text{H}$  NMR spectroscopy
  - 3-7-2. Isomerization studies of DTE-BPAs using UV-Vis spectroscopy
- 3-8. Determination of pKa values using DFT studies
- 3-9. Application of DTE-BPA- **120** towards on Enantioselective Aza-Friedel-Craft Reaction
- 3-10. Experimental section

**Chapter 4: Summary**

**Chapter 5: References**

**Acknowledgements**



## Abbreviation

ABCE	azobenzene BINOL based crown ether
ABOEG	azobenzene BINOL based oligoethylene glycol
Ac	acetyl
AMM	artificial molecular machines
APCI	atmospheric pressure chemical ionization
aq.	aqueous solution
Ar	aryl
BINOL	1,1'-bi-2-naphthol
cat.	catalyst
DAE	diarylethene
DCM	dichloromethane
DMAP	4-dimethylaminopyridine
DMF	<i>N,N</i> -dimethylformamide
DMSO	dimethyl sulfoxide
DTE	dithienylethene
ee	enantiomeric excess
eq.	equivalent
er	enantiomeric ratio
ESI	electrospray ionization
Et	ethyl
EWG	electron withdrawing group
FG	functional group
HAT	hydrogen atom transfer
HPLC	high performance liquid chromatography
HRMS	high resolution mass spectrometry
Hz	hertz
iPr	isopropyl
L	ligand
LED	light-emitting diode
M	metal
Me	methyl
MIM	mechanically interlocked molecules
MS	mass spectrometry
Ms	mesyl (methanesulfonyl)
NMR	nuclear magnetic resonance
Ph	phenyl
ppm	parts per million
PSS	photostationary state
rac	racemic
RE	rare-earth metal
rt	room temperature
SPINOL	1,1'-spirobiindane-7,7'-diol
tBu	<i>tert</i> -butyl

TfO	trifluoromethanesulfonate
THF	tetrahydrofuran
TMS	trimethylsilyl
Tol	tolyl (4-methylphenyl)
Ts	tosyl (p-toluenesulfonyl)

## Chapter 1: Background

Catalytic organic synthesis enables a vast supply of useful compounds with the architect of developing creative catalyst designs and has wide application academically as well as industrially. In 2000, Dr. List and Dr. MacMillan (Nobel Prize Winners in Chemistry 2021) independently developed a third type of asymmetric catalysis (first: natural enzyme, second: metal catalyst) to build chiral molecules *via* organocatalysis. The 2016 Nobel Prize in Chemistry was awarded to Dr. Sauvage, Dr. Stoddart, and Dr. B. L. Feringa, who raised their expectations for further basic and applied research in the future by developing artificial molecular machines (AMM).<sup>[1]</sup> If the functions of chemically synthesized catalysts can be altered by changing the geometry or conformations by various external stimuli (change of solvent, light, pH or redox processes), a variety of compounds can be designed and synthesized to reach an advanced architecture to achieve catalytic control in a continuous, regioselective and stereoselective manner. Therefore, design of next-generation catalysts with adjustable functions is a challenging task in synthetic organic chemistry. Basically, the catalyst does not change its function in the reaction once it started. However for in vivo enzymatic reaction, allosteric regulation occurs by binding of a ligand to a site other than the catalytic active site, and the catalytic structure and function change. That is why, biomolecules change their functions and behave as nanoscale machines.<sup>[2]</sup> Research on giving such mechanical functions to chemically synthesized molecules have been attracting attention in recent years.

Energetic research has been done with outstanding achievements in this field of designing mechanically interlocked molecules (MIM) using the dynamic functions of catenane, rotaxane and molecular motors.<sup>[1]</sup> One of the purposes of catalytic organic synthesis is to achieve high catalytic activity and modulate their functions in regional or chemical or stereoselective manner by mimicking exactly what biological systems can do. Therefore, many researchers are committed to developing new catalysts that enable innovative molecular conversions, and many chemically synthesized organic molecule/transition metal catalysts have been successful. In terms of approaches to take catalyst control and modulating their properties, steric selectivity as an example, the asymmetric catalyst has played a large significant role. For example, in the development of chiral drugs, enantiomers often have different biological activities, and it is necessary to clarify the differences in their activities. Since the FDA published guidelines on the handling of chiral drug development in the 1990s, the selective synthesis of mirror isomers of small molecule drugs has been one of the challenges in synthetic organic chemistry. Catalytic asymmetric synthesis enables pharmaceuticals and their synthetic intermediates as one of the methods for supplying large amounts of one enantiomer (Figure 1). At the same time, in order to achieve industrial low cost as well as environmental load, and product safety, it is desirable to reduce the amount of catalyst and/or reuse the catalyst. Along with this, in recent years, catalysts that have sufficient activity at the ppm level and catalysts that are supported on the solid phase and made recoverable have also been studied.<sup>[3,4]</sup> From these circumstances, it can be said that the practicality of catalytic organic synthesis is increasing day by day. Recently, not only chemically synthesized catalysts but also organic synthesis using enzymes has

been attracting attention. In the directional evolution method, it is possible to create catalytic activity and enhance the function that natural enzymes do not have by artificially modifying the amino acid sequence of the enzyme, and the creation of new catalysts is still academic and industrial. It turns out to be important on both sides.

### 1-1. Stimuli-responsive catalyst

Stimuli are necessary to develop a catalyst whose catalytic functions can be freely altered by changing the geometry or conformations. A catalyst whose activities changes according to stimuli-initiated regulation is called a stimulus-responsive catalyst (switchable catalyst). That means, toggling chemical reactivity of a catalyst between multiple distinct states through application of stimuli. Such stimuli induced switchable catalysts takes spatiotemporal controls over chemical reactions, which can regulate multiple process over chemical reaction to perform anomalous chemical transformations. For example, this kind of reaction control have wide applicability and can be made possible by a stimuli-responsive catalyst (Figures 1A-C). The most common type of ‘control’ achieved so far is the catalyst upregulation (on) or down regulation (off) in response to applied stimulus (Figure 1A.)

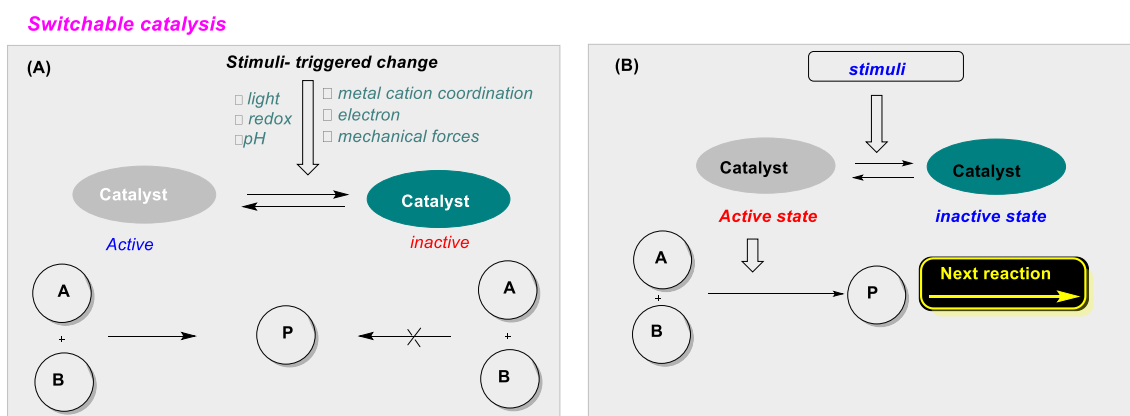


**Figure 1.** Switchable catalysis: Stimuli triggered catalyst control

However more advanced control strategies are slowly emerging in the field of switchable catalysis. Figure 1B is an example of switching between the active and inactive mode of catalyst. An active catalyst is used in the ‘A + B’ substrates to product ‘P’ reaction. In this protocol, reaction following P, the catalyst is switched to its inactive form, and in the subsequent reactions, molecular conversion can be performed without considering the influence of the catalyst. This regulation can be used to suppress mutual catalytic interference in reactions that use many catalysts at once. A more profound application in future comes in the area of asymmetric catalysis is that, if both enantiomers of the product can be obtained by controlling the function of one catalyst, there is no need to synthesize a catalyst for both photoactive substances leading to an enantiodivergent synthesis<sup>[5]</sup> that cannot be achieved by a natural enzyme. These

reaction control methods only produce a mixture of products in batches by switching catalytic activity. However, if such a catalyst is combined with flow synthesis or catalyst immobilization,<sup>[6]</sup> different products can be obtained from one flow path as needed, and it is expected to be a powerful synthesis tool in near future (In 2003, Cacciapaglia *et al.* also mentioned such a concept, but there are very few catalyst libraries available before<sup>[7]</sup> concrete applications, so first of all, the opportunity basic research on adjustable catalysts is required).

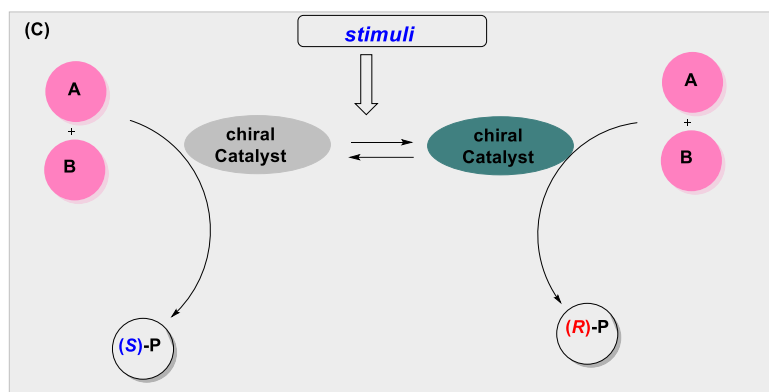
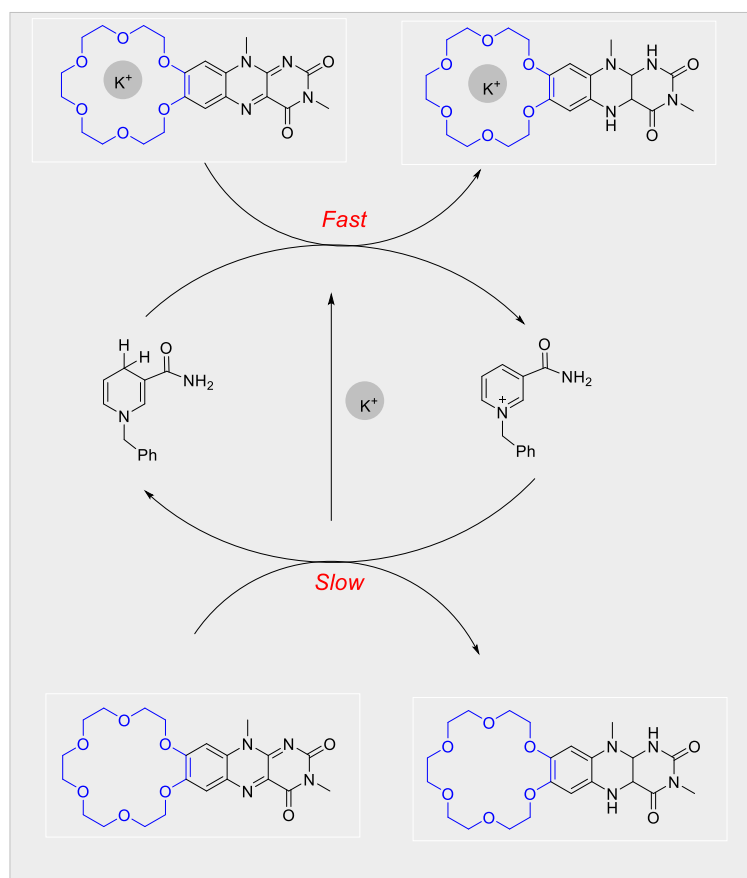


**Figure 1C.** Future application in switchable catalysis

## 1-2. Stimulus-responsive catalyst utilizing additives

### 1-2-1. Metal additives

A use of additives is one of the most practical and easy methods for creating an external stimulus-responsive catalyst as shown in Scheme 1. Generally, the function of the catalyst depends on the properties of the catalyst functional group, metal and the electronic, and steric properties of the catalyst skeleton. If these factors can be changed by adding reagents, the reaction can be indirectly controlled through changes in the function of the catalyst. In 1984, a pioneering example of reaction control using condensed crown ethers have been reported by Shinkai *et al.*<sup>[8]</sup> However, the detailed reason for this reaction acceleration is still unclear.

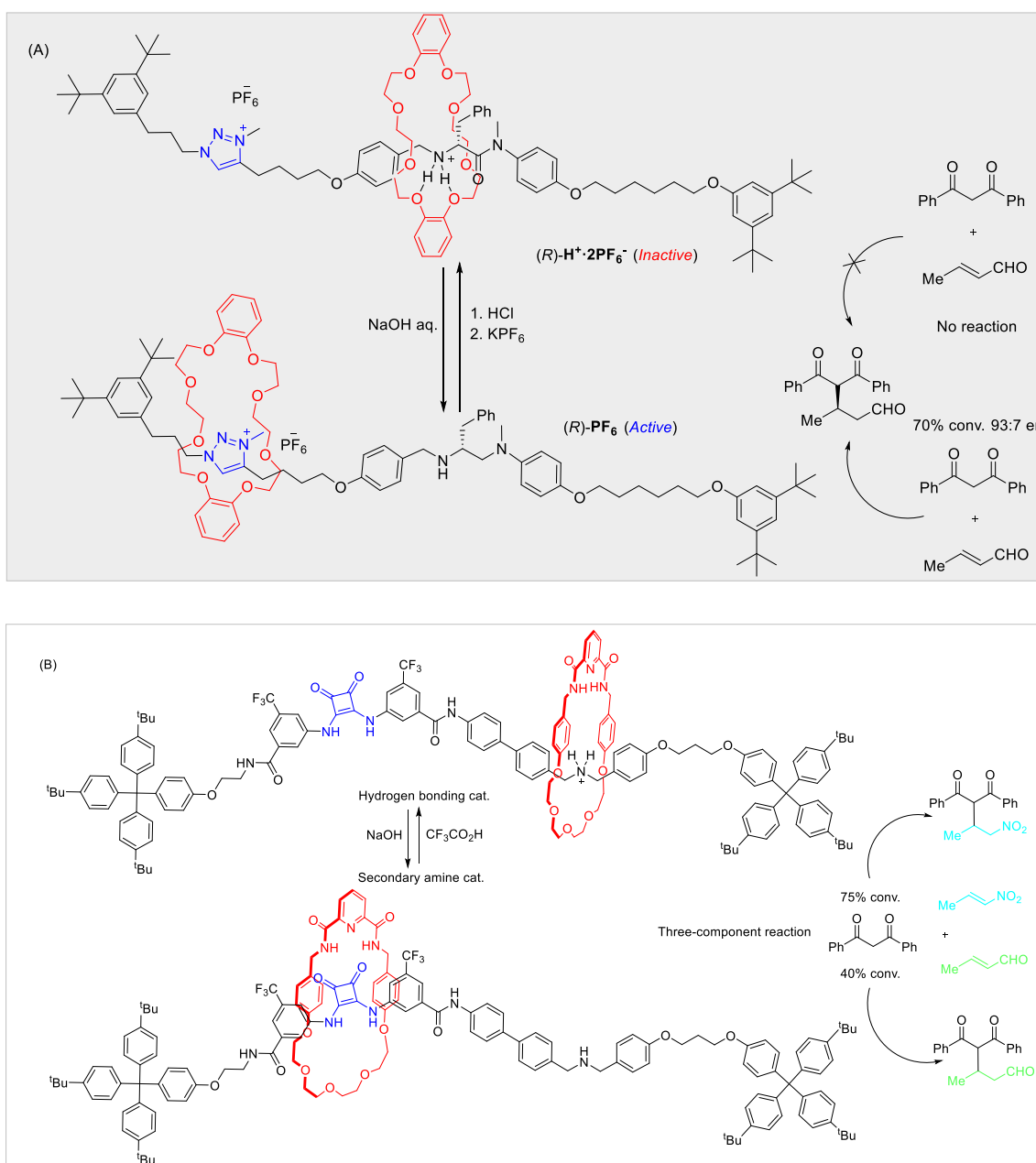


**Scheme 1.** The first report on the metal-coordination induced modulation of the reaction.

### 1-2-2. Acid-base additives

Leigh *et al.* utilized the movement of crown ether on the axis molecule of rotaxane **4** to switch the catalytic activity by adding acid or base. That is, when an ammonium salt is generated from rotaxane having an optically active secondary amine by adding an acid, the crown ether can shield the catalytically active site and suppress the function;<sup>[9]</sup> this catalyst was applied to an asymmetric conjugate addition reaction of 1,3-diphenylpropanedione to the crotonaldehyde and the activity/inactivity (ON/OFF) of the reaction could be controlled (Scheme 2A).

In addition, Leigh *et al.* introduced squaramide on the molecular axle (similar to Figure 3A) and added another electrophile to control the three-component reaction using 1,3-diphenylpropanedione, crotonaldehyde and nitrostyrene (Scheme 2B).<sup>[10]</sup> They also succeeded in controlling the selectivity of conjugate addition to crotonaldehyde. Their method has made great progress in the field of external stimulus-responsive catalysts.



**Scheme 2.** ON/OFF switching of rotaxane-based catalyst's activity by acid-base additives

Furthermore, these findings enable the creation of new functional molecules from the viewpoint of supramolecular and catalytic chemistries, still leaving a problem with the reversibility of the clause. Moreover, additives such as oxidation or reducing agents and acid or base reagents may interfere with the desired catalytic reaction or cause decomposition of substrates and products, which limits the scope of application of the catalyst. Therefore, novel external stimulus that does not remain in the reaction system is required.

### 1-3. Stimuli-responsive photoswitchable catalyst mediated by Light

Light is an attractive external regulator and has many unique specialties compared to other external stimuli. Due to its low-cost, ubiquitous, noninvasive, precise control properties initiates, and regulates complex processes with high precision in nature (photosynthesis, vision and so on).

### 1-4. Importance of photoswitchable catalyst

The advantage of capturing light as an external stimulus that controls the reaction rather than as energy to promote the catalytic reaction is that the light irradiation does not remain in the reaction system and is non-invasive, and if necessary. It is in the point that it can be irradiated/stopped (Figure 2). In addition, different effects can be expected by changing the wavelength of light. If these characteristics of light can be applied to external stimulus-responsive catalysts, it could break away from the additive-based approach (Section 1-1) and adjust the catalytic function regardless of the presence or absence of photoexcitation to the catalytic reaction. Therefore, it is conceivable to use a photoresponsive molecule that undergoes structural isomerization in response to light. It is considered that the catalytic activity can be adjusted by light if it is reflected in the change in the electronic and steric properties of the photoresponsive system. In the next section, an introduction to the photoresponsive molecules that have been used so far and the design of photoresponsive catalyst are described.

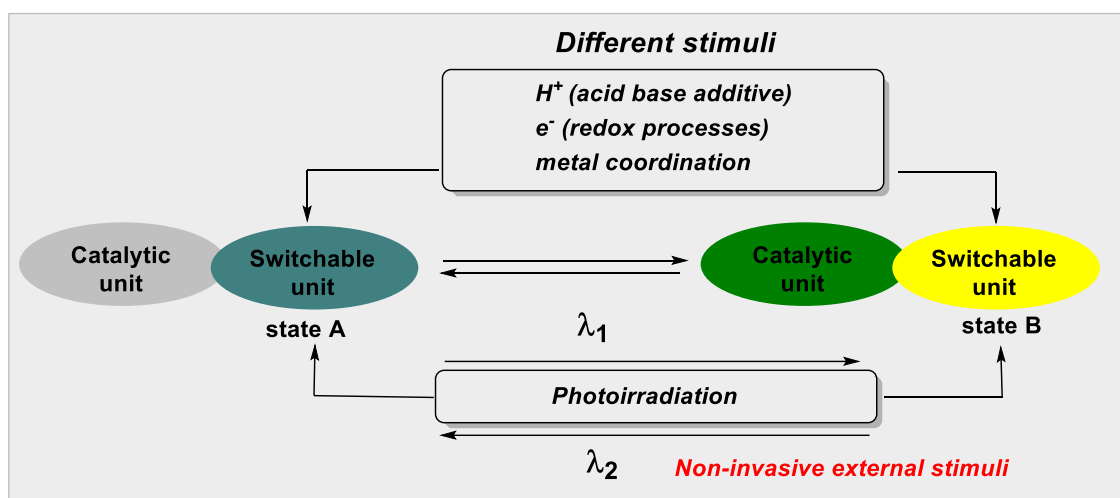


**Figure 2.** Use of light as a non-invasive external stimulus for switchable catalyst



## 1-5. Previous approaches towards photoswitchable catalyst designs

If a photoisomerizing molecule is combined with a catalyst at an appropriate position, an external stimulus response catalyst using light irradiation can be created. Such catalysts are commonly referred to as photoswitchable catalysts.

### 1-5-1. Stilbene-based catalyst

Among the molecules that are capable of showing such photoisomerization behavior, double bond photoisomerization has been known for a long time, is highly reliable with stilbene and azobenzene moieties.<sup>[11]</sup> Stilbene can be isomerized between *E*- and *Z*-forms by light irradiation, and *Z*-form of stilbene undergoes an intramolecular photocyclization reaction by continuous light irradiation. Stilbene is also converted to phenanthrene **3** by air oxidation (Figure 3). Since this process is irreversible, photoisomerization of stilbene as compared to azobenzene leaves problems with reversibility and *Z*-form stability. However, these side reactions also provide an opportunity to utilize other photoresponsive molecules with double bonds.

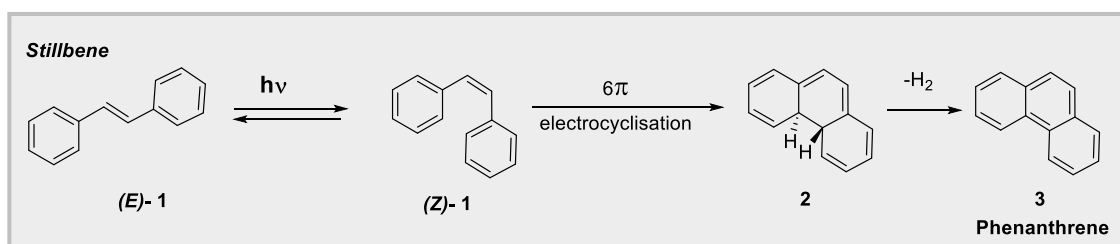
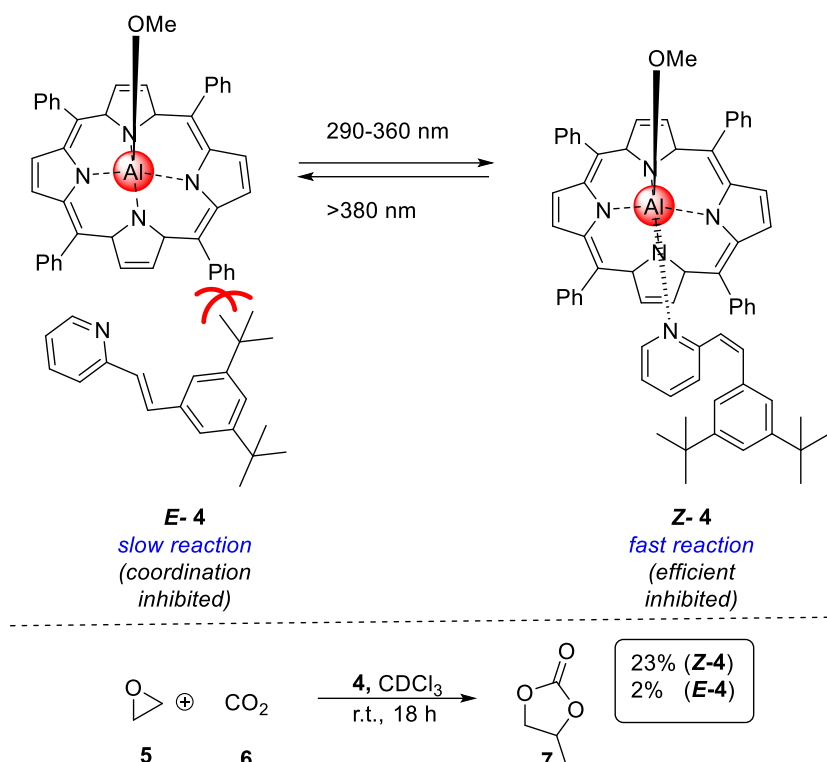


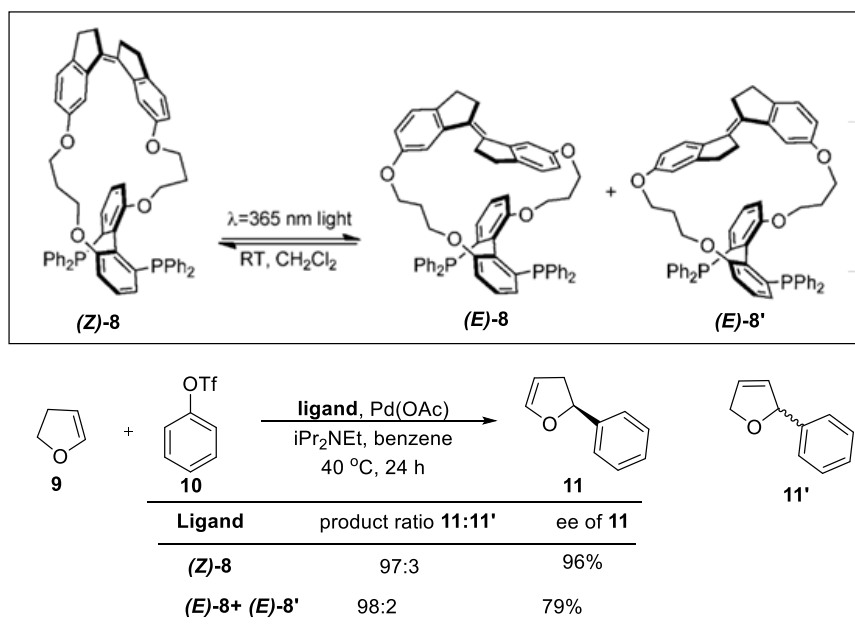
**Figure 3.** Oxidative photocyclization (*Z*)-stilbene-**1** to phenanthrene **3**.

In 1999, Inoue and co-workers carried out the seminal study in the area and achieved the photocontrol over CO<sub>2</sub> fixation mediated by aluminium porphyrin **4** (Scheme 3).<sup>[12]</sup> *Z*-configuration of the stilbene moiety engage in the activity of the system which relies on the coordination of a bulky 2-stilbazole to the Al center. The complex generated by the coordination of pyridine with Al center enhances the generation of propylene carbonate **7** from CO<sub>2</sub> and propylene oxide **5**.

A stilbene with an indane skeleton is called stiff-stilbene, because the double bond is a quaternary substitution. Craig *et al.* synthesized cross-linked axial chiral phosphine ligand with the stiff-stilbene.<sup>[13]</sup> They studied on this photoresponsive catalyst activity in the asymmetric Heck and Tsuji-Trost reaction (Scheme 4). As a result, asymmetric induction by the ligand **8** was slightly higher in the asymmetric Heck reaction after isomerization. This difference is attributed to be a coordination narrow angle of the ligand changes due to photoisomerization of stilbene.



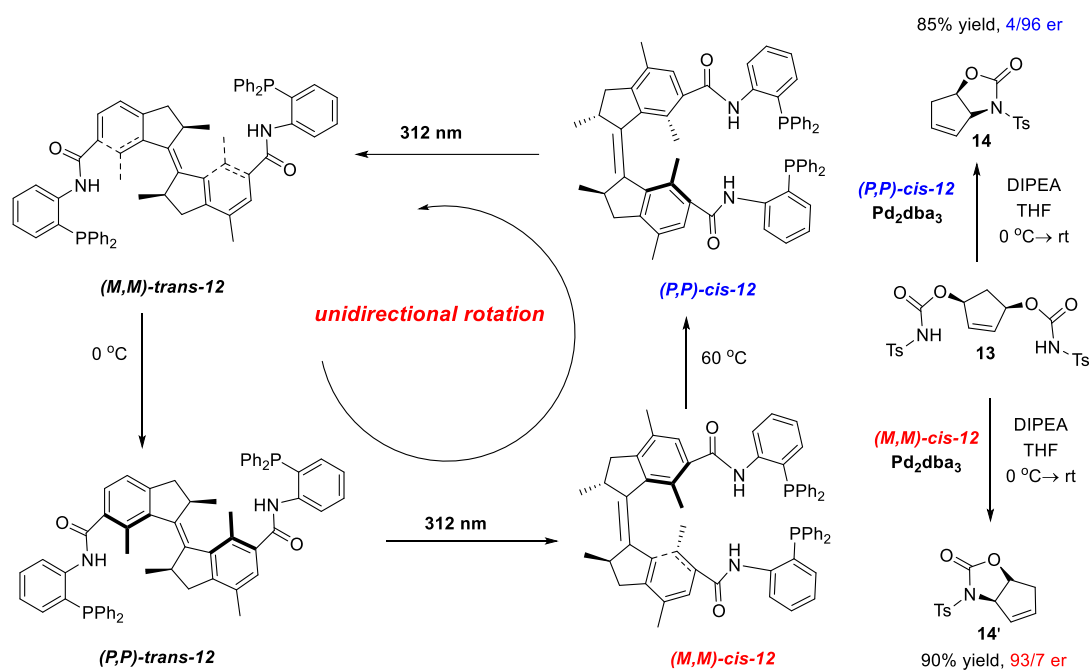
**Scheme 3.** Photoswitchable coordination of stilbazole to a porphyrin to form catalyst **4**<sup>[12]</sup>



**Scheme 4.** Photoresponsive biaryl bis(phosphine) ligand **8**<sup>[13]</sup>

In 1999, Feringa *et al.* introduced a helicity on the indane of stiff-stilbene and applied as a photoresponsive catalyst. This controls not only *cis/trans* isomerization but also rotation in one direction. This molecule behaves like a motor capable of rotating in

one direction and hence it is called a molecular motor (Scheme 5);<sup>[14]</sup> (*P,P*)- and (*M,M*)-*cis*-**12** is in a pseudo-enantiomer relationship. When it applied as an asymmetric ligand in the intramolecular allylic substitution reaction, the corresponding opposite absolute configuration products **14** and **14'** were formed.

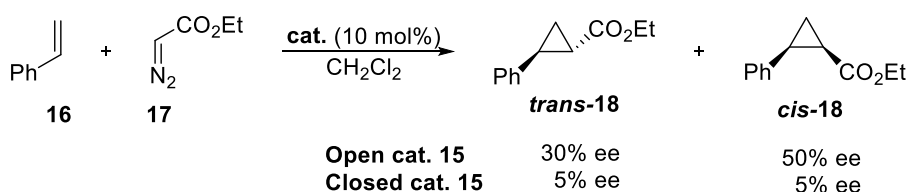
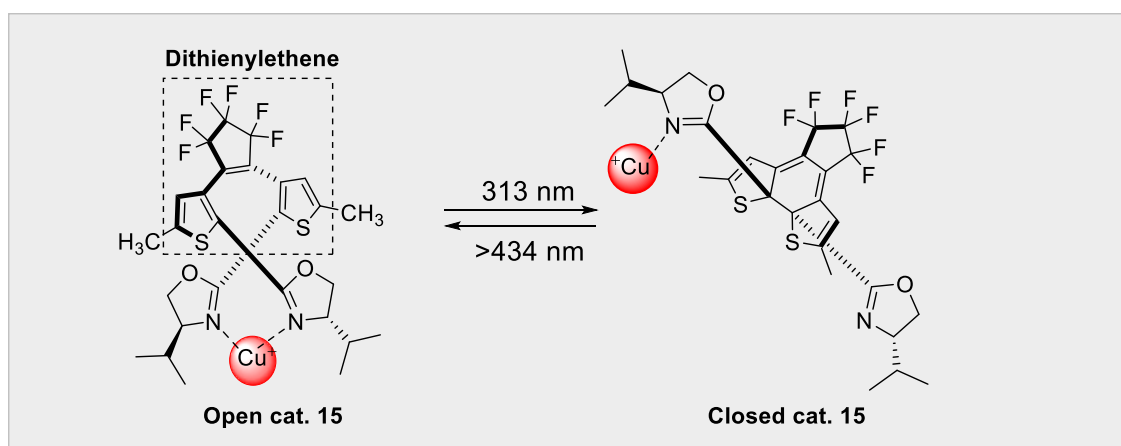


**Scheme 5.** Molecular motor-based chiral ligand and its application to enantiodivergent allylic substitution<sup>[14]</sup>

However, at least 5 steps from commercially available optically active raw materials are required to synthesize **12**. These synthetic difficulties is one reason why a few reports on photoresponsive asymmetric catalysts.

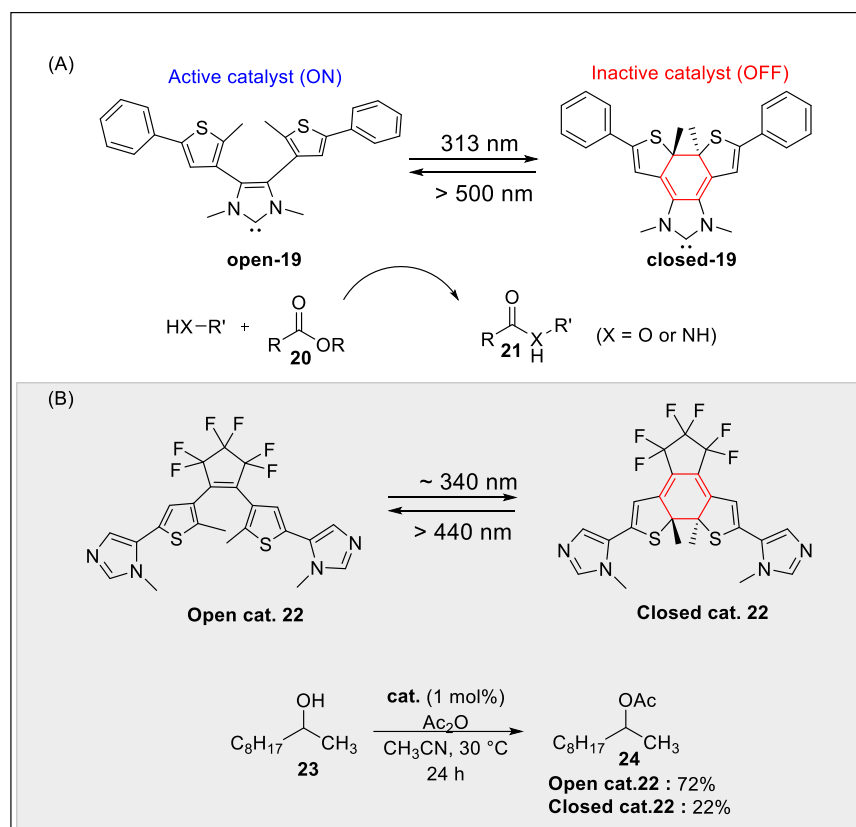
### 1-5-2. Diarylethene (DTE)-based catalyst

To suppress the production of phenanthrene from stilbene in the *cis*-form, in 1988 Irie *et al.* discovered another photochromic unit dithienylethene.<sup>[15]</sup> Dithienylethene is a molecule that repeats intramolecular cyclization by irradiation with ultraviolet light and ring opening by irradiation with visible light. Dithienylethene differs from other photoresponsive molecules in that both isomers are thermally stable. In 2005, Branda *et al.* first synthesized a photoresponsive dithienylethene oxazoline based asymmetric ligand.<sup>[16]</sup> The ligand **15** undergoes a major structural change due to photoisomerization, switching between the bidentate and monodentate coordinates for monovalent copper. Although the asymmetric induction in asymmetric cyclopropanation is low (Scheme 6).



**Scheme 6.** Photoswitchable chiral oxazoline ligand having a dithienylethene unit<sup>[16]</sup>

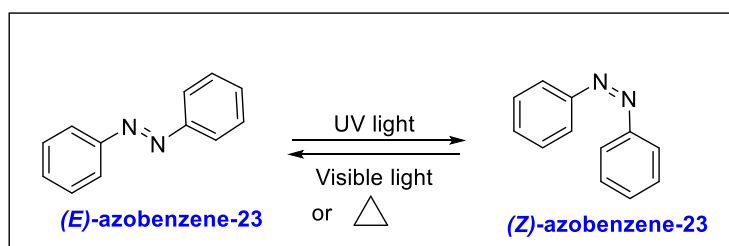
In addition, dithienylethene can change the electronic properties of the catalyst functional group because the ring closure increases the planarity of the entire molecule and expands the conjugated system. For example, NHC,<sup>[17]</sup> imidazole catalyst<sup>[18]</sup> utilizing this difference has been reported (Schemes 6A-B). However, in order to exert a change in the electronic properties of dithienylethene on the catalytic functional group, it is necessary to directly connect the catalytic functional group to the position or thiophene site, and it is difficult to develop it into an asymmetric catalysis. Moreover, it is also difficult to utilize the conformational change through photoisomerization in these catalyst designs (Actually, we explored this challenge to develop a novel chiral organocatalyst which we will discuss in Chapter 3). As a result, the utilization of other photochromic unit in developing new designs become much significant. In contrast to stilbene derivatives used in photoresponsive catalysts, the use of another photochromic unit such as azobenzene which can show a large structural difference with and without light, expanded the area of photoresponsive catalyst designing to another level.



**Scheme 6.** Photoswitchable catalysis using DTE framework

### 1-5-3. Azobenzene-based photoswitchable catalysts

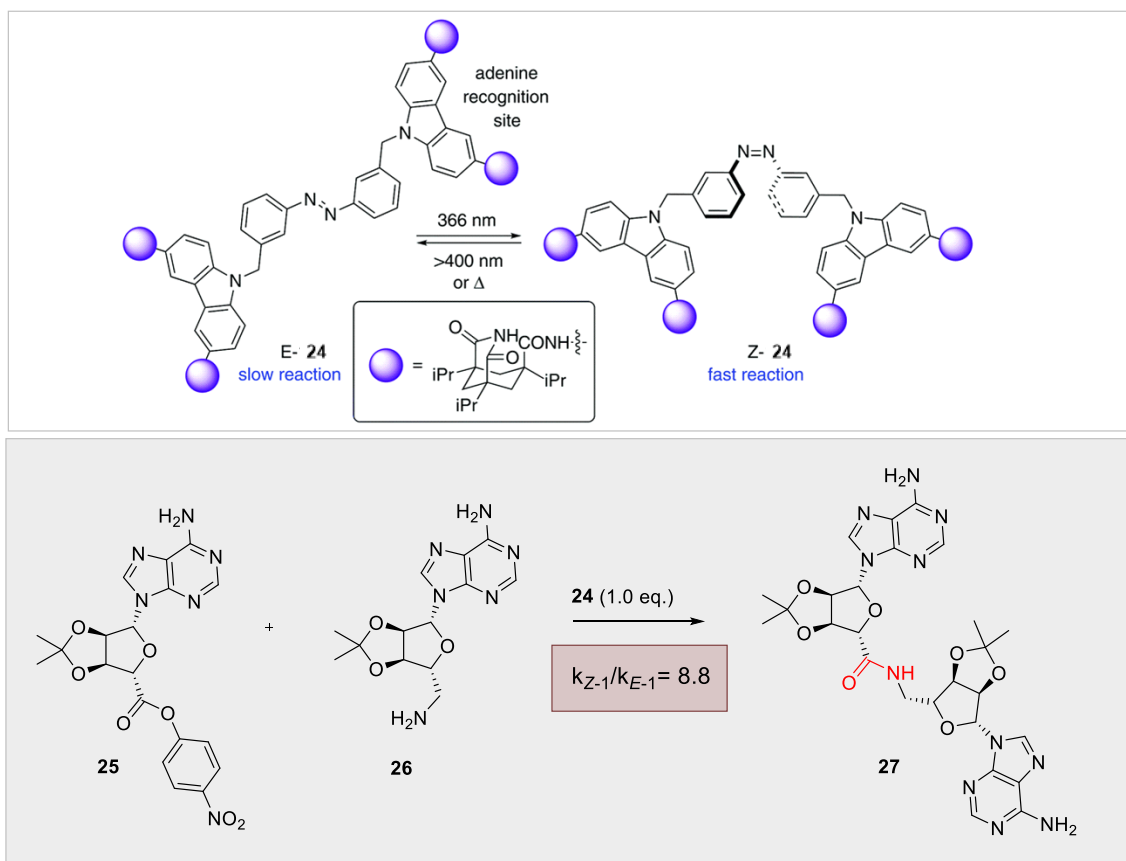
Azobenzene belongs to a class of well-studied as well as established photochromic moiety. Under photoirradiation with a particular wavelength of light, the N=N bond undertakes a photoisomerization from the *E*- to *Z*-isomer. However, the less stable *Z*-isomer will revert back to the thermodynamically more stable *E*-isomer in the absence of light. This reverse isomerization process can also be achieved by irradiating *Z*-isomer with visible light.



**Scheme 7.** Photoisomerization of azobenzene

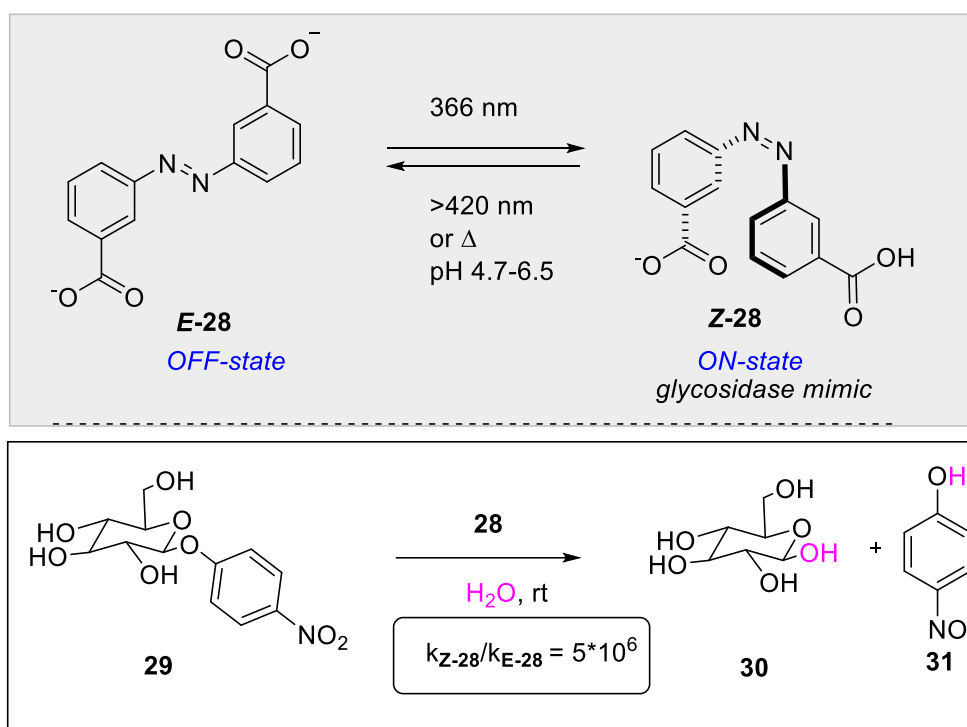
As the pioneering work utilizing azobenzene photochromic catalyst, in 1995, Würthner and Rebek demonstrated control of the catalyst linking two carbazole-based adenine receptors; a functional group consisting of the active ester was introduced to control the rate of amidation by light irradiation. The receptor site (*R*) of adenine

remotely captures two substrates *via* hydrogen bonds. In the *E*-form, the recognition sites are kept far apart from each other which results in a low reaction rate. However, upon photoirradiation, the recognition sites will come closer, resulting in cooperatively working to accelerate the condensation reaction.<sup>[19]</sup>



**Scheme 8.** Azobenzene-based adenine receptor for photoswitchable catalysis

A photoresponsive bifunctional organocatalyst based on azobenzene-tethered biscalboxylic acid **28** was developed by Samantha and co-workers.<sup>[20]</sup> The pKa modulation mediated by light through *E/Z* isomerization enhanced the activity around 6-fold under photoirradiation with 366 nm UV light (Scheme 9).

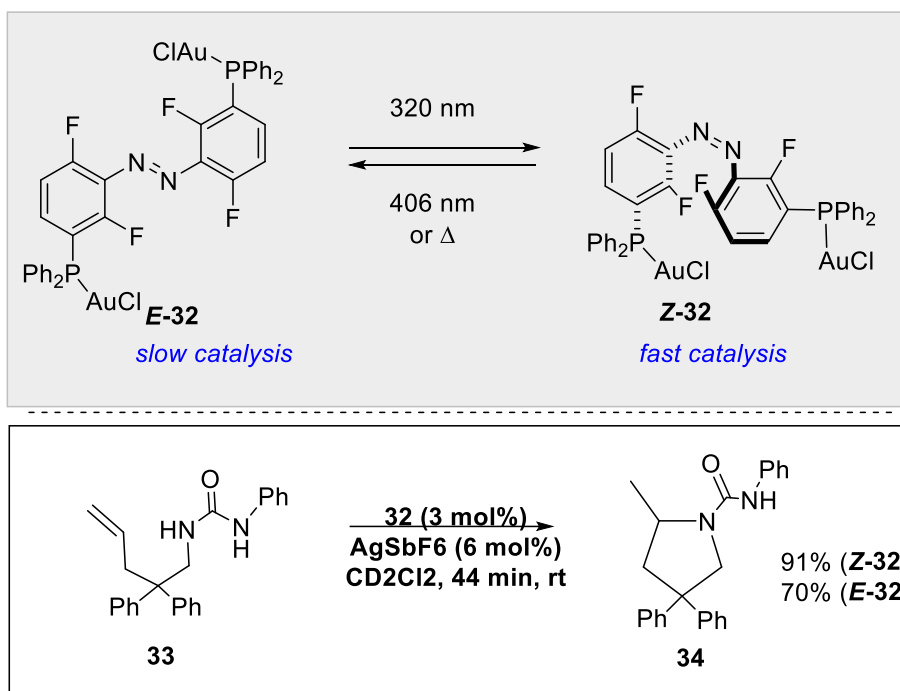


**Scheme 9.** Photoresponsive glycosidase mimic **28**.

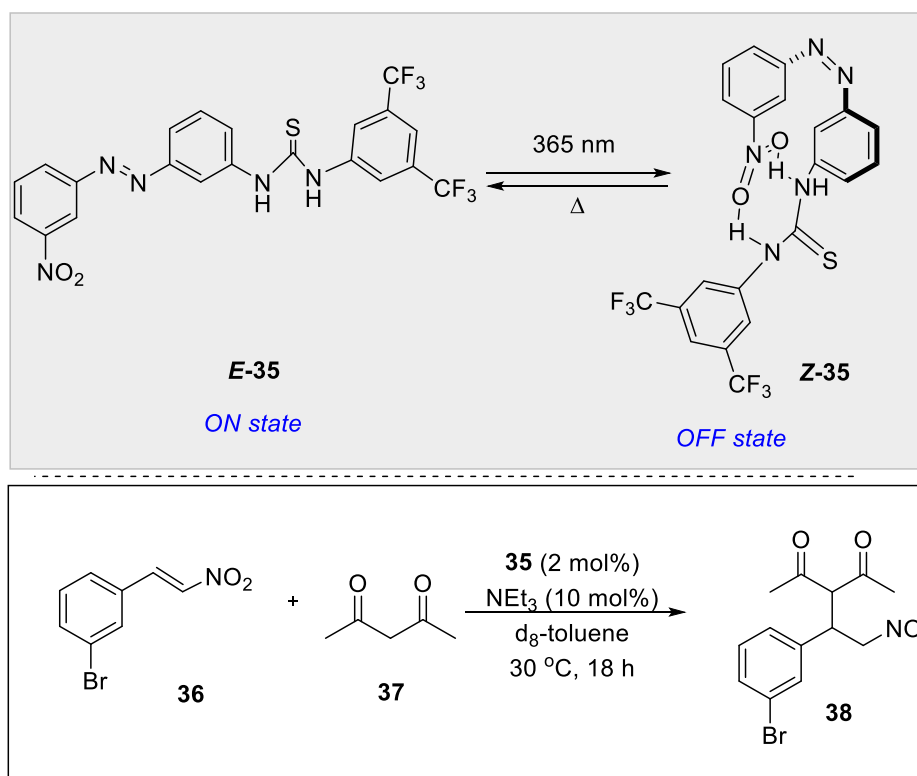
However, the asymmetric photoresponsive catalyst using azobenzene core is still limited and only a few reports have been reported so far. A requirement of different strategies to combine photoresponsive units with chiral frameworks for developing new light-based reaction control methods are much significant.

A more recent example that utilizes the azobenzene moiety as the photoswitchable linker for the catalytic activity of bimetallic gold(I) complex **32** (Scheme 10);<sup>[21]</sup> *Z*-isomer generated by 320 nm wavelength of light seems to be more active towards intramolecular hydroamination of **33** when tested both the isomers as catalyst independently. The enhanced activity results in the cooperative activation of two metal centers in the *Z*-isomer of **32**.

Another ligand system based on the azobenzene linker was developed utilizing the intramolecular hydrogen bonding interactions leading to deactivation of the catalyst **35** for thiourea catalyzed nitro-Michael addition reaction (Scheme 11).<sup>[22]</sup> Although *E*-state of the catalyst provides efficient catalyst activity, the generated *Z*-isomer of azobenzene blocks the active site of the catalyst through hydrogen bonding interaction, resulting in diminishment of the catalyst performance. However, the catalyst performance is not completely suppressed due to low PSS ratio after photoirradiation.



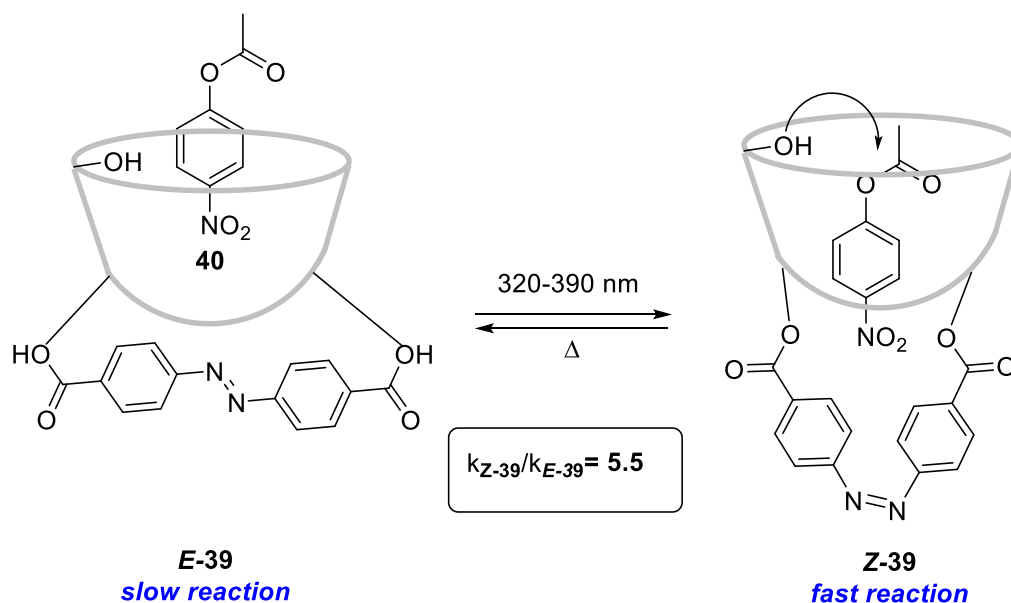
**Scheme 10.** Photoswitchable bimetallic gold complex **32** and control over the rate of intramolecular hydroamination of **33**<sup>[21]</sup>



**Scheme 11.** Photocontrol over the deactivation of organocatalyst **35**<sup>[22]</sup>



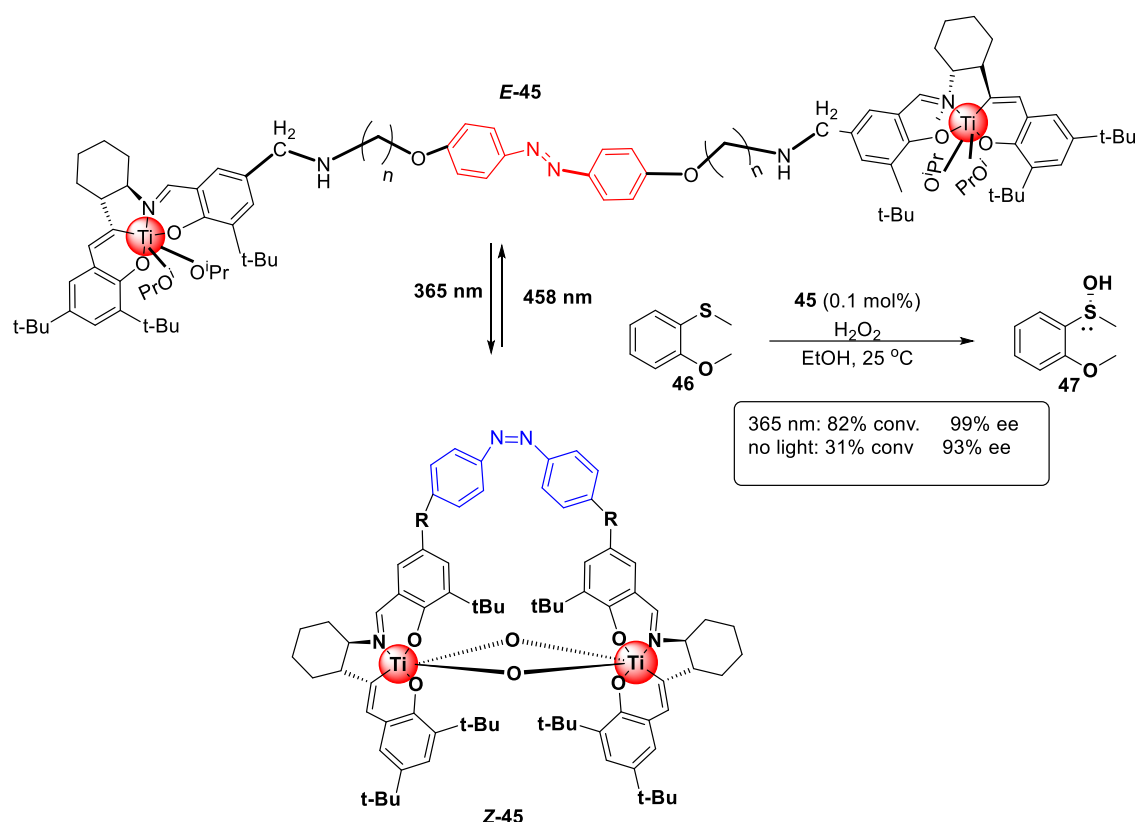
In 1981, a steric effect of  $\beta$ -cyclodextrin **39** containing an azobenzene capping unit was investigated on a hydrolysis of *p*-nitrophenylbenzoate **40**.<sup>[23]</sup> In the *E*-form of azobenzene skeleton, the substrate impedes the hydrolysis process by preventing the binding of the substrate inside the cavity. However, upon geometry change from the *E*- to *Z* isomer, the substrate is able to bind with pocket prior to hydrolysis, resulting in a 5-fold rate increasing with 38% of the *Z*-isomer in the system under 365 nm photoirradiation.



**Scheme 12.** Photocontrol over ester hydrolysis catalysed by azobenzene-capped  $\beta$ -cyclodextrin **39**<sup>[23]</sup>

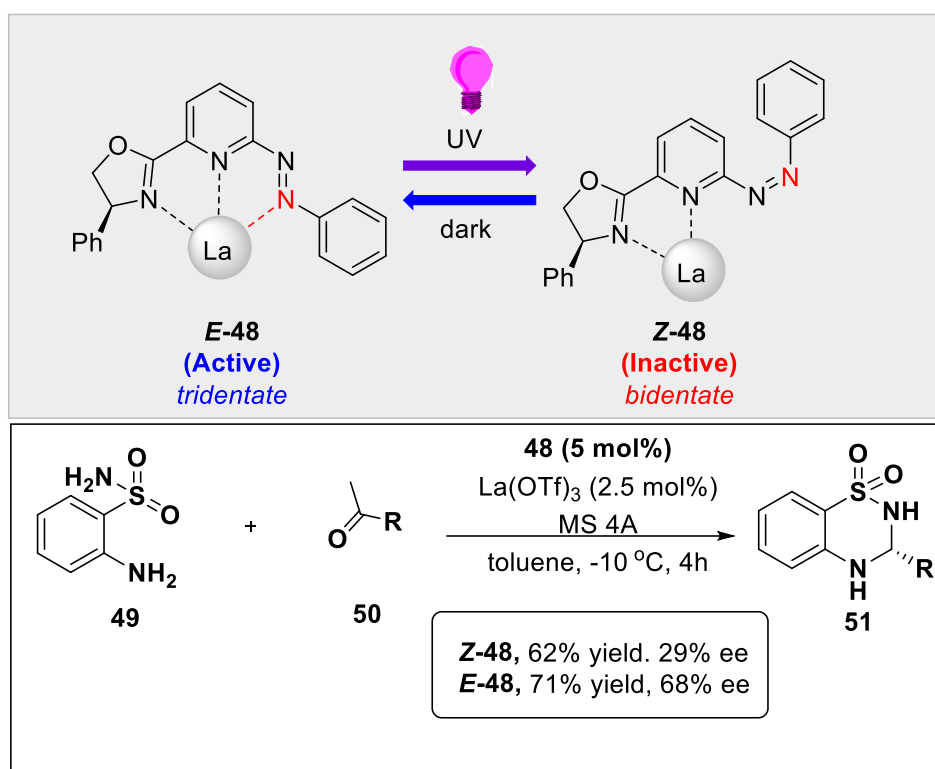
Another alternative approach based on the steric effect regulated by *E/Z* isomerization of azobenzene unit was developed for the Henry reaction with photoswitchable base **41** (Scheme 13).<sup>[24]</sup> In the thermodynamically more stable *E*-form of **41**, the nitrogen lone pair in the piperidine moiety was shielded by aromatic fragment and hinders its reactivity. However, upon photoirradiation with 365 nm UV light, the generated *Z*-isomer of **41** is able to catalyze this transformation much efficiently. About 35-fold increase in the formation of **44** was obtained with 95% of *Z*-isomer under 365 nm photoirradiation.





**Scheme 14.** The first azobenzene-based photoswitchable chiral catalyst **45**<sup>[25]</sup>

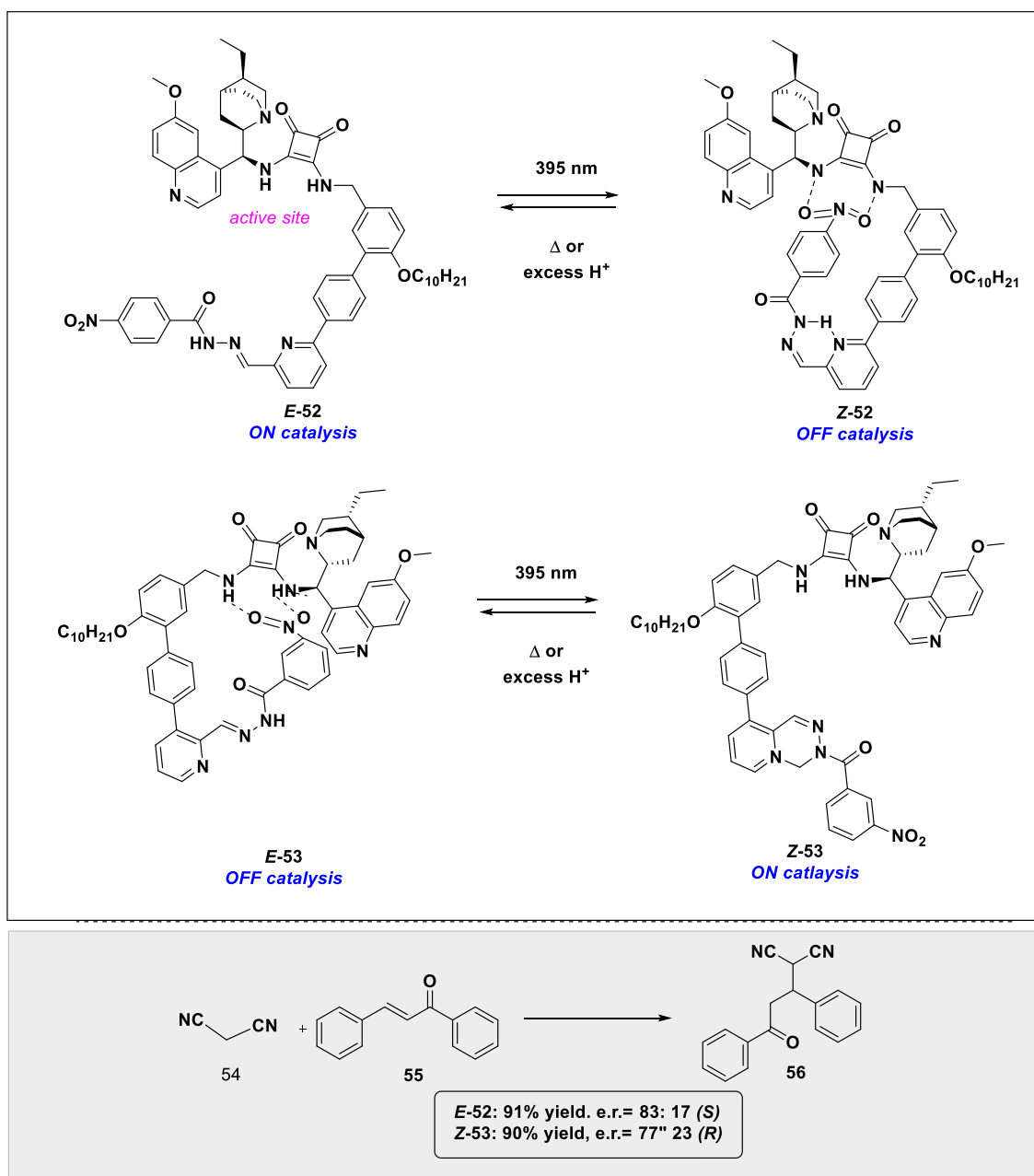
As alternative effective system utilizing azobenzene unit for photocontrol over reactivity and enantioselectivity, our group also developed chiral oxazoline-azobenzene hybrid ligand (Scheme 15).<sup>[27]</sup> Upon photoirradiation with 365 nm wavelength, the generated *Z*-isomer for the ligand lost its one of the coordination sites with the rare earth metal, leading to be less active when compared to the *E*-isomer of the catalyst. Through control experiments, the change of ee *via* photoisomerization is due to the switching of the coordination morphology between the bidentate and the tridentate system. The *E*-state ligand behaves as a tridentate system with rare earth metal. In contrast, the generated *Z*-isomer upon photoisomerization will function as a bidentate system which lowers the enantioselectivity of product **51** from 68% ee to 29% ee. To expand this area of research, our group is focusing on the development of new creative designs with this kind of photochromic units (especially azobenzene and dithienylethene moieties) to modulate the catalyst functions in response to light).



**Scheme 15.** Azobenzene chiral oxazolines **48** for photoswitchable catalysis<sup>[27]</sup>

#### 1-5-4. Hydrazone-based photoswitchable catalysts

Although the photochromic C=N bonds also possess a great space in creating photoswitchable systems utilizing imines<sup>[28]</sup> as well as hydrazones,<sup>[29]</sup> their application as photoswitchable ligands remains scarce. As shown in Scheme 16, pyridyl-acylhydrazone scaffold as a photochromic entity was utilized to develop enantioselective photoswitchable organocatalysts.<sup>[30]</sup> The main part of the catalyst includes bifunctional cinchona alkaloid-squaramide motif, which exists as the active site and is able to catalyze asymmetric Michael additions reaction. Photoswitchable hydrazine was linked with a hydrogen bond acceptor system. A photoirradiation with an appropriate wavelength of light brings the NO<sub>2</sub> group near to the squaramide motif, resulting in deactivation of the catalyst through intramolecular hydrogen bond capping. The pseudo chiral photoswitchable catalyst was also developed. These two catalysts (one is active without light and another one active with light) which differ in the regiochemistry of pyridine ring generates opposite enantiomers of product in several 1,4-addition reactions.



**Scheme 16.** Complementary pair of hydrazone-based photoswitchable organocatalysts **52** and **53**

### 1-6. Outline of my research

As described in this chapter, the catalyst activity such as a reaction rate and selectivity could be reversibly regulated by using light as an external stimulus. However, the development of photoresponsive catalysts is still in its infancy. Although new light-based reaction control methods have long required and demanded to develop effective photoresponsive catalysts, only a few examples of photoresponsive asymmetric catalysts have been reported until now. As some reasons, multistep

synthesis of chiral catalytic functional groups are required, and it is difficult to achieve compatibility with designs that obtain differences in reaction activity.

In the first part of the section, the author focused on catalysts that use aromatic azo compounds as the photoswitchable linker, which can be synthesized in a shorter process and have large structural changes as well as dipole moment due to photo induced *E/Z* isomerization. The designs of existing photoresponsive catalysts using azobenzene can be broadly divided into the following two types (Figure 4). (A) Photoisomerization of symmetric azobenzene causes functional groups to switch between single action and cooperative action, (B) photoisomerization of asymmetric azobenzene switches the shielding effect to the catalytic active site, and which changes the catalyst activity. Therefore, in this research, the author aims to use an aromatic azo compound as the photoswitchable linker. A novel photoswitchable chiral cation binding catalyst, by properly linking the azobenzene core to the chiral unit and the polyether chains which can bind alkali metals, is developed and applied to enantioselective reaction. This catalyst has the advantage over the previously reported phase transfer catalyst (ABCE)<sup>[26]</sup> from our group due to the availability of secondary interaction to stabilize the substrate molecule inside the chiral cage which promotes efficient asymmetric induction.

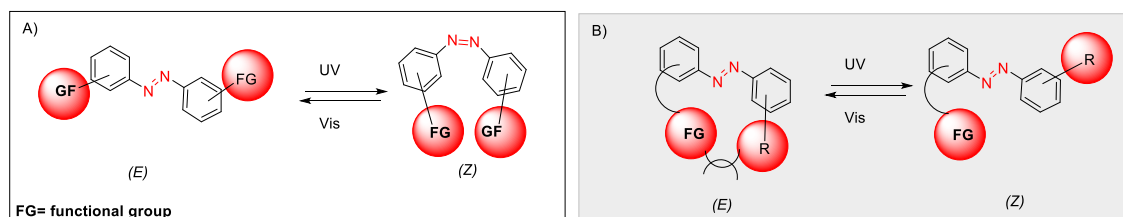


**Figure 4.** (A) Photoisomerization of symmetric azobenzene causes functional groups to switch between single action and cooperative action, (B) photoisomerization of asymmetric azobenzene switches the shielding effect to the catalytic active site

In the second part of the section, the author focused on the development of a novel chiral organocatalyst based on dithienylethene photochromic unit. To date, there are no reports utilizing this photochromic skeleton towards asymmetric organocatalysis. The photomodulation over the pK<sub>a</sub> values of catalyst is expected to control the outcome of enantioselective transformation and which will be different with two thermally stable isomers of DTEs due to their steric as well as change in electronic properties.

## Chapter 2. Photoswitchable chiral cation-binding catalyst: Photocontrol of catalytic activity on enantioselective amination synthesis

### 2-1. Introduction: Crown ether

Crown ether is a cyclic polyether discovered by Dr. Pedersen<sup>[31]</sup> in 1967, and subsequently it has evolved into the discovery of cryptand by Dr. Lehn and its application to molecular recognition and catalysts by Dr. Cram. Also, these achievements by the three researchers triggered the award of the Nobel Prize in Chemistry in 1987. The size of the pores can be used to identify inclusive metals and ammonium salts. Conventionally researchers utilize crown ether systems to solubilize insoluble alkali metal salts (higher lattice energy) in organic solvents. (Figure 5A). The ability to recognize cations of lithium, potassium, and sodium depends on the ring size of the crown ether (Figure 5B). In recent years, optically active crown ethers have been immobilized on silica gel<sup>[32a]</sup> and it is applied to ion exchange resin chromatography that utilizes the difference in pore size.<sup>[32b]</sup>

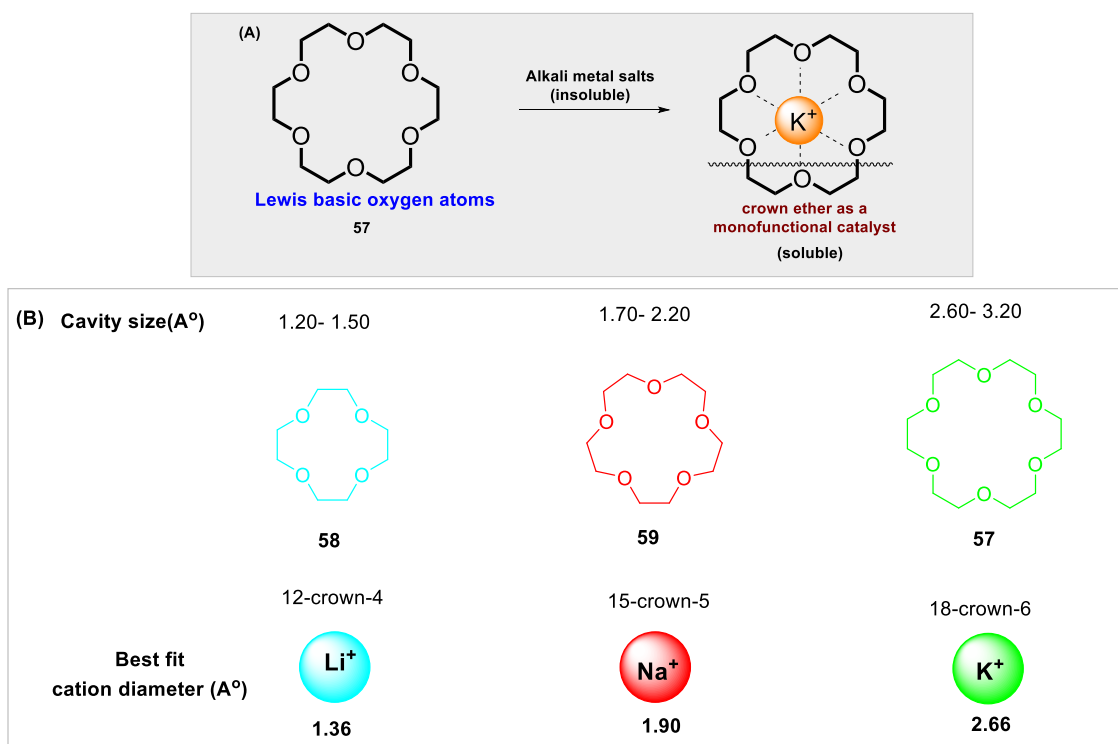


**Figure 5.** A) Crown ether as monofunctional catalyst, B) size of crown ethers and optimal cation size.

### 2-2. Photoresponsive crown ether

Research on regulating the molecular recognition ability of crown ethers by light has been conducted for a long time. In early 1980s, Takagi<sup>[33]</sup> and Shinkai<sup>[33b]</sup> independently combined azobenzene in the crown core skeleton. They synthesized and succeeded in changing the ring size of crown ether by photoisomerization of azobenzene unit.

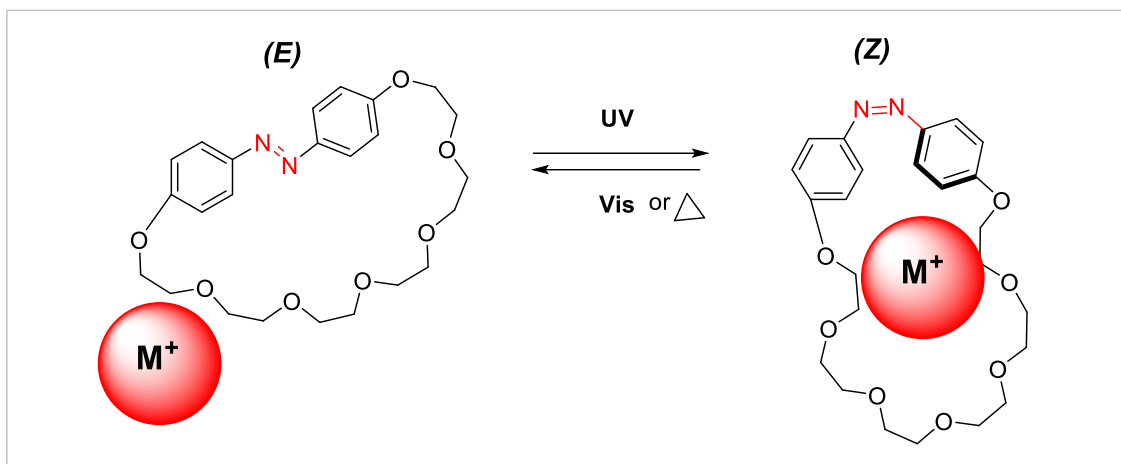


**Figure 6.** Azobenzene-containing crown ether<sup>[33]</sup>

Furthermore, Shinkai *et al.* developed another photoresponsive moiety for molecular recognition with the cross-linking two crown ethers with azobenzene (Figure 3).<sup>[34]</sup> This molecule forms a closed geometry by irradiation with ultraviolet light, and two crown ethers cooperate with each other and exhibits a high extraction ability of alkali metal salts than that of the *E*-form.

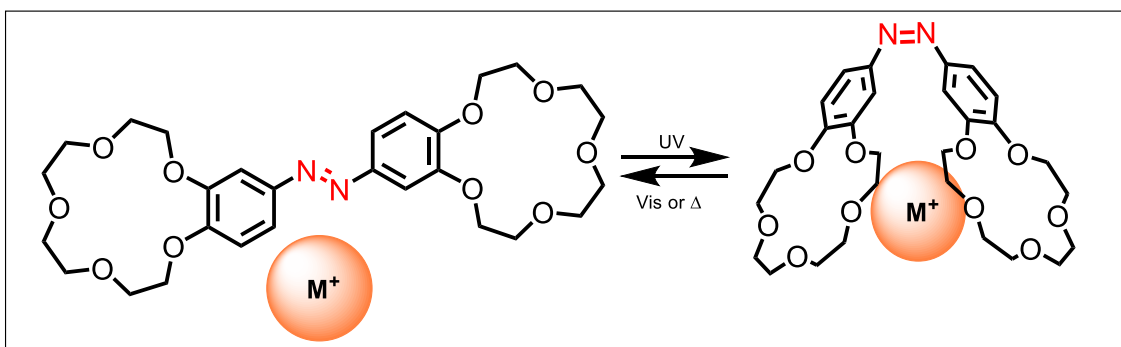
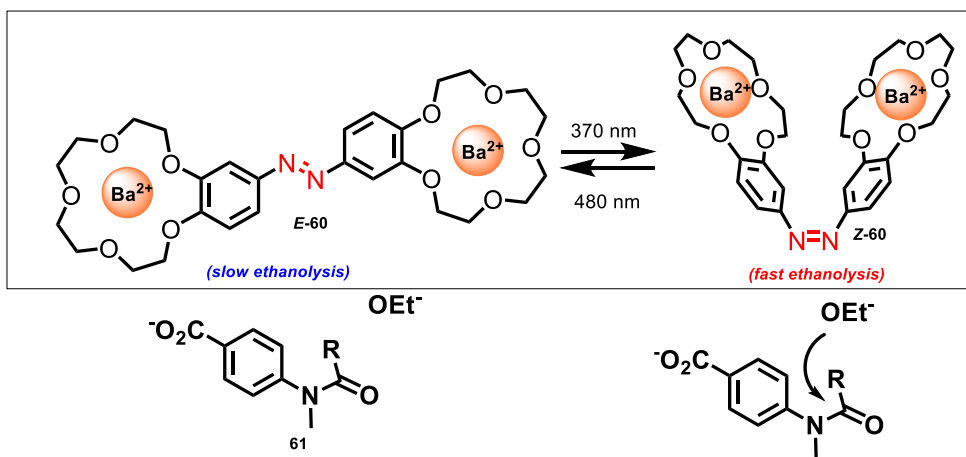


**Figure 7.** Azobenzene-bridged crown ether<sup>[35]</sup>

In 2003, Cacciapaglia *et al.* utilized barium salts under the slightly different concept by Shinkai *et al.* (Scheme 17).<sup>[35]</sup> Dinuclear barium complexes of photoresponsive bis-crown ether hosts **60** catalyzed the basic ethanolysis of tertiary acetanilides through a cooperative process in which carboxylate moiety of the substrate binds with one of the bariums centres while the other barium centre activates the nucleophilic partner, ie, ethanoate and delivers it to the carbonyl of the acetanilide. Towards the ethanolysis of anilides, the bis-barium complex of the photoresponsive azobenzene-containing *E* isomer of **60** exhibits low activity. In contrast, the *Z*-form **60** (PSS ratio *Z/E*-**5** = 95:5) obtained by photoisomerization of the azobenzene moiety worked as more active catalyst due to the proximity between two barium centres. However, the geometry resemblance between the product of reaction



and substrate resulted in a noticeable product inhibition arise from competitive coordination.

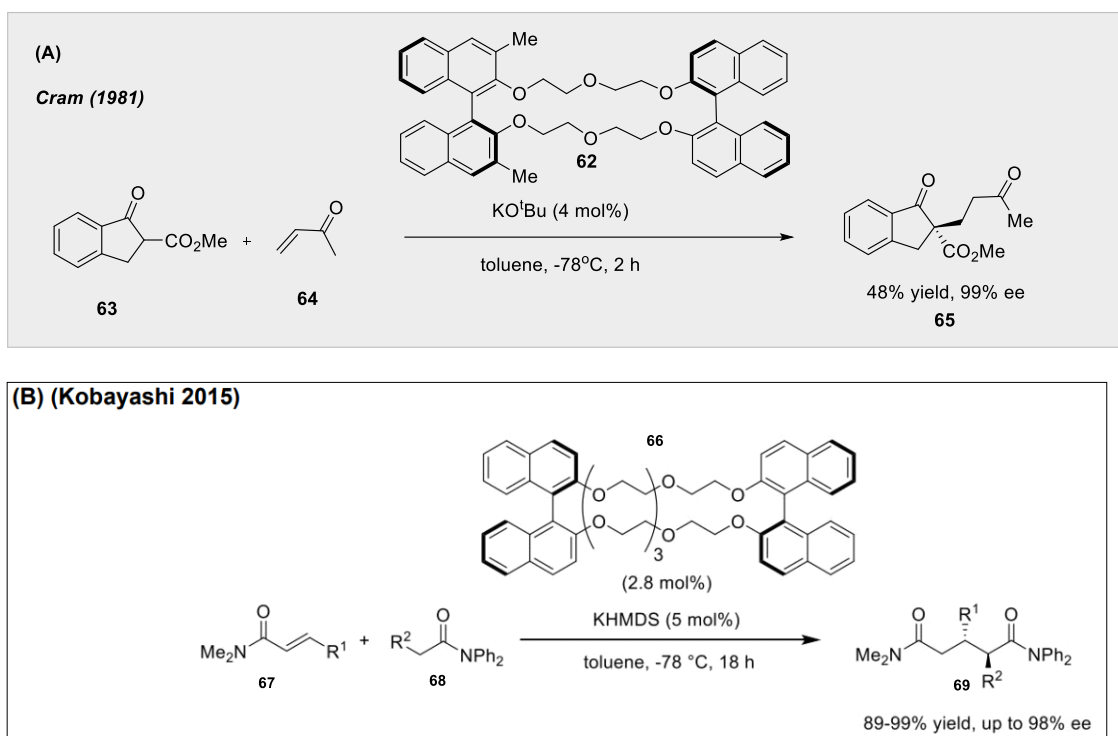


**Scheme 17.** Catalytic application of the azobenzene-bridged crown ether **60**<sup>[35]</sup>

### 2-3. Crown ether as an asymmetric phase transfer catalyst

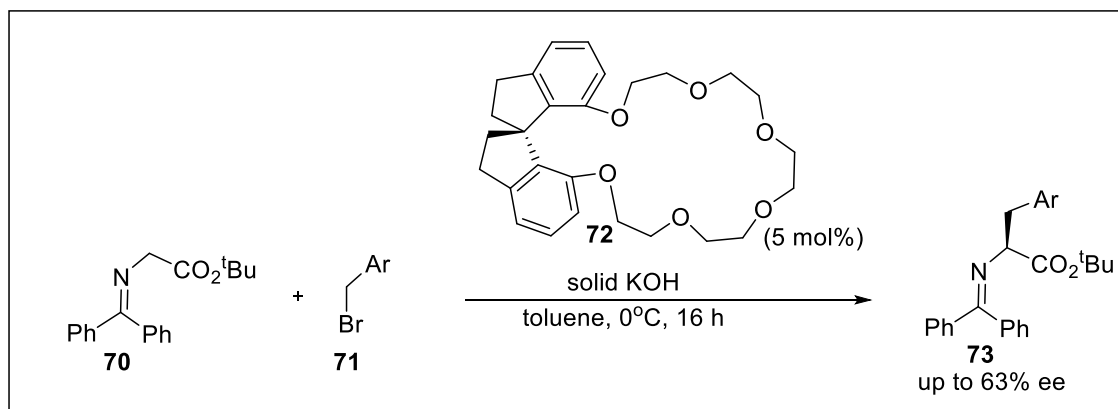
As shown in Figures 6 and 7, Cacciapaglia and Shinkai independently studied the photoresponsive crown ether for molecular recognition; one of the characteristics of crown ether molecular recognition is that it is possible to transfer an inorganic salt to an organic solvent to generate a highly active anionic species. By taking advantage of this property of crown ether it is able to utilize an ionic compound insoluble in an organic solvent for an organic reaction, and is also works as a phase transfer catalyst. This concept of phase transfer catalyst was proposed by Starks in 1971. He utilized ion-exchanged alkali metals such as sodium cyanide, which are insoluble in organic solvents, with catalytic amounts of ammonium salts and phosphonium salts, and used them as nucleophiles in organic solvents. In 1984, Dolling *et al.* reported an asymmetric quaternary ammonium salt of a cinchonine derivative as a phase transfer catalyst<sup>[36]</sup> After this report, asymmetric quaternary ammonium salt catalysts were independently developed by O'Donnell, Lygo, and Maruoka groups.

In 1981, Cram *et al.* found the value of crown ether as an asymmetric catalyst; a crown ether catalyst **62** with optically active binaphthyl skeletons was applied to the asymmetric conjugate addition reaction of ketoester **63** to methyl vinyl ketone **64**, resulting in a formation of product **65** in extremely high enantioselectivity (Scheme 18A). As other examples, in 2015, Kobayashi *et al.* succeeded in a catalytic asymmetric conjugate addition reaction of acetamide **67**, which was difficult in the past, by using crown ether together with a catalytic amount of a strong base. At this time, it has been reported that optically active crown ether **66**, which has a larger ring size than Cram *et al.* is the optimum phase transfer catalyst (Scheme 18B).<sup>[37]</sup>



**Scheme 18.** Cram's chiral crown ether and Michael reaction of  $\beta$ -ketoester to MVK

In 2005, our group reported crown ethers derived from optically active SPINOL. When the phase transfer catalyst **72** was applied to the asymmetric alkylation of glycine-Schiff salt **70** and alkyl bromide **71**, an unnatural amino acid precursor **73** can be obtained (Scheme 19).<sup>[38]</sup>

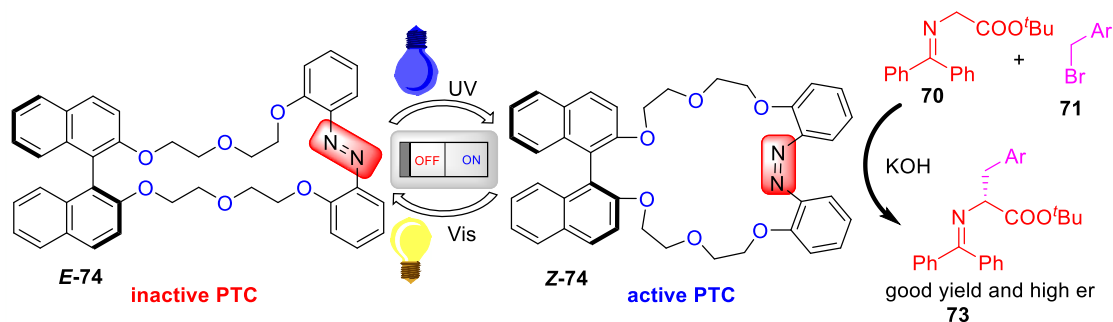


**Scheme 19.** SPINOL-derived chiral phase transfer catalyst **72**<sup>[38]</sup>

## 2-4. Development of Chiral Photoresponsive Crown Ethers

The crown ether containing azobenzene can change the recognition ability of the central metal as a photoresponsive molecule. On the other hand, crown ether has high utility value as an asymmetric phase transfer catalyst. In recent, our group reported an

azobenzene based chiral photoswitchable phase transfer catalyst **74** utilizing a crown ether-azobenzene skeleton for the first time (Scheme 20).<sup>[26]</sup> The newly developed azobenzene binaphthyl crown ether (ABCE) showed different catalytic behavior with and without photoirradiation. The *E/Z* photoisomerization of azobenzene unit in the catalytic core is responsible for the different reactivity of the ABCE system in presence of light. When applied to the enantioselective alkylation of the glycine Schiff base **70**, (*Z*)-ABCE afford chiral amino acid derivatives **73** in excellent yields with good enantiomer ratios. In contrast, (*E*)-ABCE slow down the reaction rate under similar conditions without light.



**Scheme 20.** Azobenzene based photoswitchable chiral phase transfer catalyst **74**<sup>[26]</sup>

## 2-5. OligoEGs as bifunctional promoter

As stated by Jacobsen, “the scope of cyclic crown ether approach to asymmetric catalysis has far been limited, as the naked anion is generating outside the chiral cation cage because of the absence of other secondary interactions,<sup>[39]</sup> it is difficult to create a highly organized chiral environment around naked anion. So, it is necessary to develop a new cooperative cation binding system which can utilizes the secondary interactions to stabilize the generated anion inside the chiral cage.

Then, Töke and Bako<sup>[40,41]</sup> developed bifunctional crown ethers by employing primary alcohol substituent as a secondary binding site (Figure 8). These crown ether systems utilized for Darzens reaction<sup>[40]</sup> and epoxidation;<sup>[41]</sup> free alcohol substituent resulted in higher enantioselectivities than that of using the hydroxyl protected O-methyl-protected catalysts.

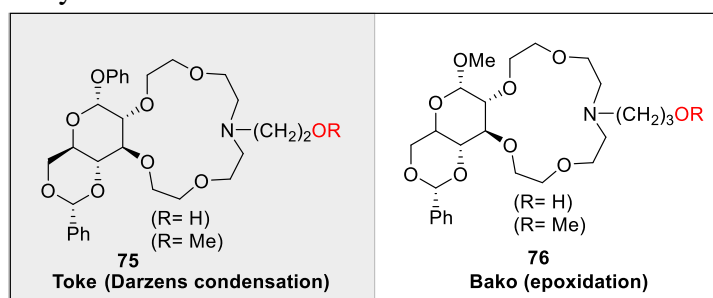


**Figure 8.** Bifunctional crown ethers as phase transfer catalyst<sup>[40,41]</sup>

These results pointed out an importance of the secondary interactions in asymmetric cation-binding catalysis.

To convert monofunctional to bifunctional catalytic system, Song *et al.* evaluated the applicability of achiral oligoethylene glycols (OligoEGs) as a promoter system for alkali metal salt-based reactions (Figure 9).<sup>[42]</sup> In the same manner like crown ether system, the coordination with the alkali metal salt and liberate the naked anion in the space to give the basic catalyst. The major difference is that, the naked anion lies in the cage itself due to the stabilizing secondary interactions like hydrogen bonding. Utilizing this hydrogen bonding interactions from one of the hydroxyl group of OligoEGs, the nucleophilicity and the basicity of the generated anion (e.g. fluoride) can be controlled and additional another hydroxyl group can be utilized to activate the substrate molecule.

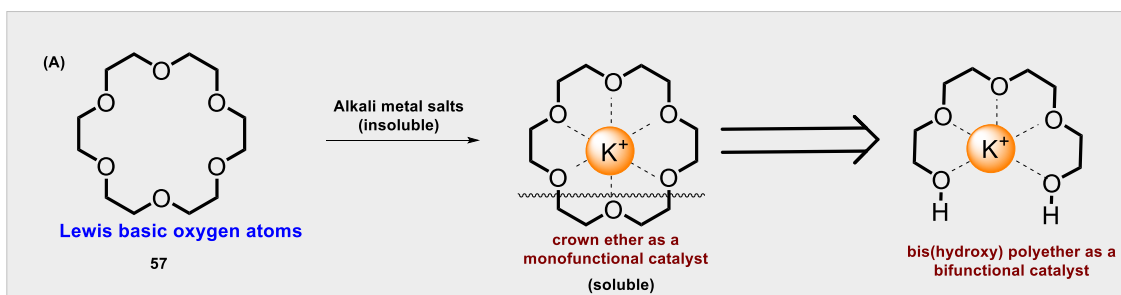
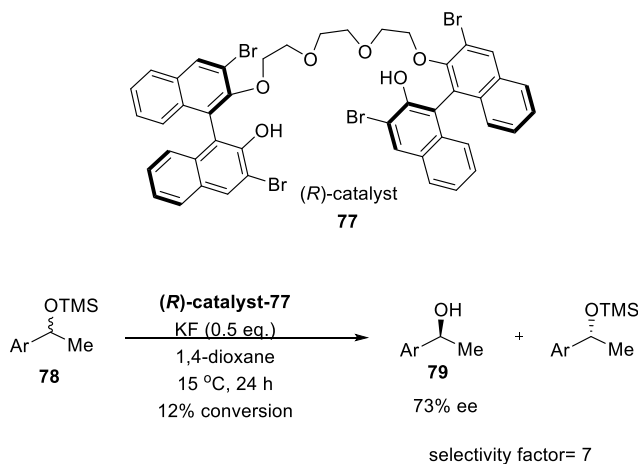


**Figure 9.** Bis (hydroxy)polyethers as bifunctional phase transfer catalyst<sup>[42]</sup>

Later, the Song group expanded this to chiral variants of oligoethylene glycols to demonstrate the applicability and usefulness of this type of chiral cation binding catalyst. The first application was demonstrated for desilylative kinetic resolution of TMS-protected secondary alcohol **79** utilizing KF (Scheme 21).<sup>[42]</sup>



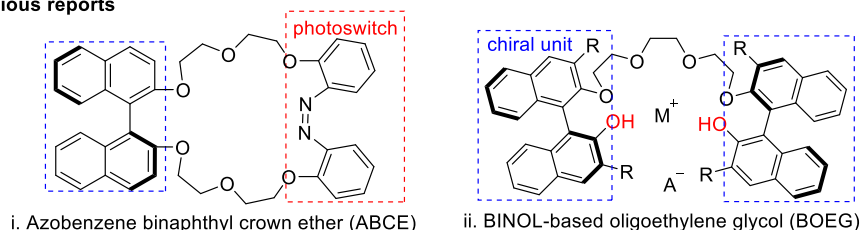
**Scheme 21.** Desilylative kinetic resolution using chiral cation binding catalyst **77**<sup>[42a]</sup>

Asymmetric environment was provided by the (*R*)-BINOL attached to both end of oligoethylene glycol with a symmetric skeleton. Further they explored the oligoethylene glycol based chiral cation binding catalyst to numerous asymmetric reactions like enantioselective protonation of TMS enol ethers of  $\alpha$ -alkyl-substituted tetralones, chromanone, and thiochromanones,<sup>[42b]</sup> catalytic enantioselective silylative kinetic resolution of racemic secondary alcohols,<sup>[42c]</sup> kinetic resolution of racemic  $\beta$ -sulfonyl ketones,<sup>[42d]</sup> enantioselective synthesis of *anti-syn*-trihalides and *anti-syn-anti*-tetrahalides *via* asymmetric  $\beta$ -elimination,<sup>[42e]</sup> asymmetric synthesis of chiral  $\alpha$ -hydroxythioesters from toxic  $\alpha$ -oxoaldehydes, asymmetric Mannich reaction with  $\alpha$ -amidosulfones.

However, the catalytic functions depend completely on the chain length of polyether moiety and the 3,3'-substituent on the BINOL backbone. Inspired from our previous work on photoswitchable chiral phase transfer catalyst (ABCE)<sup>[26]</sup> and Song's oligoethylene glycol, we hypothesized that an azobenzene core involving an oligoethylene glycol moiety with an appropriate chain length can modulate the catalyst function by adjusting the molecular switches via *E/Z* isomerization of azobenzene photochromic unit.

## 2-6. My concept:

### (A) Previous reports



### (B) This work

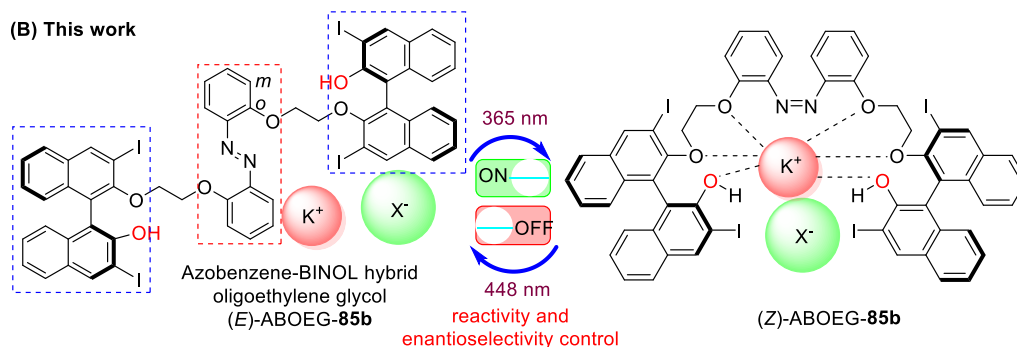
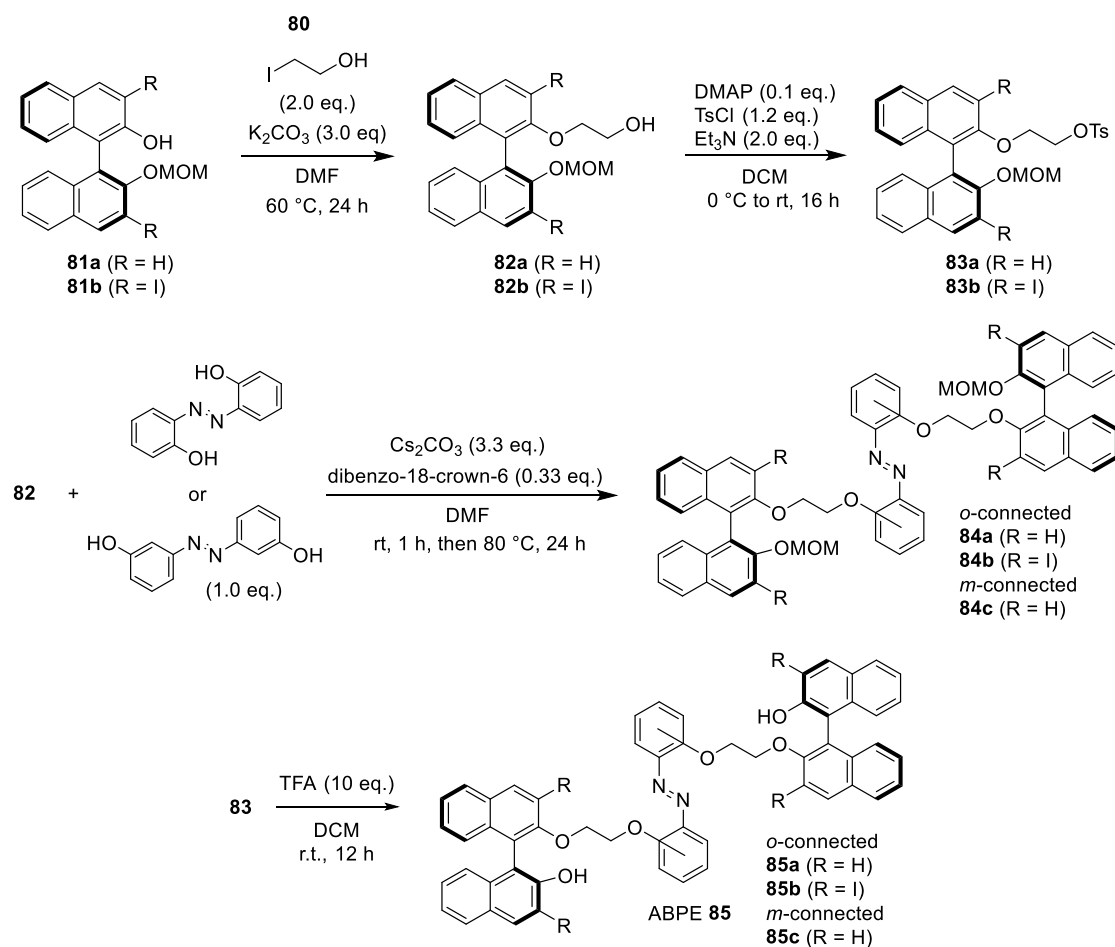


**Figure 10.** (A) Previous reports by Song and our group,<sup>[26,42]</sup> (B) this work: Azobenzene-BINOL hybrid oligoethylene glycol (ABOEG) as a photoswitchable chiral catalyst<sup>[43]</sup>

We begin our study with the synthesis of a series of chiral azobenzene base oligoethylene glycols as cation binding cages from the mono-MOM-protected BINOL<sup>[42f]</sup> and the 3,3'-disubstituted mono-MOM protected BINOL derivatives in four steps (Scheme 22).

## 2.7. General synthesis procedure for the preparation of ABOEG 85



**Scheme 22.** General synthesis procedure for the preparation of azobenzene BINOL based photoswitchable oligoethylene glycol cation binding catalysts (ABOEGs)

This includes,

- Alkylation of mono-MOM-protected BINOL-**81**<sup>[26]</sup>
- Tosylation of **82** to afford **83**
- Dihydroxyazobenzene insertion using *o*- or *m*-connected dihydroxy azobenzene as photochromic unit
- Deprotection of the MOM group using TFA to afford the final catalysts **ABOEG 85a-85c**.

The synthesis of ABOEG **85a** starts from mono-MOM-protected BINOL **81a** using 2-iodoethanol in presence of  $K_2CO_3$  as base in DMF solvent system. This provides the hydroxy alkylated product **82a** with 62% yield. The alkylated product is then subjected to tosylation utilizing a combination of triethylamine/DMAP with  $TsCl$  to afford the product **83a** with 92% isolated yield. Further, the insertion of

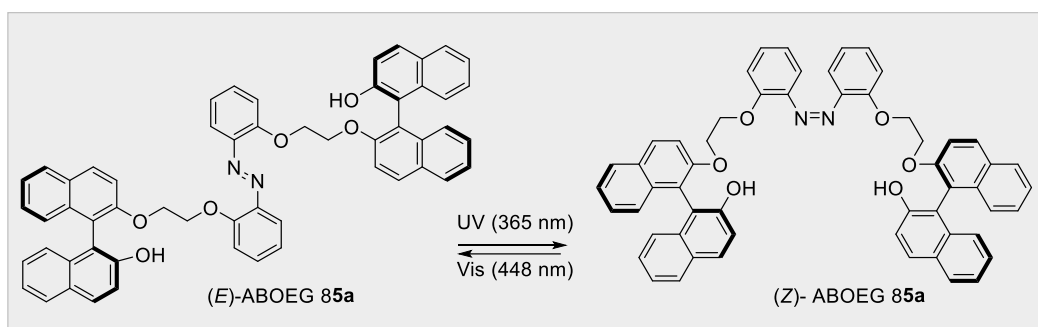
photochromic unit (2,2'-*o*-dihydroxyazobenzene) provided the MOM-protected ABOEG **84a** with moderate yield (67%). Finally, the deprotection of MOM-group was achieved using a slow addition of trifluoroacetic acid to afford the cation binding catalyst ABOEG **85a** in 72% isolated yield. Similar procedures were employed for the synthesis of ABOEG **85b** and ABOEG **85c**.

Finally, photoisomerization experiments of the newly designed chiral ABOEGs **85a** and **85b** was conducted to understand the isomerization behavior under photoirradiation and to obtain the PSS ratio under different wavelengths.

## 2-8. Photoisomerization experiment studies of ABOEG **85a**

To confirm whether our newly synthesized ABOEGs **85** were able to undergo photoisomerization and to gain further information about the photostationary ratio of the catalyst, I conducted photoisomerization experiments utilizing  $^1\text{H}$  NMR (Section 2-8-1) and UV-vis spectroscopy (Section 2-8-2).

### 2-8-1. Photoisomerization experiment studies using $^1\text{H}$ NMR



As shown in Figure 11, the catalyst showed an *E/Z* isomerization ratio of 88/12 after purification. This isomerization ratio was improved by dissolving ABOEG **85a** in toluene and heat up to over 80 °C for 1 hour. Heating the catalyst increased the *E*-isomer in ratio near to 100%. Then I irradiated with 365 nm UV for 30 minutes to the sample of ABOEG **85a** in  $\text{CDCl}_3$  (containing *E/Z* = >99:1). The PSS ratio of ABOEGs **85a** reached up to *E/Z* = 14:86. Moreover, the reversible isomerization of the catalyst ABOEG **85a** reached *E/Z* = 65:35 on exposure to visible light of wavelength 448 nm for 30 minutes. The reversible switching behavior of our new photoresponsive catalyst encourage as to examine the photoisomerization behavior using UV-vis spectroscopy (Section 2-8-2, Figure 12).

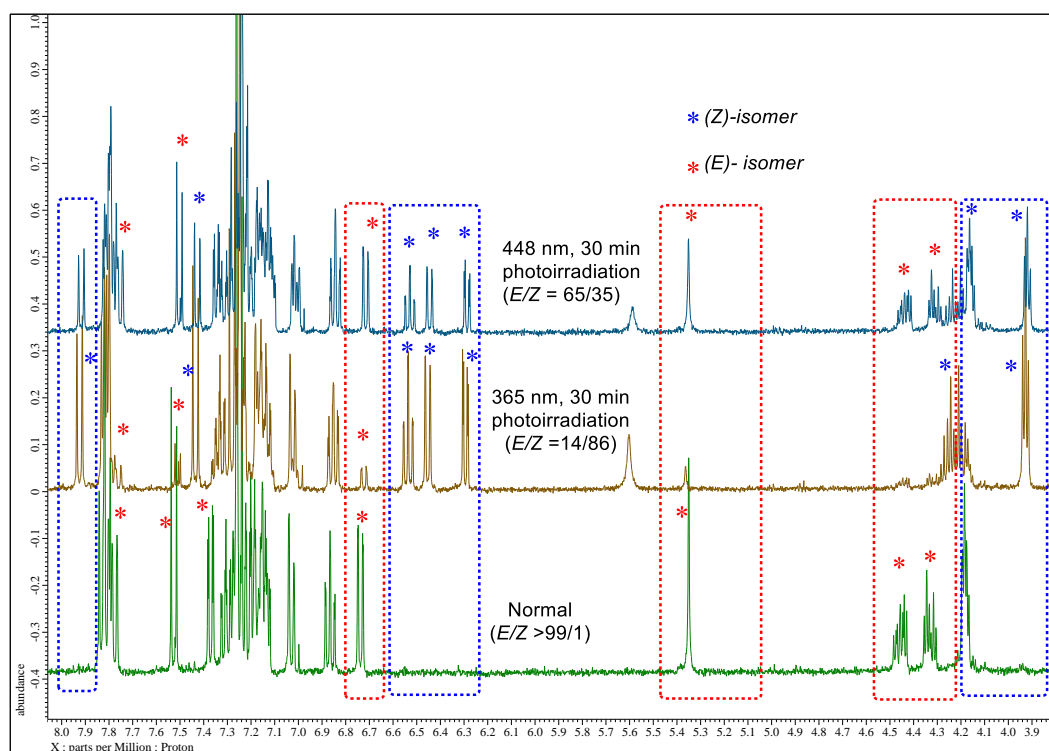


**Figure 11.** Photoisomerization experiment studies of ABOEG **85a** by  $^1\text{H}$  NMR analysis (in  $\text{CDCl}_3$ )

## 2-8-2. Photoisomerization experiment studies using UV-vis spectroscopy

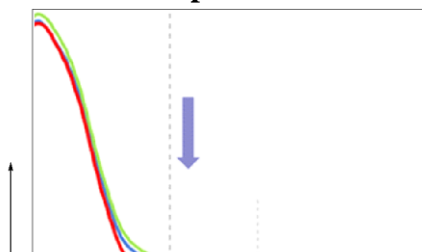


**Figure 12.** Changes in the UV-vis spectra of ABOEG **85a** (in toluene, 100  $\mu\text{M}$ )

UV irradiation (365 nm) to a sample ABOEG **85a** for 1 hour decreased the  $\pi \rightarrow \pi^*$  band along with a slight increment in the  $n \rightarrow \pi^*$  transition. This ensures the formation of the (Z)-isomer of **85a**. ABOEG **8a** showed reversible photoswitchable behavior upon visible light irradiation (448 nm for 1 hour). Similar photoisomerization



experiments were performed for **ABOEG 8b** having 3,3'-iodo substituents on the BINOL-backbone. **ABOEG 8b** shows a similar isomerization behavior like **ABOEG 85a** with a PSS ratio of  $E/Z = 13:87$  under 365 nm UV irradiation and  $E/Z = 63:37$  on exposure to visible light of wavelength 448 nm for 30 minutes (Figure 13).

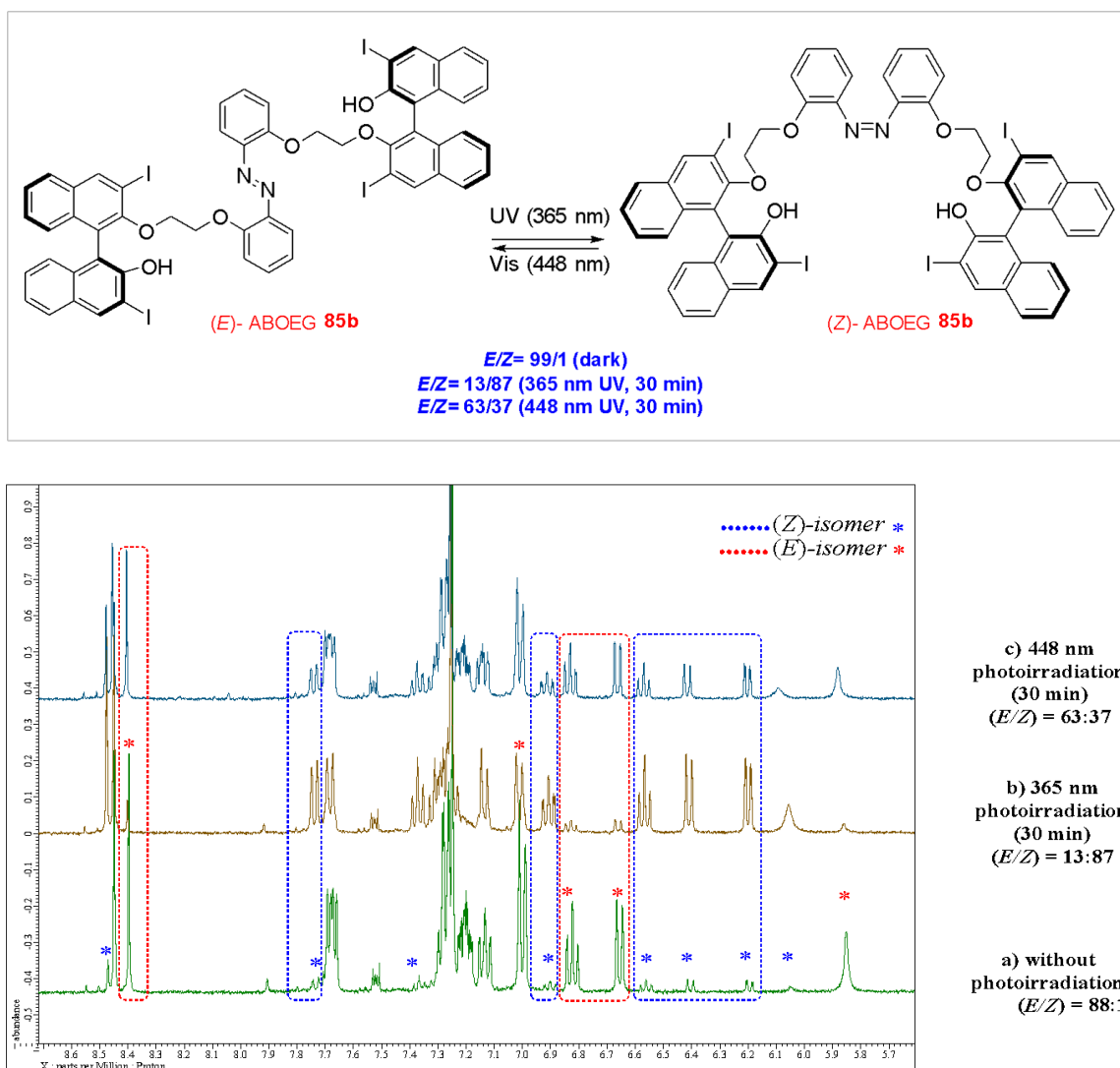


**Figure 13.** Photoisomerization experiments of **ABOEG 85b** using  $^1\text{H}$  NMR (in  $\text{CDCl}_3$ )

Then numerous other **ABOEGs** having longer ether chain length (**ABOEG 85e** and **85g**) were synthesized as well as bearing different substituents like phenyl at 3,3'-position of BINOL backbone (**ABOEG 85d**). Their photoisomerization ability also confirmed by  $^1\text{H}$  NMR analysis and UV-Vis spectroscopy (Figure 14).

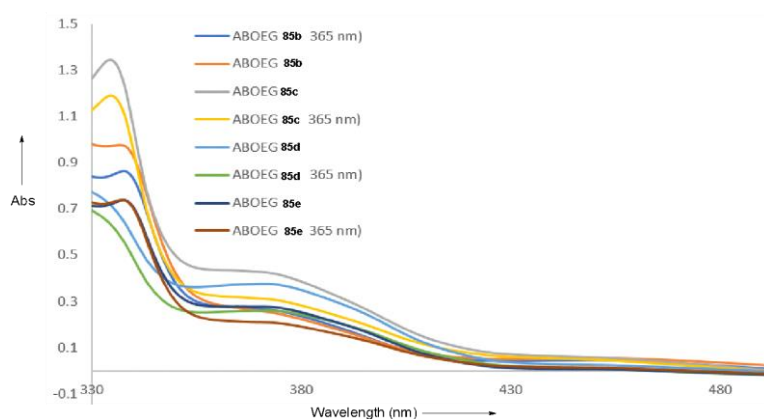
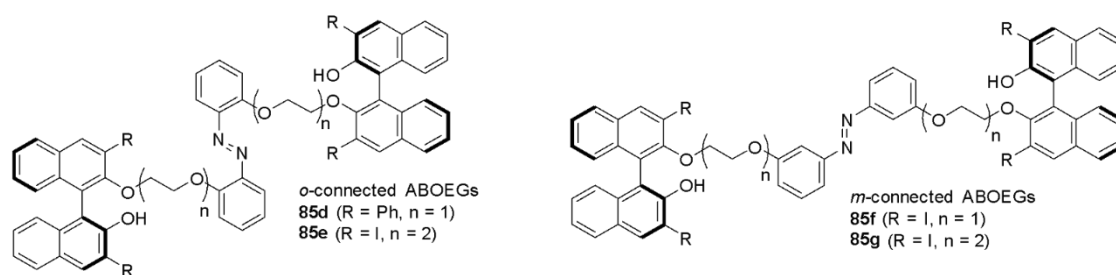


**Figure 14a.** Changes in the UV-vis spectra with UV irradiation (365 nm) to **ABOEGs** (in toluene, 100  $\mu$ M)

When we analyzed the photochemical isomerization of all the newly synthesized ABOEGs, a similar trend in the absorption was observed. In all cases,  $\pi \rightarrow \pi^*$  band goes down after irradiating with 365 nm light and a slight enhancement in the absorption corresponds to  $n \rightarrow \pi^*$  transition (Figure 14a).

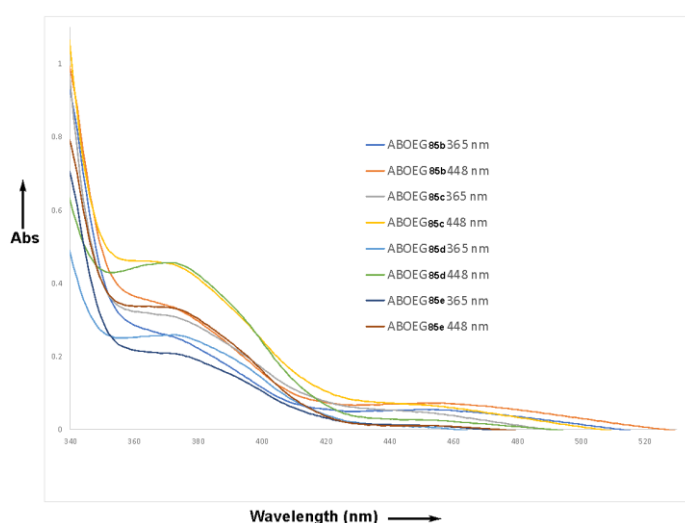


**Figure 14b.** Changes in the UV-vis spectra with UV as well as visible light irradiation to **ABOEGs** (in toluene, 100  $\mu$ M)

However, the initial pattern after purification was not recovered completely for any of these catalysts due to the existence of more amount of Z-isomer even after 448 nm, visible light irradiation (Figure 14b).

**Table 1.** Solvent effect of ABOEG **85b** on the photostationary state (PSS)ratio.

Entry	Solvent	Photoisomerization ratio ( <i>E/Z</i> ) determined by <sup>1</sup> H NMR
1	CDCl <sub>3</sub>	13:87
2	toluene-d <sub>8</sub>	14:86
3	acetone-d <sub>6</sub>	1:99
4	methanol-d <sub>4</sub>	low solubility
5	DMSO-d <sub>6</sub>	1:99

Procedure: Solvent effect to the PSS ratio was determined by taking 6.0 mg of ABOEG **85b** in an NMR tube. Then, dissolved in 0.5 mL of respective deuterated solvent was added and analyzed using <sup>1</sup>H NMR. ABOEG **85b** seems to be not soluble in Methanol-d<sub>4</sub>. Photoirradiation time (365 nm): 30 minutes

Interestingly, polar solvents like acetone-d<sub>6</sub> and DMSO-d<sub>6</sub> showed excelled photochemical isomerization (Table 1, Entries 3 and 5) on comparison with low polar solvents like CDCl<sub>3</sub> and toluene (Table 1, Entries 1 and 2).

**Table 2.** Photoisomerization experiments under different wavelengths (30 minutes).

Entry	Wavelength (nm)	Photoisomerization ratio ( <i>E/Z</i> ) determined by <sup>1</sup> H NMR
1	normal	88:12
<b>2</b>	<b>365</b>	<b>13:87</b>
3	385	24:76
4	395	33:67
5	405	51:49
<b>6</b>	<b>448</b>	<b>63:37</b>
7	468	57:43
8	521	56:44
9	631	62:38

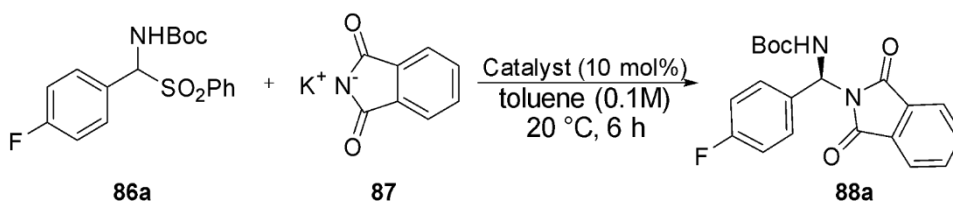
In Table 2, a range of wavelengths from 356 to 631 nm were optimized to find the suitable wavelength for achieving maximum PSS ratio. It was found that, UV light of 365 nm can provide minimum *E/Z* ratio (maximum Z isomer) on comparison with other wavelengths like 385 and 395 nm. Concomitantly, 448 nm visible light seems to be effective for achieving maximum *E/Z* isomer ratio (Table 2, entry 6).

**Table 3.** Photoisomerization ratio of ABOEGs **85** under 365 nm UV irradiation

Entry	Catalyst	Light	Photoisomerization ratio ( <i>E/Z</i> ) determined by <sup>1</sup> H NMR
1	ABOEG <b>85a</b>	Dark	99:1
2		365 nm	14:86
3	ABOEG <b>85b</b>	Dark	99:1
4		365 nm	13:87
5	ABOEG <b>85c</b>	Dark	66:34
6		365 nm	12:88
7	ABOEG <b>85d</b>	Dark	93:7
8		365 nm	13:87
9	ABOEG <b>85e</b>	Dark	95:5
10		365 nm	15:85
11	ABOEG <b>85f</b>	Dark	99:1
12		365 nm	12:88
13	ABOEG <b>85g</b>	Dark	92:8
14		365 nm	19:81

After optimizing the wavelength for an effective *E* to *Z* (365 nm) and *Z* to *E* (448 nm) isomerizations, I initially analyzed the PSS ratio of the synthesized ABOEGs with respect to 365 nm photoirradiation for a period of 30 minutes (Table 3). All of the newly synthesized catalyst ABOEGs **85** were able to undergo a good photoisomerization behavior. I have examined the ability of ABOEGs to function as asymmetric photoswitchable catalyst. Since ABOEGs **85** seem to have some features which are similar to those of Songs chiral BINOL-based oligoethylene glycols (BOEGs, Figure 1A-ii), the reaction of  $\alpha$ -amidossulfones **86a** with potassium salt of phthalimide **87** was investigated (Table 4).

## 2-9. ABOEG **85** catalyzed enantioselective Mannich type reaction



When a catalyst loading of 10 mol% of ABOEG **85a** bearing a 2,2'-dioxy azobenzene photochromic unit was applied to the aminalization reaction under 365 nm UV irradiation, the yield of desired aminal **88a** reduced on comparison with that obtained without light (55% and 80%, respectively). Moreover, **88a** did not exhibit any enantioselectivity under both the condition (Entries 1 and 2).

**Table 4.** Enantioselective Mannich-type reaction of  $\alpha$ -amidosulfone **86a** with potassium phthalimide **87** using ABOEGs **85**.

Entry	Catalyst	Wavelength (nm)	<i>E/Z</i> ratio	Yield <sup>b</sup> [%]	ee <sup>d</sup> [%]
1	ABOEG <b>85a</b>	365	14:86	55	Rac
2	ABOEG <b>85a</b>	no light	100:0	80	Rac
3	ABOEG <b>85b</b>	365	13:87	<b>92 (90)<sup>c</sup></b>	<b>86</b>
4	ABOEG <b>85b</b>	no light	99:1	<b>34 (31)<sup>c</sup></b>	<b>30</b>
5	ABOEG <b>85c</b>	365	15:85	55	Rac
6	ABOEG <b>85c</b>	no light	95:5	37	Rac
7	ABOEG <b>85d</b>	365	12:88	34	Rac
8	ABOEG <b>85d</b>	no light	64:36	38	Rac
9	ABOEG <b>85e</b>	365	12:88	83	38
10	ABOEG <b>5e</b>	no light	93:7	51	24
11	ABOEG <b>85f</b>	365	12:88	51	14
12	ABOEG <b>85f</b>	no light	99:1	39	24
13	ABOEG <b>85g</b>	365	19:81	74	32
14	ABOEG <b>85g</b>	no light	92:8	58	44

<sup>a</sup>General reaction conditions: **86a** (0.1 mmol), **87** (0.22 mmol) in toluene (0.1 M) at 20 °C for 6 h. <sup>b</sup><sup>1</sup>H-NMR yield using 1,3,5-trimethoxybenzene as an internal standard. <sup>c</sup>Isolated yield. <sup>d</sup>Enantiomeric ratio was determined by HPLC analysis (DAICEL Chiralpak OD-H). Racemization of **88a** did not proceed during the reaction and HPLC measurements.

Interestingly, the reaction utilizing ABOEG **85b** with iodo groups at the 3,3'-position of the BINOL backbone enhanced both the catalytic activity as well as enantioselectivity under photoirradiation, provided **88a** in 90% yield with 86% ee probably due to the extra stabilization offered by the iodo substituent to potassium cations inside the cation binding chiral cage (Entry 3). In contrast, the reaction carried out under dark results in a drastic drop-in catalyst activity, providing **88a** in 31% yield with 30% ee (Entry 4). These different results could be explained based on the different photostationary state ratios under UV irradiation and dark. When ABOEG **85d** possessing phenyl substituent at the 3,3'-position of the BINOL backbone was applied, the reactions seem to be much sluggish and afforded **88a** in 34% yield under UV irradiation and 38% under dark with no observable enantioselectivity (Entries 7 and 8, respectively). Then we synthesized long chain ABOEG **85e**, which has a longer chain length when compared to that of ABOEG **85b**, resulted in moderate reactivity and low selectivity, which signifies the importance of the polyether chain length for

enantioinduction (Entries 9 and 10). After that, I have synthesized *m*-connected dihydroxy azobenzene based ABOEGs **85c**, **85f**, **85g** were used in the Mannish type reaction. However, no satisfactory results were obtained owing to the weak coordination *m*-cage with the potassium cation (Entries 5, 6, and 11–14).

### 2-9-1. Optimization of Reaction Conditions

Next I investigated the effect of catalyst loading (Table 5). Among a catalyst amount of 1, 2.5, 5, 10, and 20 mol% I screened, a use of 10 mol% of catalyst resulted in highest yield and enantioselectivity of aminal **88a** with 365 nm light (entry 7). In contrast, 34% yield and 30% ee of **88a** was observed under the dark.

**Table 5a.** Effect of catalyst loading

entry	wavelength (nm)	catalyst (mol%)	yield (%)	ee (%) <sup>b</sup>
1	365	1	18	17
2	no light	1	trace	--
3	365	2.5	35	32
4	no light	2.5	13	10
5	365	5	57	52
6	no light	5	23	22
<b>7</b>	<b>365</b>	<b>10</b>	<b>92</b>	<b>86</b>
<b>8</b>	<b>no light</b>	<b>10</b>	<b>34</b>	<b>30</b>
9	365	20	96	82
10	no light	20	46	48

<sup>a</sup>General reaction conditions: **86a** (0.1 mmol), **87** (0.22 mmol) in toluene (0.1 M) at 20 °C for 6 h. <sup>b</sup>Determined by HPLC (DAICEL Chiralpak OD-H).

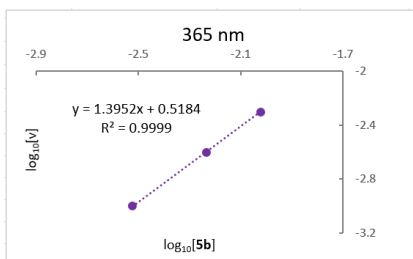
**Table 5b.** Measurement of catalytic order of ABOEG **85b**<sup>a</sup>

Entry	Wavelength (nm)	Catalyst (mol%)	<sup>1</sup> H NMR yield of <b>88a</b> (%) <sup>b</sup>	%Ee of <b>88a</b> <sup>c</sup>
1	365	1	18	17
2	no light	1	5	--
3	365	2.5	35	32
4	no light	2.5	13	10
<b>5</b>	<b>365</b>	<b>5</b>	<b>57</b>	<b>52</b>
<b>6</b>	<b>no light</b>	<b>5</b>	<b>23</b>	<b>22</b>

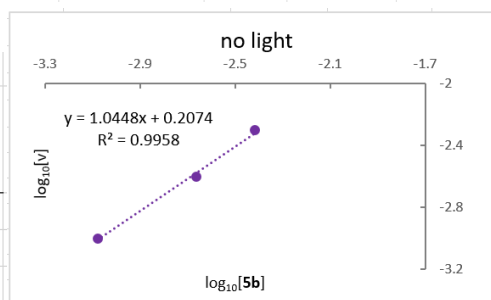
<sup>a</sup>General reaction conditions: **86a** (0.1 mmol), **87** (0.22 mmol) in toluene (0.1 M) at 20 °C for 6 h. <sup>b</sup>Using 1,3,5-trimethoxybenzene as an internal standard. <sup>c</sup>Determined by HPLC (DAICEL Chiralpak OD-H).

Reaction time- 6 h, Solvent- 1 mL

	365 nm		
5b mol%	v (mmol/cm <sup>3</sup> · h)	log <sub>10</sub> [v]	log <sub>10</sub> [5b]
1	0.00	-2.5228787	-3
2.5	0.01	-2.2340832	-2.602059991
5	0.01	-2.0222764	-2.301029996



	no light		
5b mol%	v (mmol/cm <sup>3</sup> · h)	log <sub>10</sub> [v]	log <sub>10</sub> [5b]
1	0.000833333	-3.0791812	-3
2.5	0.002166667	-2.6642079	-2.60206
5	0.003833333	-2.4164234	-2.30103



Next, I have measured the order of the catalyst ABOEG **85b**. The reaction order with respect to the catalyst ABOEG **85b** was calculated when using catalyst loadings of 1, 2.5, and 5 mol %. The reaction was found to be first order in the catalyst under no light, and 1.4<sup>th</sup> order in the catalyst with irradiation of 365 nm, probably due to the *E/Z* mixture.

**Table 6.** Effect of solvent to reactivity and enantioselectivity<sup>a</sup>

entry	catalyst (wavelength)	Solvent	yield (%) <sup>b</sup>	ee (%) <sup>c</sup>
1	ABOEG <b>85b</b> (365 nm)	Mesitylene	87	78
2	ABOEG <b>85b</b> (no light)	Mesitylene	39	33
3	ABOEG <b>85b</b> (365 nm)	DCM	81	20
4	ABOEG <b>85b</b> (no light)	DCM	trace	...
5	ABOEG <b>85b</b> (365 nm)	THF	96	rac
6	ABOEG <b>85b</b> (no light)	THF	94	rac
7	ABOEG <b>85b</b> (365 nm)	1,4-dioxane	82	12
8	ABOEG <b>85b</b> (no light)	1,4-dioxane	74	rac
9	ABOEG <b>85b</b> (365 nm)	Toluene	92	86
10	ABOEG <b>85b</b> (no light)	Toluene	34	30

<sup>a</sup>General reaction conditions: **86a** (0.1 mmol), **87** (0.22 mmol) and 10 mol% of catalyst in toluene (0.1 M) at 20 °C for 6 h. <sup>b</sup>Determined by <sup>1</sup>H-NMR using 1,3,5-trimethoxybenzene as an internal standard. <sup>c</sup>Determined by HPLC (DAICEL Chiralpak OD-H).

Among the catalyst we screened, toluene was better reaction solvent than others (Table 6).

**Table 7.** Effect of photoisomerization ratio on reactivity and enantioselectivity<sup>a</sup>

entry	wavelength (nm)	Photoisomerization ratio ( <i>E/Z</i> )	yield (%) <sup>b</sup>	ee (%)
1	365	13:87	96	86
2	395	33:67	82	74
3	405	57:43	71	60
4	-	98:2	34	35

<sup>a</sup>General reaction conditions: **86a** (0.1 mmol), **87a** (0.22 mmol) in toluene (0.1 M) at 20 °C for 6 h. <sup>b</sup><sup>1</sup>H-NMR yield using 1,3,5- trimethoxybenzene as an internal standard.

<sup>c</sup>Determined by HPLC.

To confirm whether the *Z*-isomer of ABOEG **85b** is actually responsible for higher enantioinduction, asymmetric reaction with different wavelengths of light was carried out. Each of these wavelengths can provide different isomerization ratios. It was found that, with decreased *Z/E* ratio using different wavelengths of light, enantioselectivity of amination seems to be dropped. This signifies that the *Z*-isomer of ABOEG **85b** can provide more suitable chiral environment for proper metal coordination in comparison with a *E*-isomer of ABOEG **85b**.

## 2-9-2. Coordination experiment of catalyst ABOEG **85b**

To understand the coordination behavior of potassium cation with the two distinct coordination environments of ABOEG **85b**, coordination experiment was conducted using <sup>1</sup>H NMR spectroscopy studies using DMSO-*d*<sub>6</sub> (Figure 15). DMSO is selected over other solvents owing to the higher solubility of **87** on comparison with CDCl<sub>3</sub> and toluene *d*<sub>8</sub>. Acetonitrile may also be an effective solvent for coordination studies. The details of the procedures were explained below.

Procedure: To a flame dried test-tube was added ABOEG **85b** in DMSO-*d*<sub>6</sub> and irradiate with 365 nm UV irradiation for 30 min. After that, 2.0 eq. of potassium phthalimide was added and stirred for another 30 min. Further, the crude mixture was submitted for <sup>1</sup>H NMR analysis. Same procedure was carried out without light for reaction with *E*-isomer of ABOEG **85b**.



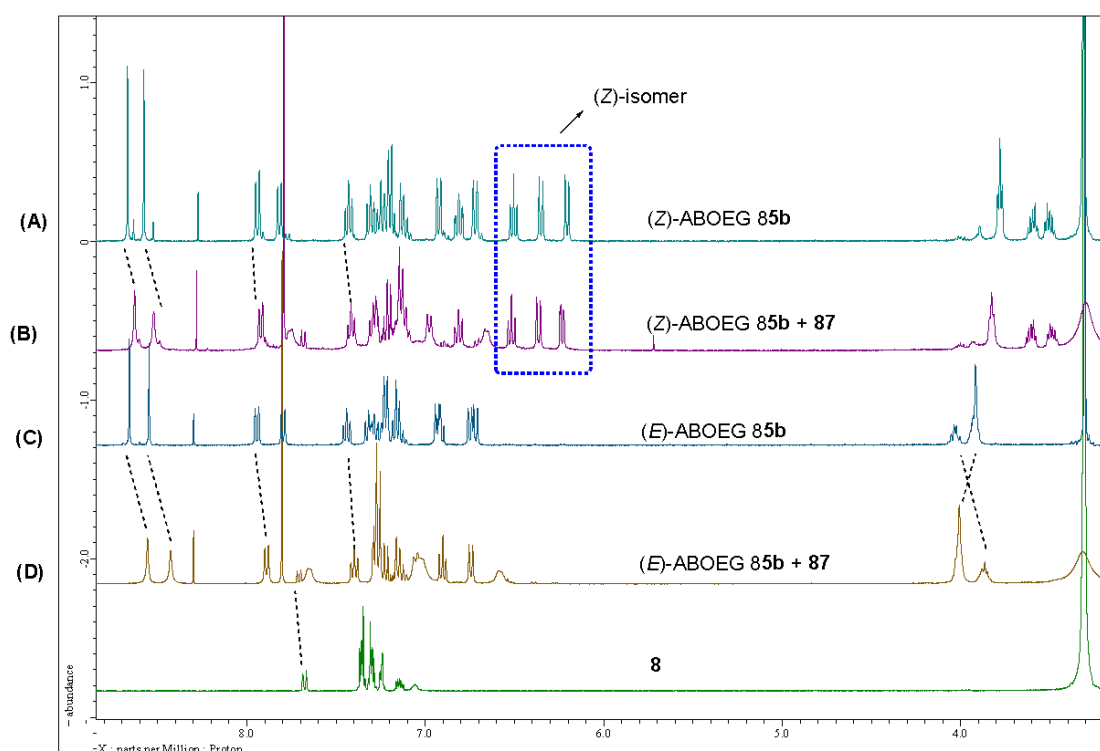


**Figure 15.** Coordination studies of catalyst ABOEG **85b**.  $^1\text{H}$  NMR of (A) (Z)-ABOEG **85b** upon 365 nm UV irradiation for 30 min, (B) (Z)-ABOEG **85b**+**87** upon 365 nm UV irradiation for 30 min (1 mM in DMSO- $d_6$ ) and (C) (E)-ABOEG **85b** under dark, (D) (E)-ABOEG **85b**+**87** (1 mM in DMSO- $d_6$ ).

**Table 8:** *E/Z* ratio of ABOEG **85b** and **85b-87** in the photostationary state (PSS).

Entry	Compounds	Light (wavelength (nm))	PSS ratio ( <i>E/Z</i> )
1	ABOEG <b>85b</b>	dark	99/1
2	ABOEG <b>85b</b>	UV (365 nm)	2/98
3	ABOEG <b>85b-8</b>	dark	99/1
4	ABOEG <b>85b-8</b>	UV (365 nm)	1/99
5	ABOEG <b>85b</b>	448 nm	63/37
6	ABOEG <b>85b-87</b>	448 nm	64/36

Determined by  $^1\text{H}$  NMR of ABOEG **85b** after photoirradiation for 30 min (1 mM) in DMSO

From the coordination experiments (Table 8), both *E*- and *Z*-ABOEGs **85b** could coordinate with potassium cation **87**; the reverse isomerization of *Z*-ABOEG **85b** with 448 nm is not affected with potassium cation coordination (Table 8, entry 6). Furthermore, symmetric peak shifting indicates that two BINOL moieties in the catalyst may take part in cation coordination.

### 2-9-3. Thermal stability and half-life measurement of (Z)-ABOEG 85b

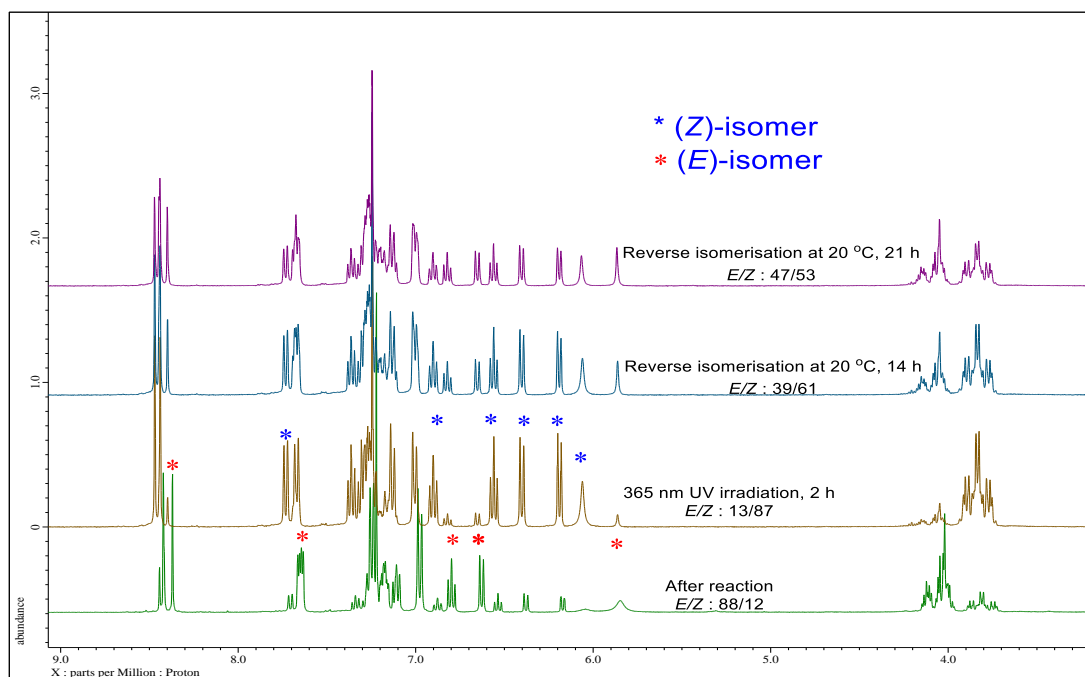


**Figure 16a.** Half-life measurement of (Z)-ABOEG **85b** in CDCl<sub>3</sub> using <sup>1</sup>H NMR

The half-life of the designed cation cage (Z)-ABOEG **85b** was measured at 20 °C. ABOEG **85b** was obtained with a PSS ratio of  $E/Z$ -ABOEG **85b** = 88:12 after purification using column chromatography. Heating in toluene at 80 °C for 2 h improved the PSS ratio to  $E/Z$ -ABOEG **85b** = 99:1. Then, exposure to UV irradiation for 2 h under 365 nm resulted in PSS ratio to  $E/Z$ -ABOEG **85b** = 13:87. After that, it was allowed to undergo reverse isomerization at 20 °C. A plot showing the thermal isomerization with respect to temperature over 40 h was demonstrated in Figure 16b. A linear plot with negative slope of 1.75 and a y intercept of 87.5 was obtained. From the plot, the half-life of Z-**85b** was measured to be 25 h (in CDCl<sub>3</sub>).

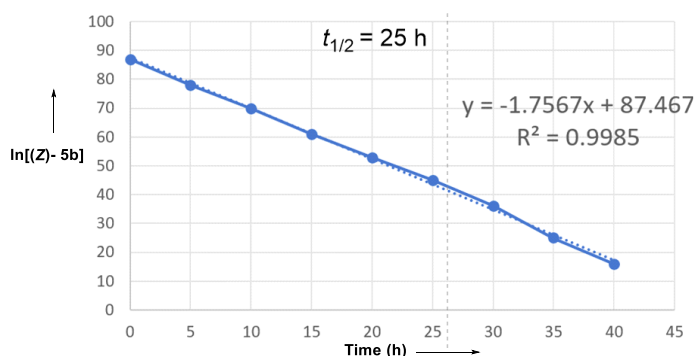
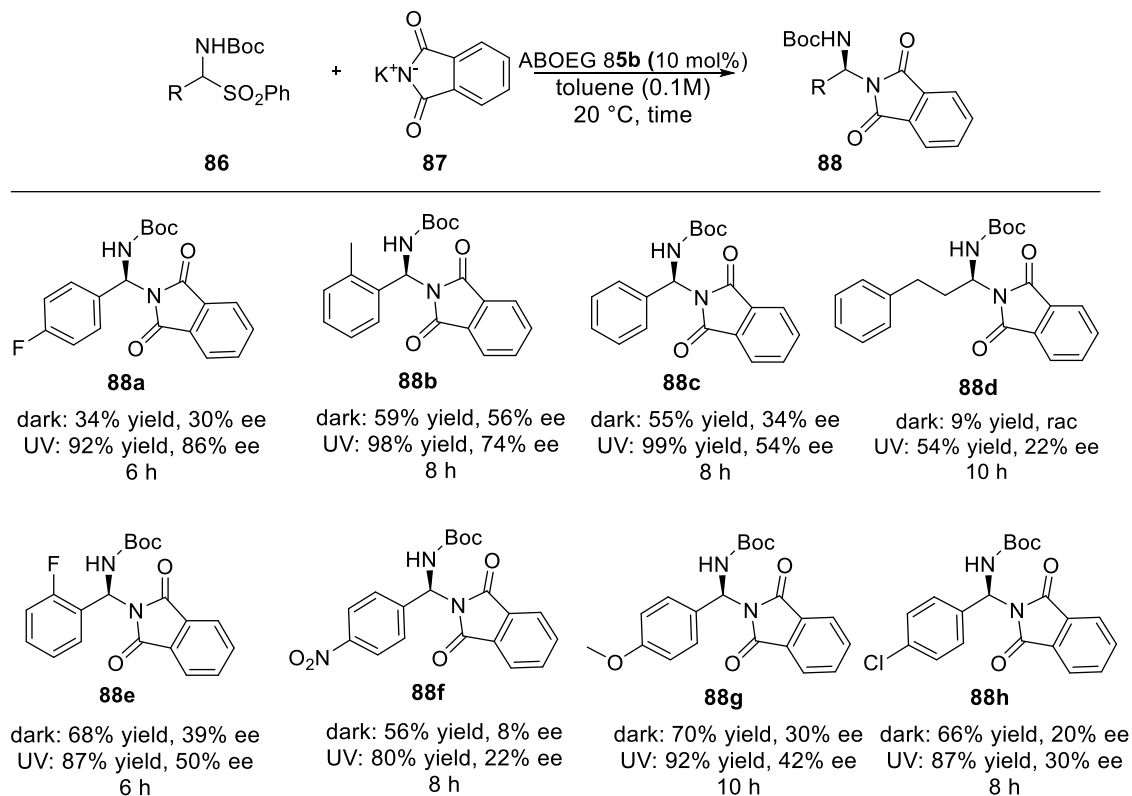


**Figure 16b.** Half-life of (Z)- **85b** was determined by <sup>1</sup>H-NMR measurement at 20 °C

## 2-9-4. Substrate scope

**Scheme 23.** Evaluation of yield and ee modulation with different  $\alpha$ -amidosulfones **86**<sup>a-h</sup>



<sup>a</sup>General reaction conditions: **86** (0.1 mmol), **87** (0.22 mmol) in toluene (0.1 M) at 20 °C. <sup>b</sup><sup>1</sup>H-NMR yield using 1,3,5-trimethoxybenzene as the internal standard.

<sup>c</sup>Determined by HPLC analysis (DAICEL Chiralpak OD-H, AS-H and IBN-5).

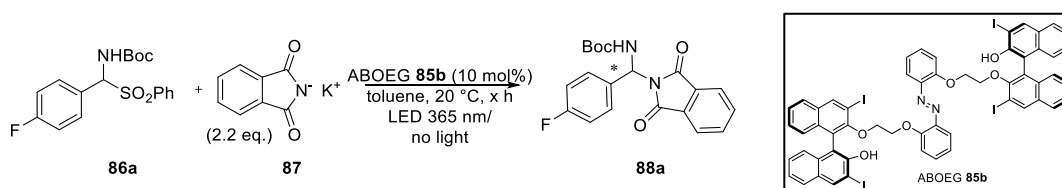
Next, I investigated the scope of our ABOEG **85b** to modulate its function towards other  $\alpha$ -amidosulfones to afford the respective aminals **88a-c**.  $\alpha$ -Amidosulfones **86b** having an *o*-Me group in the aromatic ring promoted the product **88b** formation with a significant difference in yields (98% vs. 59%) and enantioselectivities (74% vs. 56%) when carried out under 365 nm light irradiation or dark conditions for 8 h.  $\alpha$ -Amidosulfones **86c** bearing a phenyl group afforded the aminal product **88c** in good yields with a moderate enantioselectivity upon light irradiation. In dark condition, both the yield and enantioselectivity of **88c** drastically dropped. I further investigated the modulation ability of catalyst ABOEG **85b** for aliphatic substrate **86d**. The reaction rate seems to be much enhanced under 365 nm UV irradiation, when compared to that under dark conditions. Unfortunately, aminal **88d** was obtained with low enantioselectivity (22% ee) under light and in a racemic form in the absence of light. Substrate containing an ortho fluoro substituent on the aromatic ring **86e** provided aminal **88e** with moderate reactivity control (87% vs. 68%) yield as well as ee (50% vs. 39%) with and without

light. Other para-substituted amidosulfones (**86f**, **86g** and **86h**) were investigated, showed a similar trend in modulation behavior with excellent yield under UV irradiation albeit with low enantioselectivity.

### 2-9-5. Time course studies

To a flame dried test tube equipped with LED lamp (PER-AMP, Techno Sigma Co., Ltd., 365 nm) maintained at a distance of 0.5 cm away from the reaction tube were added catalyst **85** (0.01 mmol, 10 mol%) and toluene (0.1 M, 1 mL). The solution was stirred at 20 °C for 30 min under photoirradiation. Potassium phthalimide **87** (commercially available) (0.22 mmol, 2.2 eq.) was subsequently added at 20 °C and continued stirring for another 30 min. Then, starting material **86** (0.1 mmol, 1.0 eq.) was added at 20 °C. The reaction mixtures were stirred and expose to UV light during the reaction at different time intervals. After that, water was added to the reaction and the resulting solution was extracted with EtOAc. The combined organic layer was dried over Na<sub>2</sub>SO<sub>4</sub> and concentrated in *vacuo* to give crude mixture. The crude mixture was purified by silica gel column chromatography using hexane-acetone as an eluent (8/1) to provide the desired product **88a**. The reaction in dark conditions was carried out following the same procedure without photoirradiation.

**Table 9.** Time course study for enantioselective Mannich type reaction<sup>a</sup>



Entry	Light (wavelength)	Time (h)	% Yield of <b>88a</b> <sup>b</sup>	%Ee of <b>88a</b> <sup>c</sup>
1	365 nm no light	1	10	68
		1	trace	33
2	365 nm no light	3	25	70
		3	< 10	32
3	365 nm no light	4	59	82
		4	18	33
4	365 nm no light	6	92	86
		6	34	30
5	365 nm no light	12	98	84
		12	94	34

<sup>a</sup>General reaction conditions: **86a** (0.1 mmol), **87** (0.22 mmol) in toluene (0.1 M) at 20 °C for x h. <sup>b</sup><sup>1</sup>H-NMR yield using 1,3,5-trimethoxybenzene as an internal standard.

<sup>c</sup>determined by HPLC analysis (DAICEL Chiralpak OD-H)

Each reaction was set up separately and quenched after the respective time according to general procedure. Yield of **88a** was determined by  $^1\text{H-NMR}$  using 1,3,5-trimethoxybenzene as an internal standard. The enantioselectivity is determined by chiral high-performance liquid chromatography (HPLC) after purification using preparative thin-layer chromatography (TLC).

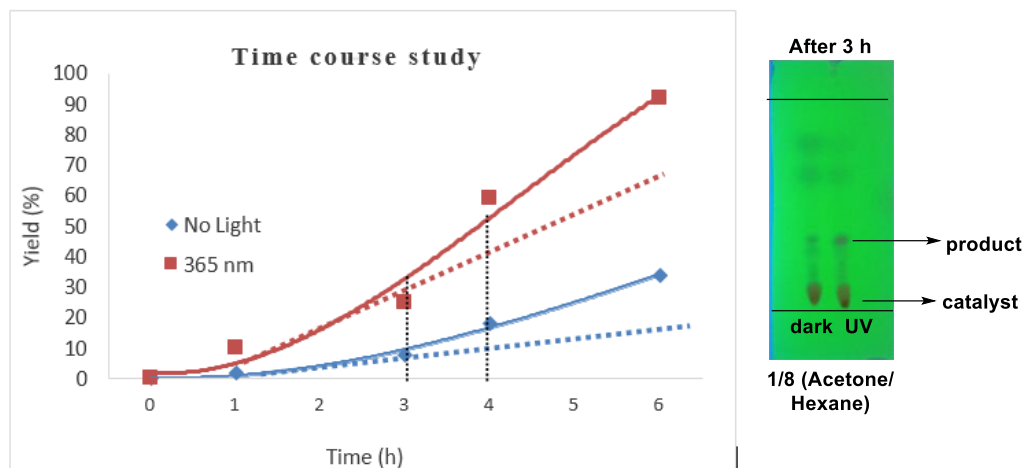


**Figure 17.** Plot of time course study with and without photoirradiation

Here, from 3 to 4 hours (Table 9, Entries 2 and 3), a drastic jump in the reaction rate under photoirradiation was observed. This enhancement may preferably due to the generation of an active species under photoirradiation. The deviation from linearity was also demonstrated by plotting the yield on y axis with respect to time on x axis (Figure 17). An induction period of initial 2 hours was observed.

#### 2-9-6. Mass spectra of ABOEG **85b**-K<sup>+</sup> complex

To further understand the complexation of ABOEG **85b** with potassium cation or other intermediates in the reaction system, mass spectra were analyzed using electron spray ionization technique (Figure 18). The detailed explanation of sample preparation method explained below.

#### Sample preparation method

A well flame dried test tube under nitrogen atmosphere, contained a magnetic stirrer bar was charged with catalyst ABOEG **85b** (0.1 eq) in toluene (0.1 M) and the solution was irradiated with 365 nm LED for 30 minutes at 20 °C maintained using a thermoflask containing water. After that, potassium phthalimide **87** (2.2 eq.) was added to the solution and stir the solution for further 30 minutes. After separation of organic layer using EtOAc as solvent and dried using Na<sub>2</sub>SO<sub>4</sub>, Crude phase was collected and subjected to ESI-MS analysis; calculated for C<sub>56</sub>H<sub>38</sub>I<sub>4</sub>N<sub>2</sub>O<sub>6</sub>K: m/z ([M+K]<sup>+</sup>) 1380.8540, found 1380.8534.

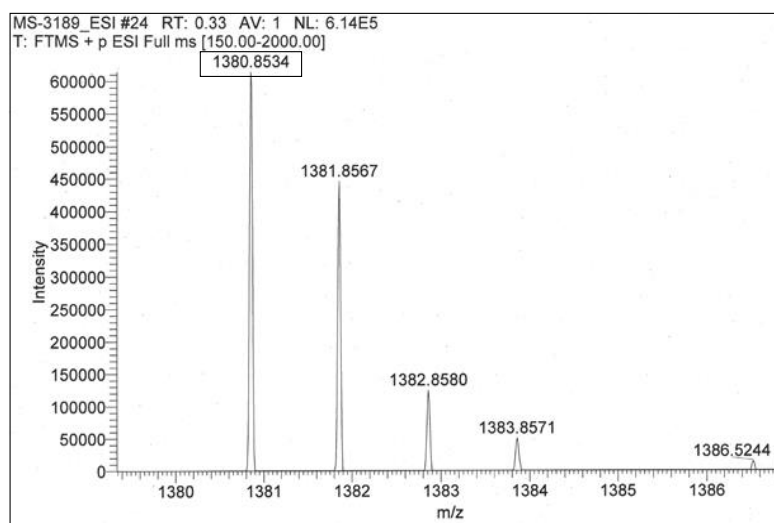
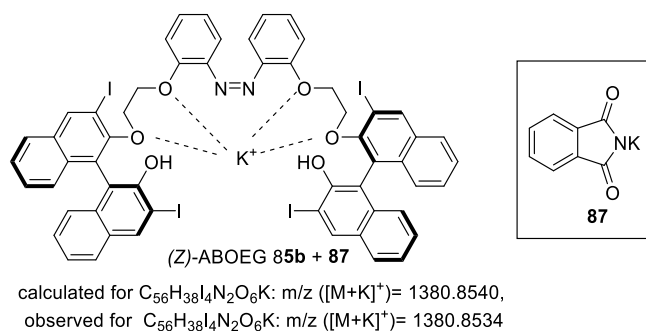


**Figure 18.** ESI-MS analysis of Z-ABOEG **85b**-K<sup>+</sup> complex

After confirming that our catalyst ABOEG **85b** is able to coordinate with K<sup>+</sup> using <sup>1</sup>H NMR studies as well as mass spectra analysis. I also carried out the control experiments to further understand the mechanism of catalyst coordination for chiral induction.

## 2-9-7. Control experiments

Initially, to understand the reactivity difference under 365 nm photoirradiation and dark, I have analyzed the crude <sup>1</sup>H NMR charts for both reactions. (Figure 19). I observed the persistence of intermediate imine generated from the starting material amidosulfone **86c** for the reaction in dark. However, there is no peak corresponds to the intermediate imine when the reaction was performed with 365 nm photoirradiation for the same reaction time (8 hours: complete conversion). This clearly indicates that the reaction is faster with photoirradiation (365 nm) compared to dark.

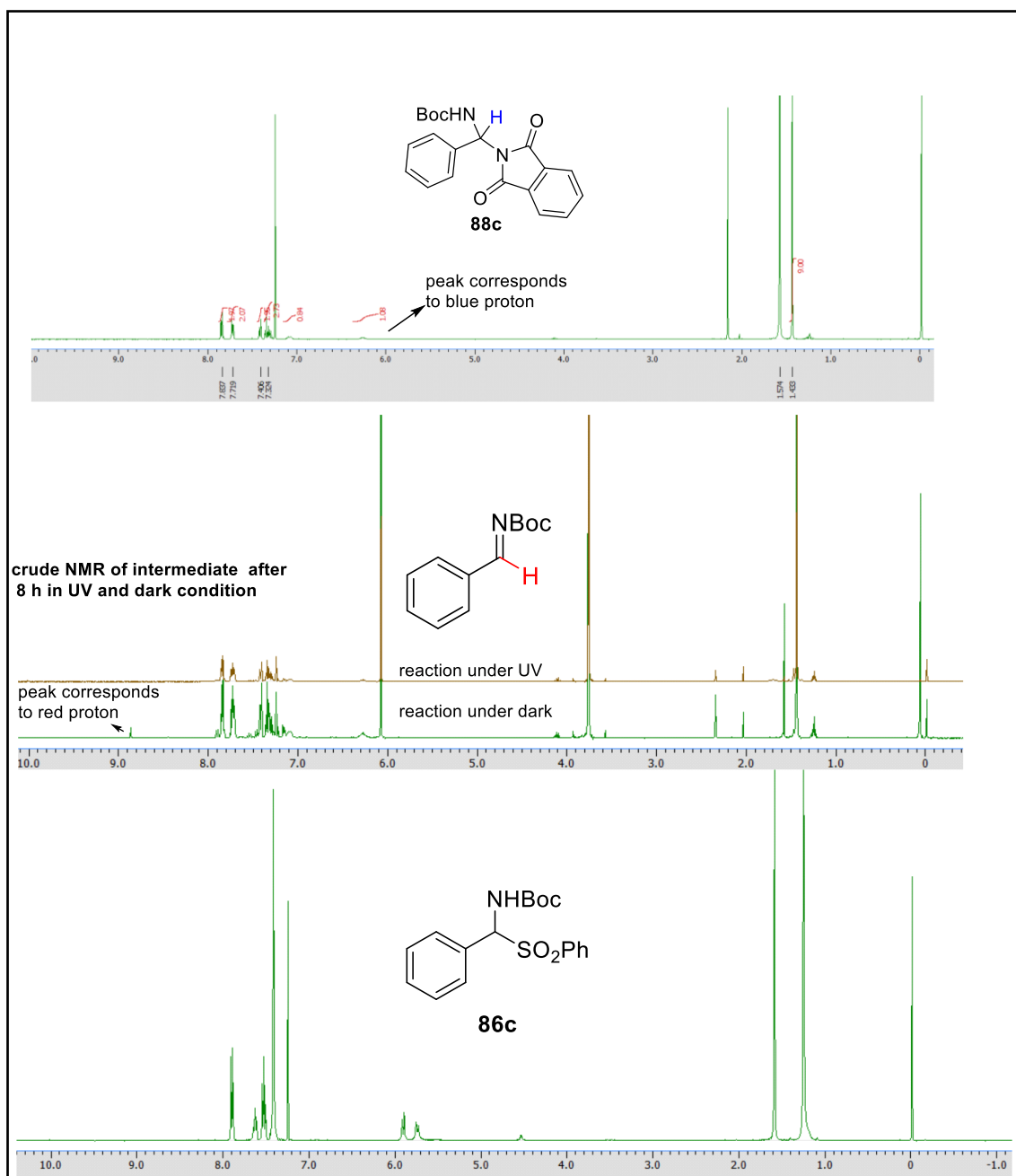
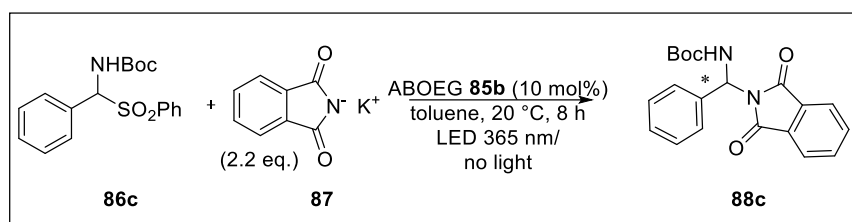
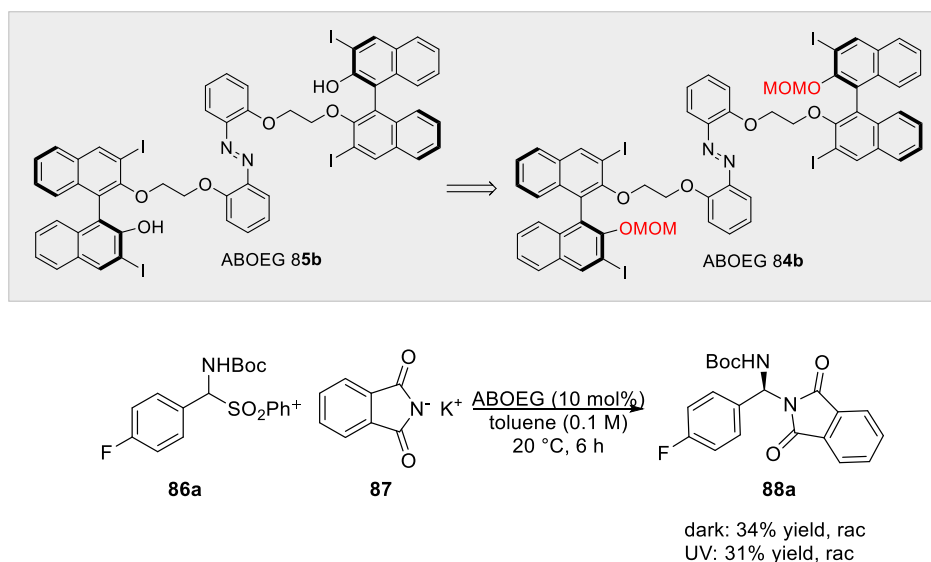


**Figure 19.** <sup>1</sup>H NMR (in CDCl<sub>3</sub>) spectrum for reactions carried with and without photoirradiation after 8 h

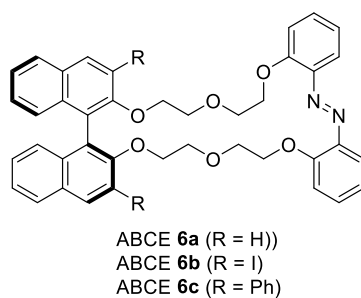
To gain further insight into the mechanism of action of ABOEG **85b** toward asymmetric induction, I focused initially to understand the role of phenolic hydrogen bonding in the catalyst. For that I have used ABOEG **84b** catalyst, whose hydroxyl groups are protected with methoxymethane (MOM) group. As shown in Scheme 24, ABOEG **84b** provided racemic product with no difference in yield with and without light.



**Scheme 24.** Effect of hydrogen bonding of catalyst

To further confirm the role of hydrogen bonding interaction, I have utilized our Azobenzene based crown ether (ABCE **89**)<sup>[26]</sup> toward this asymmetric aminalization reaction. The results are summarized in Table 10.

**Table 10.** Azobenzene based crown ether (ABCE **89**)<sup>[26]</sup> toward this asymmetric aminalization reaction.

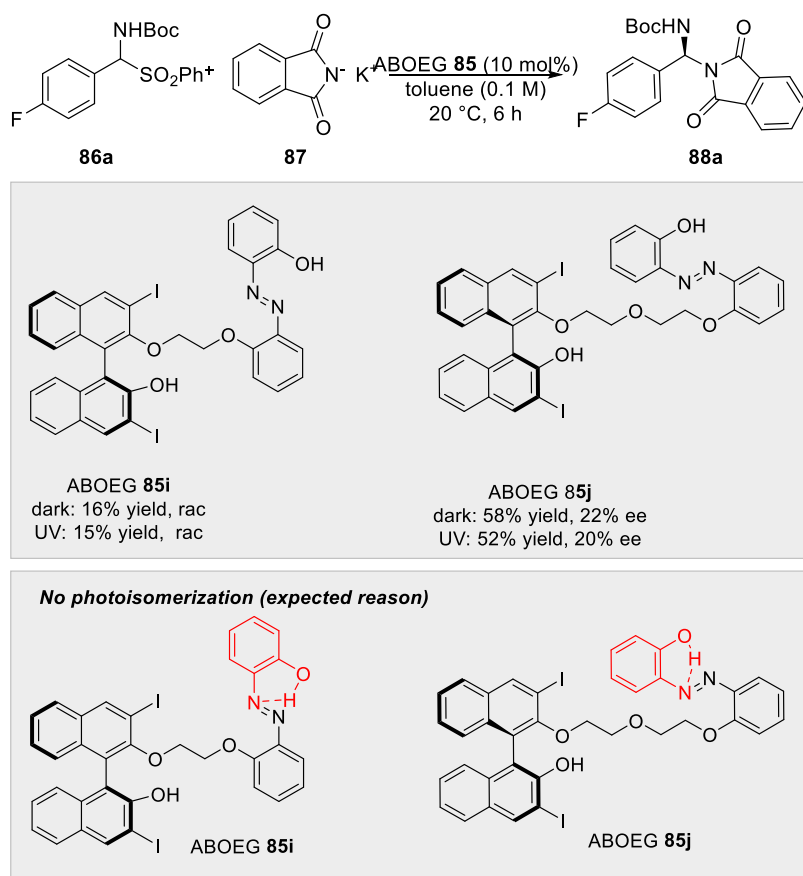


Entry	Catalyst (wavelength)	<i>E/Z</i> ratio	yield (%)	ee (%)
1	ABCE <b>89a</b> (365 nm)	12:88	60	10
2	ABCE <b>89a</b> (no light)	84:16	90	Rac
3	ABCE <b>89b</b> (365 nm)	11:89	60	10
4	ABCE <b>89b</b> (no light)	92:8	90	30
5	ABCE <b>89c</b> (365 nm)	13:87	22	Rac
6	ABCE <b>89c</b> (no light)	93:7	31	Rac



From the above control experiments using ABOEG **4b** and ABCE **6**, it is evident that phenolic hydrogen plays a crucial role in reactivity as well as enantioselectivity for this reaction.

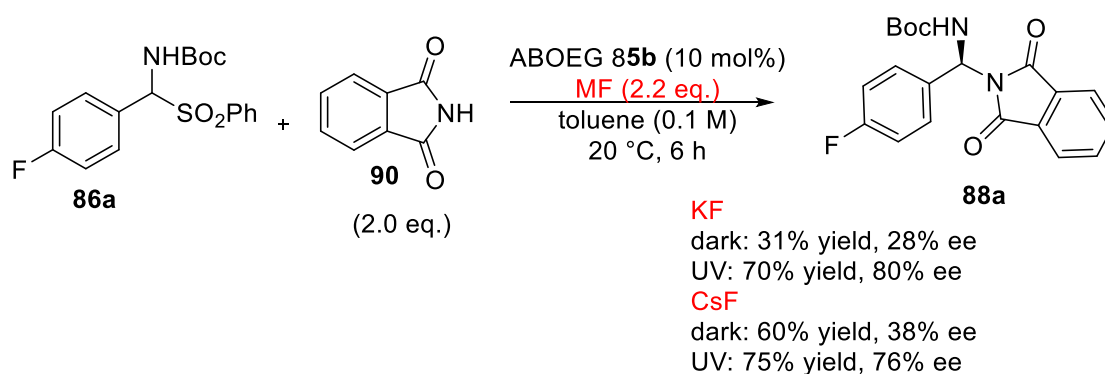
After confirming the importance of secondary interaction for enantioinduction, I have focused on the importance of two BINOL moieties in the catalyst skeleton for coordination with metal cation (Scheme 25). For that I have prepared two kinds of catalyst ABOEG **85i** and ABOEG **85j** which are different in terms of their chain length. Interestingly, ABOEG **85i** did not exhibit any enantioinduction under light and dark. However longer chain length catalyst ABOEG **85j** bearing three oxygen atoms gave very low enantioselectivity. But no modulation was observed. These two results suggest that the two BINOL moieties are important for a proper metal coordination as well as the chain length also play an important role in enantioselectivity. Another important property I have observed is the photoisomerization behavior of these two catalysts. Even though ABOEGs **85i** and **85j** bear a photoresponsive azobenzene moiety, they did not undergo photoisomerization in presence of 365 nm photoirradiation for 2 hours. The expected reason for this behavior is due to the hydrogen bonding interaction of phenolic group of azobenzene with the lone pairs on nitrogen as shown below.



**Scheme 25.** Effect of BINOL dimeric skeleton on enantioselectivity

## Effect of metal salts

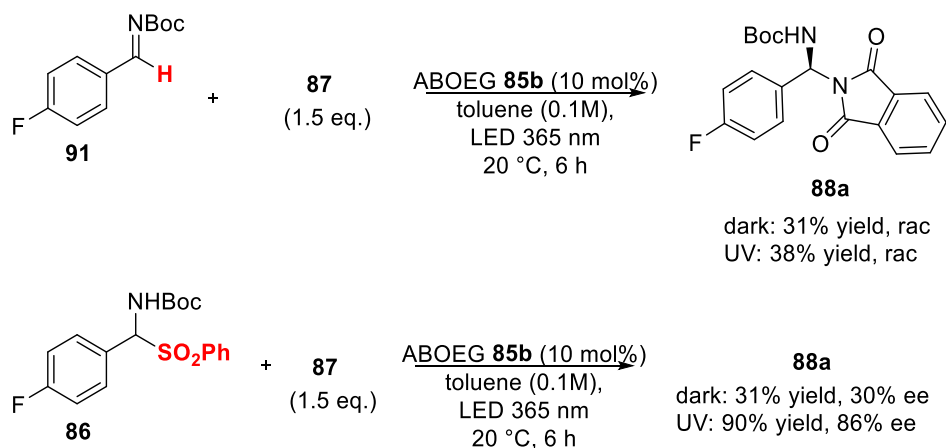
I also analyzed the effect of various metal salts for this reaction. Instead of taking directly the potassium phthalimide nucleophile **87**, I took the corresponding phthalimide **90** and *in situ* generate the potassium phthalimide by reacting with metal fluorides. Interestingly, I could achieve the same reproducibility with KF as metal salt. However, when we tried using a bigger cation like Cs, the reactivity and enantioselectivity seems to be enhanced under dark presumably due to the formation of a much suitable cation binding cage of *E*-ABOEG **85b** for Cs<sup>+</sup> than K<sup>+</sup> under dark conditions.



**Scheme 26.** Effect of metal salts

## Effect of PhSO<sub>2</sub> group

To further understand the role of sulfinate group (SO<sub>2</sub>Ph) to the selectivity, we have carried out the reaction with the intermediate imine under similar reaction conditions. The presence of the intermediate is previously confirmed by crude NMR analysis (Figure 19, section 2-9-7).

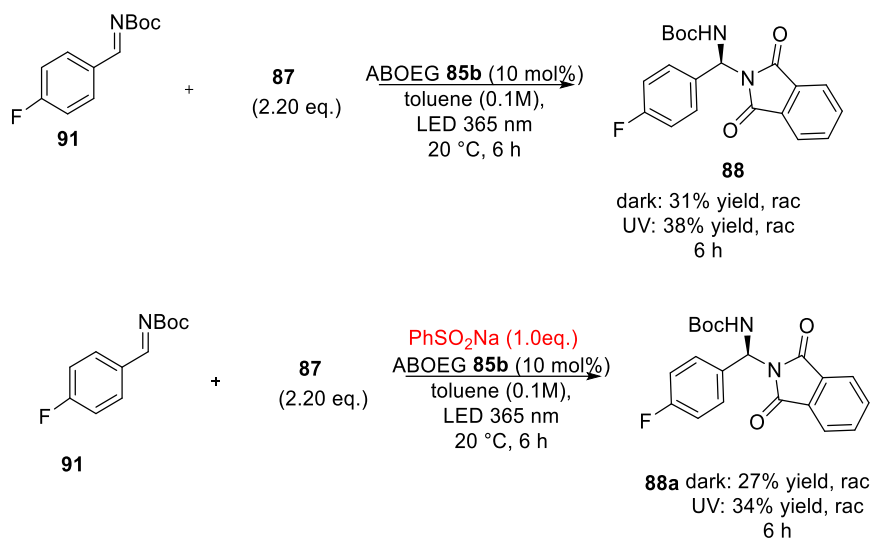


**Scheme 27.** Effect of PhSO<sub>2</sub> group

Unfortunately, I could not observe any enantioselectivity and difference in yield for aminal **88a**, which signifies the importance of SO<sub>2</sub>Ph group for enantioinduction.

### Effect of sulfinate salts (RSO<sub>2</sub>Na)<sup>[42g]</sup>

Based on the result obtained in Scheme 27, I investigated the effect of adding PhSO<sub>2</sub>Na to the reaction system. However, no noticeable improvement of enantioselectivity was observed. Even though, our control experiments with NaSO<sub>2</sub>Ph salt did not show any noticeable difference in the catalyst activity. It may affect the PSS ratio of catalyst. To understand this, we also determined the photostationary state ratio (*E/Z*) of catalyst in presence of PhSO<sub>2</sub>Na (Figure 20). Unfortunately, the obtained results are similar for that without salt.



**Scheme 28.** Effect of sulfinate salts (RSO<sub>2</sub>Na)<sup>[42g]</sup>

### analysis of sodium sulfinate salt to photostationary state ratio (*E/Z*) of ABOEG **85b**

Further, the presence of metal salts (sulfinate) can sometimes influence the isomerization kinetics due to the ion recognition. This might be positively or negatively affecting the catalyst due to the differences in terms of life time of the *Z*-isomer upon binding cations. Thus, further studies, photoisomerization and UV-Vis analysis were conducted with sodium sulfinate or potassium sulfinate salts. Based on this, I investigated the thermal isomerization of the ABOEG **85b** at 20 °C with sodium sulfinate salt. Interestingly, thermal half-life of ABOEG **85b** seems to be enhanced (25 to 34 hours) in presence of sulfinate salt (Figure 21A). UV-Vis analysis was also carried out with sodium sulfinate (Figure 21B).

In summary, we have designed a new photoswitchable chiral cation-binding catalyst utilizing azobenzene photochromic unit for the development of azobenzene based -BINOL hybrid oligoethylene glycols (ABOEGs) that can control the reactivity and enantioselectivity towards the synthesis of optically pure amins. The catalyst control has achieved through *E/Z* isomerization of the azobenzene unit. The ABOEGs showed a good reversible isomerization behavior in response to 448 nm visible light irradiation, irrespective of the coordination with metal cations. The *E/Z* photoisomerization property of the catalyst can be utilized to control the reactivity and enantioselectivity due to the distinct coordination ability with metal cations achieved under different chiral environment. Further investigations related to the mechanism and catalyst modulation behavior are in progress.

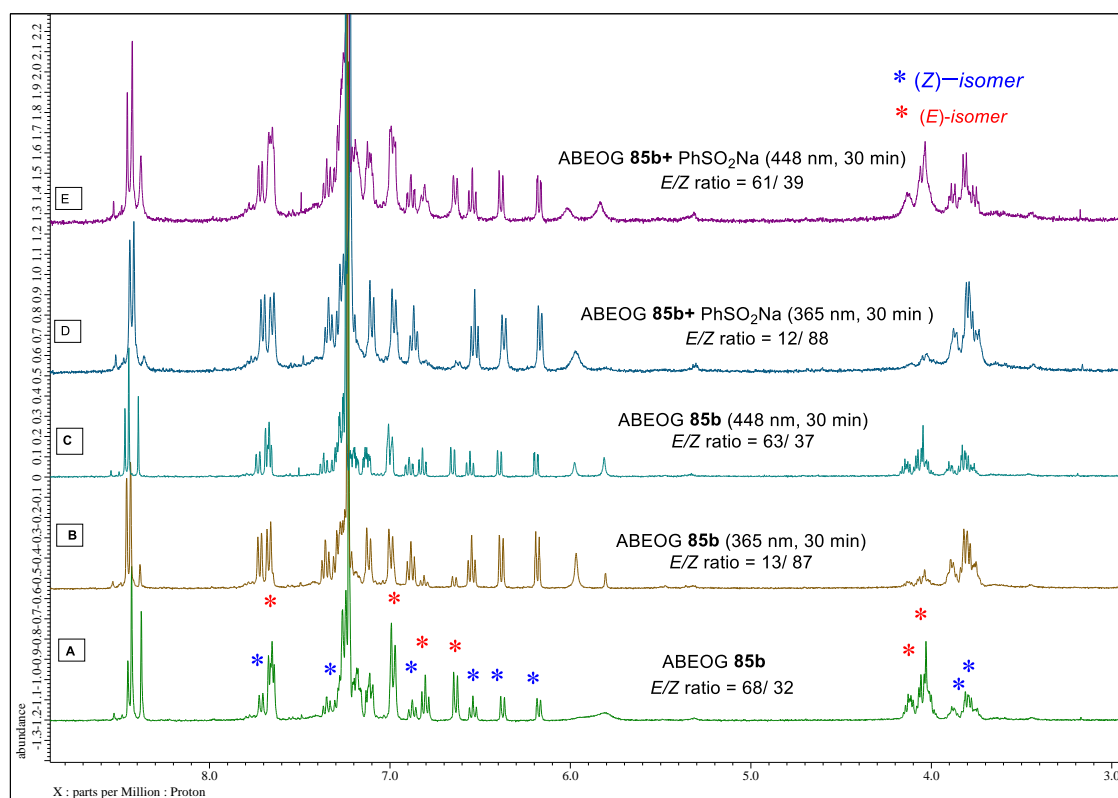


**Figure 20.** Photoisomerization studies of catalyst ABOEG **85b** with  $\text{PhSO}_2\text{Na}$ . ( $^1\text{H}$  NMR of (A) ABOEG **85b** after purification (B) ABOEG **85b** upon 365 nm UV irradiation for 30 min, (C) ABOEG **85b** upon 448 nm UV irradiation for 30 min, (D) ABOEG **85b** +  $\text{PhSO}_2\text{Na}$  (1: 5 ratio) upon 365 nm UV irradiation for 30 min and (E) ABOEG **85b** +  $\text{PhSO}_2\text{Na}$  (1: 5 ratio) upon 448 nm UV irradiation for 30 min, in  $\text{CDCl}_3$ )

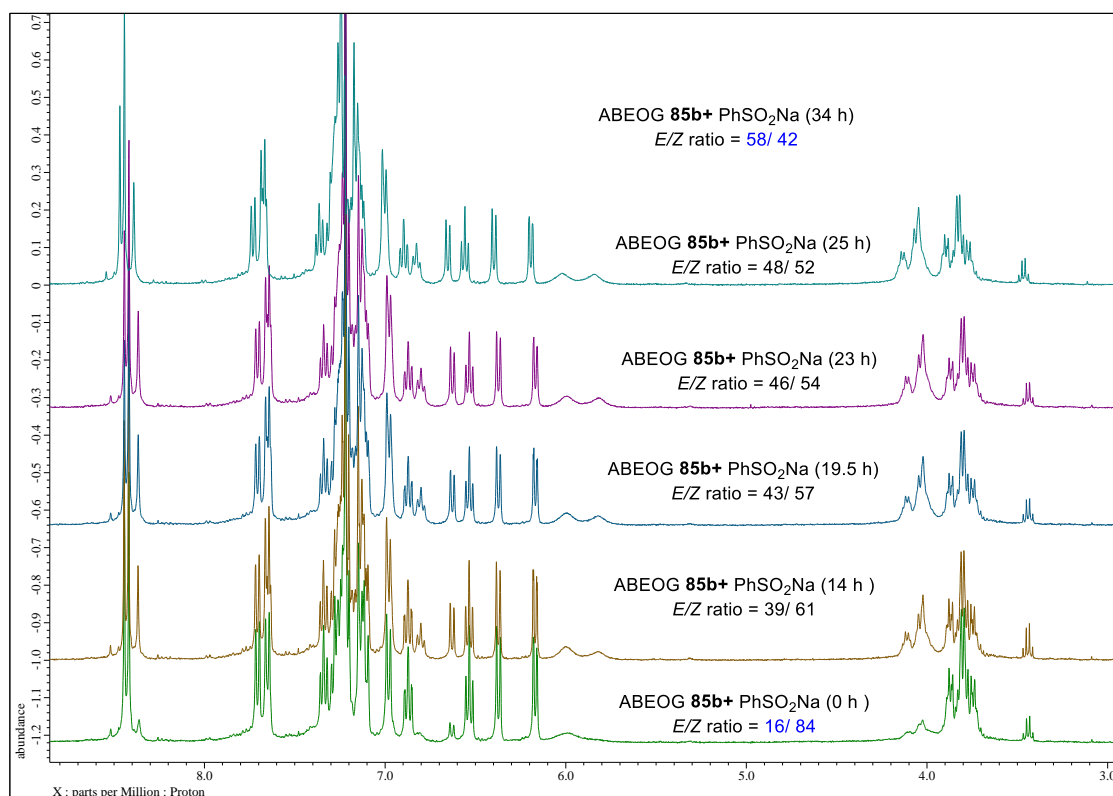


**Figure 21A.** Half-life measurement of (Z)-ABOEG **85b**+ PhSO<sub>2</sub>Na at 20 °C in CDCl<sub>3</sub> using <sup>1</sup>H NMR

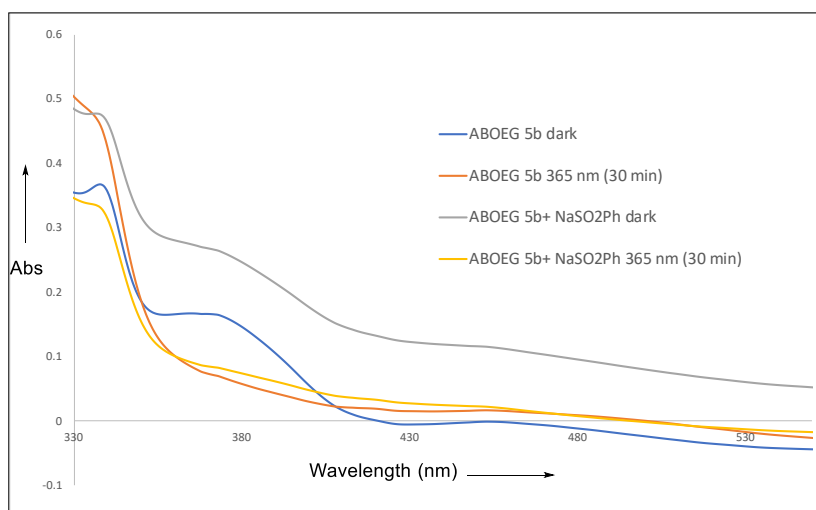


**Figure 21B.** UV-vis spectra of ABOEG **85b** with PhSO<sub>2</sub>Na (in toluene, 50 μM)

## 2-10. Experimental section

### 2-10-1. General information

$^1\text{H}$ - and  $^{13}\text{C}$ -NMR spectra were recorded with a JEOL JMN ECS400 FT NMR NMR ( $^1\text{H}$ -NMR 400 MHz,  $^{13}\text{C}$ -NMR 100 MHz).  $^1\text{H}$ -NMR spectra are reported as follows: chemical shift in ppm relative to the chemical shift of  $\text{CHCl}_3$  at 7.26 ppm, DMSO at 2.50 ppm,  $(\text{CH}_3)_2\text{CO}$  at 2.05 ppm,  $\text{CH}_3\text{OH}$  at 3.31 ppm & 4.78 ppm,  $\text{C}_6\text{H}_5\text{CD}_3$  at 2.30 ppm and 7.19 ppm, integration, multiplicities (s = singlet, d = doublet, t = triplet, q = quartet, m = multiplet), and coupling constants (Hz).  $^{13}\text{C}$ -NMR spectra reported in ppm relative to the central line of triplet for  $\text{CDCl}_3$  at 77 ppm. ESI-MS spectra were obtained with JMS-T100LC (JEOL), LTQ Orbitrap XL mass analyzer (Thermo Fischer SCIENTIFIC). HPLC analyses were performed on a JASCO HPLC system (JASCO PU 980 pump and UV-975 UV/Vis detector). UV spectra were recorded on JASCO v-770. Column chromatography on  $\text{SiO}_2$  was performed with Kanto Silica Gel 60 (40-100  $\mu\text{m}$ ). Commercially available organic and inorganic compounds were used without further purification. UV and visible light irradiations were performed with LED lamp (PER-AMP, Techno Sigma Co., Ltd.).

### 2-10-2. Reaction setup

The reaction setup is shown in Figure 22 below. The light setup consists of a self-made light source configuration, utilizing Thermo Scientific UC reactor. As shown in Figure 22, the test tube was covered with aluminum foil and the commercially available LED lamp (PER-AMP, Techno Sigma Co., Ltd.) with various wavelengths (range: 340 to 631 nm) kept at a distance of 0.5 cm from the test tube were used for photoirradiation. For the reactions to carry out under room temperature, setup was testube was immersed in water up to half length of the tube. To maintain a constant room temperature the reaction was performed in a Thermo-stainless-steel chamber. The temperature of water bath was monitored inside the chamber during the progress of experiment to check any deviations and did not exceed the room temperature (18–24  $^{\circ}\text{C}$ )

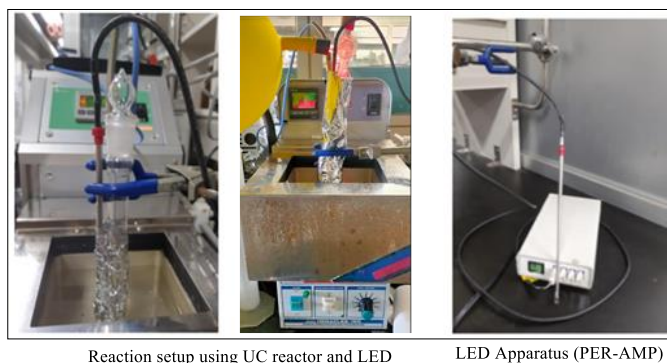
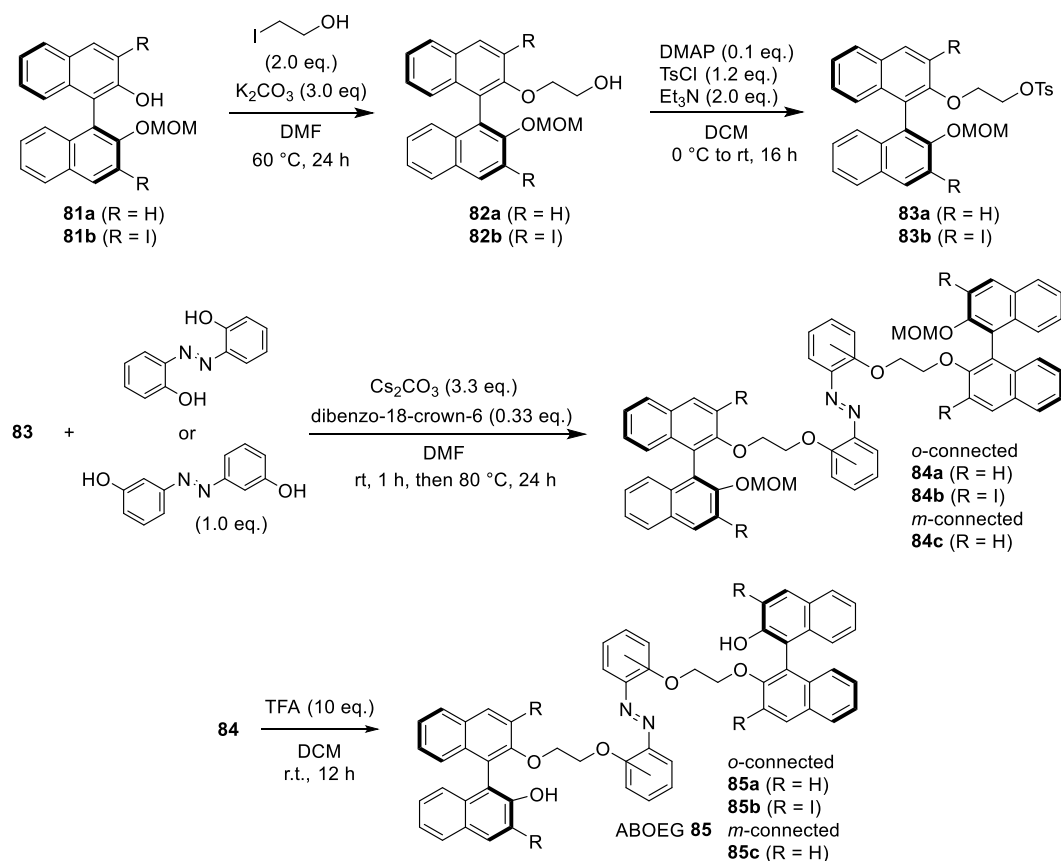


**Figure 22.** Reaction setup for photochemical reaction

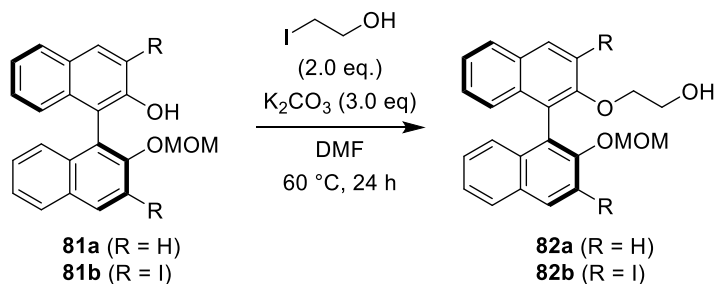
### 2-10-3. General synthesis procedure for the synthesis of ABOEG 85



**Scheme 29.** General synthesis procedure for the synthesis of azobenzene BINOL based photoswitchable oligoethylene glycol (ABOEGs)

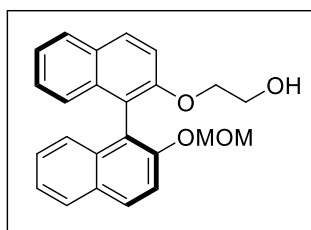
### 2-10-4. Typical synthesis procedure for the synthesis of ABOEG 85

#### General procedure for synthesis of 82<sup>[26]</sup>

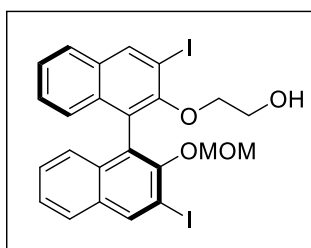


A flame dried flask under nitrogen atmosphere was charged with mono MOM protected (*S*)-BINOLs **81**<sup>[42f]</sup> (0.50 mmol, 1.0 eq.) in DMF (0.1 M, 5.0 mL),  $\text{K}_2\text{CO}_3$  (1.5 mmol, 3.0 eq.) and 2-(2-iodoethoxy)ethanol (1 mmol, 2.0 eq.) was added at room temperature. The solution was then allowed to stir at 60 °C in an oil bath for a period of 24 hours. After confirming the starting materials complete consumption on TLC analysis,

the reaction was quenched with saturated  $\text{NH}_4\text{Cl}$  aq. Then, EtOAc (20 mL) was added to the mixture and washed with brine (30 mL). The organic layer was separated, dried over  $\text{Na}_2\text{SO}_4$  and concentrated in *vacuo* to give crude mixture. The mixture was then purified by silica gel column chromatography using hexane- EtOAc (5/5) as an eluent for (*S*)- **82a**, hexane- EtOAc (7/3) to provide desired product **82**.

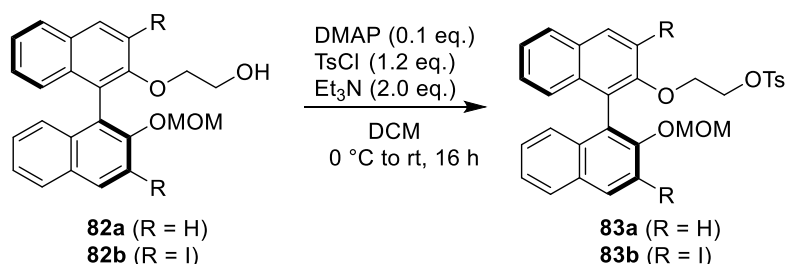


(*S*)-**82a**: 115 mg, 0.37 mmol, 62% isolated yield; yellow solid;  $^1\text{H}$ -NMR (400 MHz,  $\text{CDCl}_3$ )  $\delta$  7.99-7.88 (m, 4H), 7.57 (dd,  $J$  = 8.9 Hz, 1H), 7.39 (m,  $J$  = 8.9 Hz, 3H), 7.27-7.20 (m, 4H), 5.07 (d,  $J$  = 8.9 Hz, 1H), 4.95 (d,  $J$  = 8.4 Hz, 1H), 4.22-4.05 (m, 2H), 3.58 (d,  $J$  = 8.9 Hz, 2H), 3.08 (s, 3H), 2.22 (s, 1H);  $^{13}\text{C}$ -NMR (100 MHz,  $\text{CDCl}_3$ )  $\delta$  153.7, 152.3, 134.0, 133.7, 130.1, 129.5, 129.3, 128.0, 127.9, 126.5, 126.4, 125.3, 125.3, 124.3, 123.8, 121.7, 120.0, 117.9, 115.1, 95.7, 70.9, 61.1, 55.9; HRMS (ESI)  $m/z$   $[\text{M}+\text{Na}]^+$  Calcd for  $\text{C}_{24}\text{H}_{22}\text{O}_4\text{Na}$  397.1410; Found 397.1407. IR (KBr) 3456(br), 3054, 2934, 2825, 1558, 1493, 1444, 1221, 1156, 1074  $\text{cm}^{-1}$ ; mp: 80-83  $^\circ\text{C}$ .



(*S*)-**82b**: 198 mg, 0.31 mmol, 64% isolated yield; yellow solid;  $^1\text{H}$ -NMR (400 MHz,  $\text{CDCl}_3$ )  $\delta$  8.54 (d,  $J$  = 7.8 Hz, 2H), 7.80 (t,  $J$  = 7.8 Hz, 2H), 7.43 (t,  $J$  = 7.6 Hz, 2H), 7.33-7.26 (m, 2H), 7.15 (t,  $J$  = 7.8 Hz, 2H), 4.83 (d,  $J$  = 6.0 Hz, 1H), 4.68 (d,  $J$  = 6.0 Hz, 1H), 3.79 (s, 1H), 3.43-3.37 (m, 3H), 2.58 (s, 3H), 1.81 (s, 1H);  $^{13}\text{C}$ -NMR (100 MHz,  $\text{CDCl}_3$ )  $\delta$  153.0, 152.2, 140.6, 139.9, 134.1, 133.5, 132.3, 132.2, 127.5, 127.2, 126.9, 126.3, 126.1, 126.0, 125.9, 125.7, 125.3, 99.6, 92.5, 92.2, 74.6, 61.9, 56.6; HRMS (ESI)  $m/z$   $[\text{M}+\text{Na}]^+$  Calcd for  $\text{C}_{24}\text{H}_{20}\text{I}_2\text{O}_4\text{Na}$  648.9343; Found 648.9338. IR (KBr) 3460 (br), 3054, 2924, 2852, 2368, 1618, 1461, 1265, 1145, 1025  $\text{cm}^{-1}$ ; mp: 51-54  $^\circ\text{C}$ .

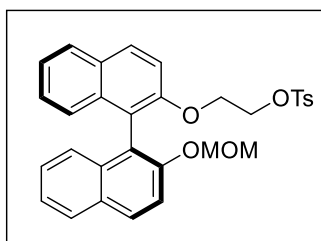
### General procedure for synthesis of **83**<sup>[26]</sup>



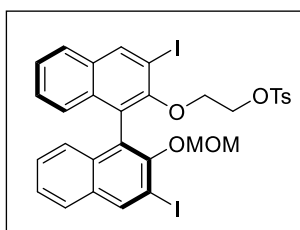
To a solution of **82** (0.42 mmol, 1.0 eq.) in DCM (0.1 M, 4.2 mL), DMAP (0.042 mmol 0.10 eq.) and  $\text{Et}_3\text{N}$  (0.84 mmol, 2.0 eq.) were added at 0  $^\circ\text{C}$  under nitrogen atmosphere. TsCl (1.2 eq.) was added to the above solution for a period of 2 min. This solution was allowed to warm up to room temperature. After being stirred for 16 h, saturated  $\text{NH}_4\text{Cl}$  aq. was added to the solution. The resulting mixture was extracted with



DCM (20 mL). The combined organic layer was dried over Na<sub>2</sub>SO<sub>4</sub> and concentrated in *vacuo* to give crude mixture. The crude mixture was purified by silica gel column chromatography using hexane-ethyl acetate (6/4) as an eluent (*S*)- **83a**, hexane- EtOAc (8/2) for (*S*)- **83b** to provide desired product **83**.

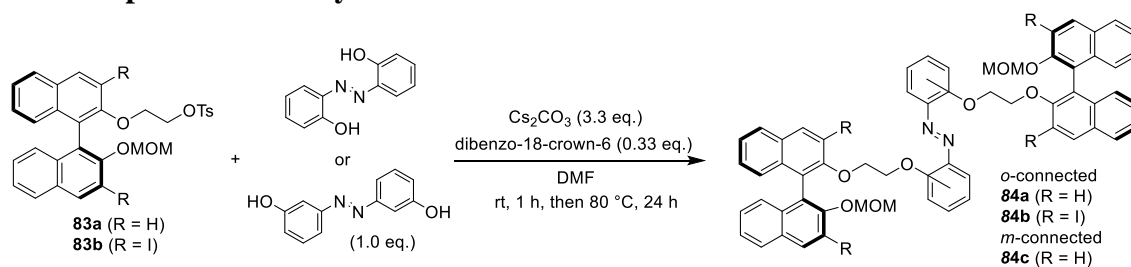


(*S*)-**83a**: 205 mg, 0.39 mmol, 92% isolated yield; yellow solid; <sup>1</sup>H-NMR (400 MHz, CDCl<sub>3</sub>) δ 8.00 (d, *J* = 8.2 Hz, 1H), 7.91-7.84 (m, 3H), 7.53-7.51 (m, 2H), 7.42-7.38 (m, 2H), 7.33-7.26 (m, 3H), 7.23-7.16 (m, 4H), 7.00 (d, *J* = 8.2 Hz, 1H), 4.93 (s, 1H), 4.17-4.09 (m, 2H), 3.99-3.96 (m, 2H), 2.40 (s, 3H); <sup>13</sup>C-NMR (100 MHz, CDCl<sub>3</sub>) δ 153.8, 152.8, 144.7, 134.1, 134.0, 132.6, 130.0, 129.9, 129.8, 129.7, 129.6, 128.0, 127.9, 126.6, 126.5, 125.7, 125.5, 124.3, 124.1, 121.5, 120.7, 117.2, 116.6, 95.3, 68.2, 67.8, 55.9, 21.7; HRMS (ESI) *m/z* [M+Na]<sup>+</sup> Calcd for C<sub>31</sub>H<sub>28</sub>O<sub>6</sub>SNa 551.1499; Found 551.1484. IR (KBr) 3587, 3521, 3303, 3060, 2961, 2924, 2374, 1923, 1624, 1509 cm<sup>-1</sup>; mp: 79-82 °C.



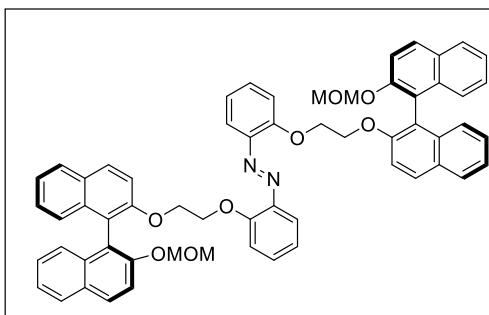
(*S*)- **83b**: 245 mg, 0.39 mmol, 94% yield; yellow solid; <sup>1</sup>H-NMR (400 MHz, CDCl<sub>3</sub>) δ 8.50 (d, *J* = 9.2 Hz, 2H), 7.78 (t, *J* = 9.2 Hz, 2H), 7.59 (d, *J* = 9.2 Hz, 2H), 7.40-7.45 (m, 2H), 7.13 (d, *J* = 8.7 Hz, 1H), 7.05 (d, *J* = 8.7 Hz, 1H), 4.79 (d, *J* = 6.0 Hz, 1H), 4.66 (d, *J* = 6.0 Hz, 1H), 2.56 (s, 3H), 2.44 (s, 3H); <sup>13</sup>C-NMR (100 MHz, CDCl<sub>3</sub>) δ 152.9, 152.0, 144.7, 140.6, 139.9, 133.9, 133.4, 132.3, 129.8, 128.0, 127.4, 127.2, 126.8, 126.4, 126.1, 125.9, 125.9, 125.7, 99.4, 92.6, 91.5, 70.1, 68.3, 56.5, 21.8; HRMS (ESI) *m/z* [M+Na]<sup>+</sup> Calcd for C<sub>31</sub>H<sub>26</sub>I<sub>2</sub>O<sub>6</sub>SNa 802.9432; Found 802.9420. IR (KBr) 3054, 2695, 2374, 2308, 1988, 1352, 1173, 922 cm<sup>-1</sup>; mp: 48-51 °C.

### General procedure for synthesis of **84**<sup>[26]</sup>

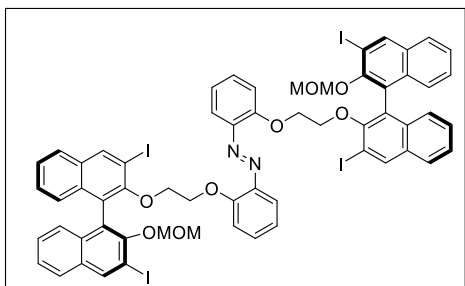


To a solution of **83** (0.28 mmol, 1.0 eq.), Cs<sub>2</sub>CO<sub>3</sub> (0.924 mmol, 3.3 eq.) and dibenzo-18-crown-6 (0.0924 mmol, 0.33 eq.) in DMF (10 mL) was added 2,2'-dihydroxyazobenzene (0.28 mmol, 1.0 eq.) or 3,3'-dihydroxyazobenzene at room temperature. The solution was stirred for 1 h under nitrogen atmosphere at room temperature and then warmed up to 70 °C in an oil bath. After 24 h, saturated NH<sub>4</sub>Cl aq. was added to the solution. The resulting mixture was extracted with EtOAc (20 mL) and washed with brine (30 mL). The combined organic layer was dried over Na<sub>2</sub>SO<sub>4</sub> and

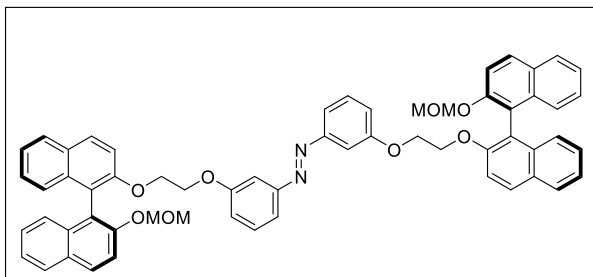
concentrated in *vacuo* to give crude mixture. The crude mixture was purified by silica gel column chromatography using hexane-ethyl acetate (6/4) for (S)-**84a** and (S)-**84c**, hexane-ethyl acetate (8/2) for (S)-**84b** as an eluent to provide **84** as orange solid with *E/Z* = 78:22 for (S)-**84a**, 88:12 for (S)-**84b**, 80:20 for (S)-**84c**. The desired product **4** was dissolved into toluene and heated at 80 °C for 1 h to achieve maximum *E/Z* = 99:1 for (S)-**84a**, 99:1 for (S)-**84b**, and 92:8 for (S)-**84a**.



(S)-**84a**: 175 mg, 0.19 mmol, 67% isolated yield; orange solid, *E/Z* = 99:1; <sup>1</sup>H-NMR (400 MHz, CDCl<sub>3</sub>) δ 7.97 (d, *J* = 9.2 Hz, 2H), 7.91 (d, *J* = 9.2 Hz, 2H), 7.86 (t, *J* = 8.2 Hz, 4H), 7.71 (dd, *J* = 8.2 Hz, 4H), 7.52 (q, *J* = 8.2 Hz, 4H), 7.34-7.32 (m, 4H), 7.21 (dd, *J* = 8.2 Hz, 2H), 7.18-7.14 (m, 5H), 6.67 (dd, *J* = 8.2 Hz, 4H), 5.05 (d, *J* = 6.9 Hz, 2H), 4.92 (d, *J* = 6.9 Hz, 2H), 4.30 (d, *J* = 8.2 Hz, 4H), 3.96 (t, *J* = 8.2 Hz, 4H), 3.11 (s, 6H); <sup>13</sup>C-NMR (100 MHz, CDCl<sub>3</sub>) δ 160.6, 154.2, 152.8, 147.1, 134.2, 134.1, 130.0, 129.8, 129.6, 129.5, 128.0, 128.0, 126.5, 126.4, 125.7, 125.5, 124.2, 124.1, 124.1, 121.5, 121.2, 117.4, 116.8, 114.8, 95.4, 68.8, 67.1, 55.9; HRMS (ESI) *m/z* [M+Na]<sup>+</sup> Calcd for C<sub>60</sub>H<sub>50</sub>N<sub>2</sub>O<sub>8</sub>Na 949.3459; Found 949.3450. IR (KBr) 3048, 2951, 2928, 2825, 1613, 1591, 1498, 1449, 1325, 1237 cm<sup>-1</sup>; mp: 92-95 °C.



(S)-**84b**: 240 mg, 0.17 mmol, 58% isolated yield; orange solid, *E/Z* = 99:1; <sup>1</sup>H-NMR (400 MHz, CDCl<sub>3</sub>) δ 8.46-8.51 (m, 2H), 8.42 (t, *J* = 7.8 Hz, 2H), 7.74 (d, *J* = 7.8 Hz, 2H), 7.66 (d, *J* = 7.8 Hz, 2H), 7.37-7.41 (m, 2H), 7.28-7.35 (m, 5H), 7.16-7.22 (m, 4H), 7.10 (t, *J* = 7.8 Hz, 5H), 6.86 (d, *J* = 7.8 Hz, 2H), 6.59-6.65 (m, 2H), 4.75-4.82 (m, 2H), 4.68 (d, *J* = 5.5 Hz, 2H), 4.08-4.12 (m, 3H), 3.90 (d, *J* = 5.5 Hz, 2H), 3.82-3.73 (2H), 3.43-3.51 (m, 1H), 2.57 (s, 6H); <sup>13</sup>C-NMR (100 MHz, CDCl<sub>3</sub>) δ 156.31, 154.5, 154.3, 152.8, 148.9, 144.3, 143.2, 134.1, 132.1, 129.9, 129.7, 129.7, 129.4, 127.9, 126.4, 126.3, 125.6, 125.5, 125.5, 124.1, 124.0, 121.3, 121.2, 121.1, 120.8, 120.5, 118.4, 117.3, 117.1, 116.5, 115.1, 112.9, 95.2, 69.2, 68.9, 68.7, 67.6, 55.9; HRMS (ESI) calcd for C<sub>60</sub>H<sub>46</sub>I<sub>4</sub>N<sub>2</sub>O<sub>8</sub>Na: *m/z* ([M+Na]<sup>+</sup>) 1452.9325, found. 1452.9329. IR (KBr) 3058, 2955, 2925, 2853, 1734, 1598, 1385, 1345, 1230, 1159 cm<sup>-1</sup>; mp: 85-88 °C.

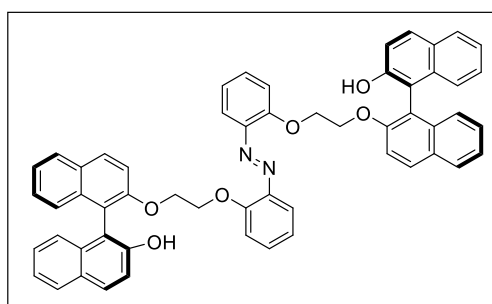
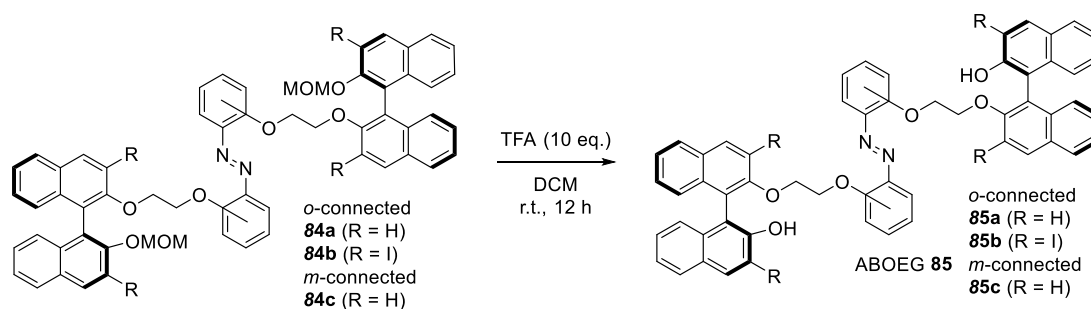


(S)-**84c**: 165 mg, 0.17 mmol, 64% isolated yield; orange solid, *E/Z* = 85:15; <sup>1</sup>H-NMR (400 MHz, CDCl<sub>3</sub>) δ 7.79-7.92 (m, 8H), 7.46-7.58 (m, 5H), 7.10-7.32 (m, 14H), 6.89 (t, *J* = 7.6 Hz, 2H), 6.66 (d, *J* = 8.2 Hz, 2H), 5.00 (d, *J*

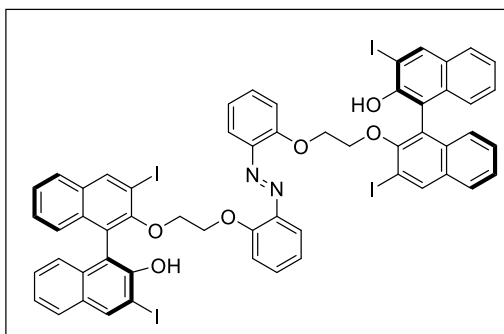
= 6.9 Hz, 2H), 4.88 (q,  $J$  = 3.5 Hz, 2H), 4.29-4.40 (m, 3H), 4.16 (m,  $J$  = 10.4, 5.2 Hz, 4H), 3.82 (t,  $J$  = 5.3 Hz, 1H), 3.06 (s, 6H).  $^{13}\text{C}$ -NMR (101 MHz,  $\text{CDCl}_3$ )  $\delta$  156.32, 154.55, 152.79, 143.28, 134.09, 132.06, 129.95, 129.76, 129.64, 129.43, 127.96, 126.36, 125.62, 125.57, 124.07, 123.98, 121.32, 121.17, 120.52, 117.43, 117.38, 117.08, 116.53, 115.23, 113.01, 95.31, 69.17, 69.07, 68.69, 55.87; HRMS (ESI)  $m/z$   $[\text{M}+\text{H}]^+$  Calcd for  $\text{C}_{60}\text{H}_{50}\text{N}_2\text{O}_8\text{Na}$  949.3459; Found 949.3447; IR (KBr) 3041, 2938, 2928, 2821, 1619, 1588, 1489, 1437, 1325, 1231  $\text{cm}^{-1}$ ; mp: 65-68  $^\circ\text{C}$ .

### General procedure for synthesis of **85**

Trifluoroacetic acid (2.3 mmol, 10 eq.) was added to a solution of **84** (0.23 mmol, 1.0 eq.) dropwise in DMF at 0  $^\circ\text{C}$ . After addition, the solution was stirred at room temperature for a period of 6 h. Then, saturated NaCl aq. was added to the solution and extracted with EtOAc (10 mL). The combined organic layer was dried over  $\text{Na}_2\text{SO}_4$  and concentrated in *vacuo* to give crude mixture. The crude mixture was purified by silica gel column chromatography using hexane-ethyl acetate (6/4) as an eluent for (*S*)-**85a** and (*S*)-**85c** and hexane-ethyl acetate (8/2) for (*S*)-**85b** to provide **85** with  $E/Z$  = 88:12 for (*S*)-**85a**, 86:14 for (*S*)-**85b**, and 90:10 for (*S*)-**85c**. The desired product **85** was dissolved into toluene and heated at 80  $^\circ\text{C}$  for 1 h to achieve maximum  $E/Z$  = 99:1 for (*S*)-**85a**, 99:1 for (*S*)-**85b**, and 95:5 for (*S*)-**85c**.

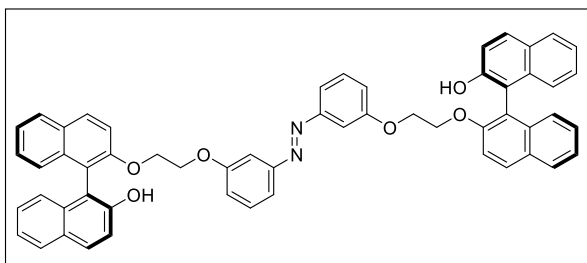


(*S*)-**85a**: 140 mg, 0.17 mmol, 72% isolated yield; orange solid;  $E/Z$  = 99:1;  $^1\text{H}$ -NMR (400 MHz,  $\text{CDCl}_3$ )  $\delta$  8.05 (d,  $J$  = 9.2 Hz, 2H), 7.83-7.93 (m, 6H), 7.73 (dd,  $J$  = 6.9, 8.2 Hz, 4H), 7.55 (d,  $J$  = 9.2 Hz, 2H), 7.40 (t,  $J$  = 6.9 Hz, 2H), 7.26-7.33 (m, 10H), 7.16-7.21 (m, 4H), 7.05 (d,  $J$  = 8.2 Hz, 2H), 6.72 (d,  $J$  = 9.2 Hz, 4H), 4.99 (s, 2H), 4.30-4.39 (m, 4H), 4.03 (t,  $J$  = 8.2 Hz, 4H);  $^{13}\text{C}$ -NMR (100 MHz,  $\text{CDCl}_3$ )  $\delta$  160.4, 155.3, 151.39, 147.20, 131.07, 130.10, 129.98, 129.19, 128.26, 127.42, 126.5, 125.3, 124.9, 124.8, 124.3, 123.3, 117.7, 117.5, 116.6, 115.1, 114.9, 68.7, 67.0; HRMS (ESI)  $m/z$   $[\text{M}+\text{Na}]^+$  Calcd for  $\text{C}_{56}\text{H}_{42}\text{N}_2\text{O}_6\text{Na}$  861.2935; Found 861.2928. IR (KBr) 3528 (br), 3057, 2956, 2930, 1913, 1619, 1596, 1460, 1380, 1147  $\text{cm}^{-1}$ ; mp: 102-105  $^\circ\text{C}$ .



(*S*)-**85b**: 223 mg, 0.17 mmol, 72% isolated yield; orange solid; *E/Z* = 99:1; <sup>1</sup>H-NMR (400 MHz, CDCl<sub>3</sub>) δ 8.45 (s, 2H), 8.39 (s, 2H), 7.67 (d, *J* = 8.2 Hz, 4H), 7.12-7.30 (m, 12H), 7.00 (d, *J* = 7.8 Hz, 4H), 6.82 (t, *J* = 7.8 Hz, 2H), 6.65 (d, *J* = 8.2 Hz, 2H), 5.83 (s, 2H), 4.01-4.14 (m, 8H); <sup>13</sup>C-NMR (100 MHz, CDCl<sub>3</sub>) δ 155.7, 154.1, 149.6, 142.8, 140.6, 139.7, 133.6, 133.4, 132.5, 131.9, 130.4,

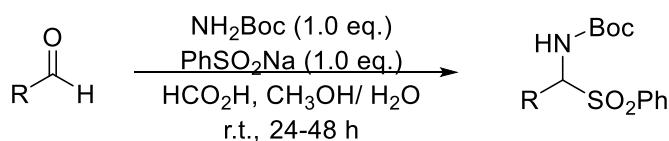
127.6, 127.5, 127.1, 127.0, 126.1, 125.2, 125.0, 124.4, 123.2, 121.2, 117.8, 115.2, 114.5, 92.6, 87.1, 71.7, 68.7; HRMS (ESI) *m/z* [M+Na]<sup>+</sup> Calcd for C<sub>56</sub>H<sub>38</sub>I<sub>4</sub>N<sub>2</sub>O<sub>6</sub>Na 1364.8801; Found 1364.8792. IR (KBr) 3476 (br), 3058, 2927, 1929, 1719, 1615, 1589, 1485, 1447, 1352 cm<sup>-1</sup>; mp: 92-95 °C.



(*S*)-**85c**: 156 mg, 0.18 mmol, 79% isolated yield; orange solid; *E/Z* = 95:5; <sup>1</sup>H-NMR (400 MHz, CDCl<sub>3</sub>) δ 7.75-7.83 (m, 8H), 7.50-7.52 (m, 2H), 7.36 (dd, *J* = 8.0 Hz, 2H), 7.11-7.31 (m, 14H), 7.02 (d, *J* = 8.0 Hz, 2H), 6.85 (t, *J* = 8.0 Hz, 2H), 6.72 (d, *J* = 8.0 Hz,

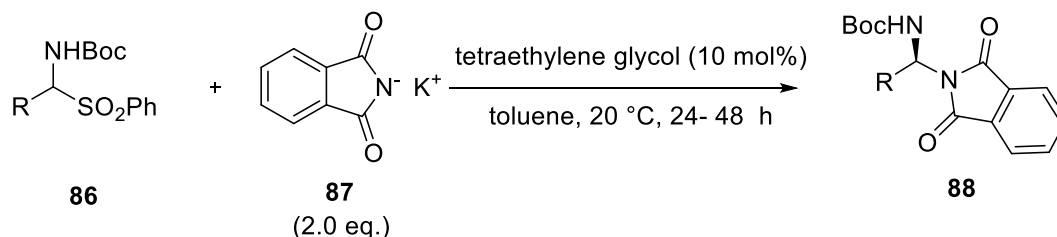
2H), 5.37 (s, 2H), 4.41-4.45 (m, 2H), 4.30-4.33 (m, 2H), 4.16 (d, *J* = 8.0 Hz, 4H); <sup>13</sup>C-NMR (100 MHz, CDCl<sub>3</sub>) δ 151.9, 132.2, 132.1, 132.0, 127.8, 126.8, 126.27, 123.8, 123.2, 122.1, 120.6, 117.0, 116.5, 114.7, 68.9; HRMS (ESI) *m/z* [M+Na]<sup>+</sup> Calcd for C<sub>56</sub>H<sub>42</sub>N<sub>2</sub>O<sub>6</sub>Na 861.2935; Found 861.2928; IR (KBr) 3513 (br), 3427, 3057, 2926, 2873, 1945, 1700, 1620, 1590, 1485 cm<sup>-1</sup>; mp: 81-83 °C.

### General procedure for the synthesis of α-amido sulfones **86**



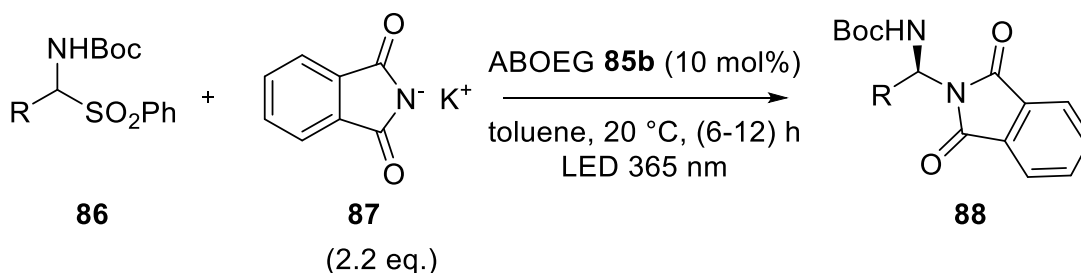
Synthesis of the α-amido sulfones **86** were carried out according to the literature procedures.<sup>[42h]</sup> Representative procedure: A flame dried 100 mL flask was charged with respective aldehyde (20 mmol), NH<sub>2</sub>Boc (20 mmol), PhSO<sub>2</sub>Na (20 mmol). Methanol (10 mL), H<sub>2</sub>O (20 mL), and HCO<sub>2</sub>H (3 mL) was added sequentially and the reaction mixture was allowed to stir at room temperature for 24–48 hours. The white precipitate was filtered from the solution, washed with distilled water (30 ml) and collected the solid by filtration in a Büchner funnel and washed with hexane/dichloromethane (10/1 mL). The solid is transferred to a flask and dried under reduced pressure. α-Amido sulfones **86a–d** are known compounds in literature.

## General procedure for the synthesis of aminoral **88**



To a flame dried round bottom flask equipped with a magnetic stirrer bar, starting material **86** (0.1 mmol, 1.0 eq.) was added at 20 °C in toluene (0.1 M, 1 mL). Potassium phthalimide **87** (commercially available) (0.2 mmol, 2.0 eq.) was subsequently added at 20 °C followed by tetraethylene glycol as achiral catalyst (0.01 mmol, 10 mol%). The reaction mixtures were stirred for 24-48 h. After completion of the reaction, water was added to the reaction and the resulting solution was extracted with EtOAc. The combined organic layer was dried over Na<sub>2</sub>SO<sub>4</sub> and concentrated in *vacuo* to give crude mixture. The crude mixture was purified by silica gel column chromatography using hexane-acetone as an eluent to provide the desired products **88**. Aminoral **88a–h** are known compounds in literature. <sup>[42h]</sup>

## 2-10-5. General procedure for the ABOEG **85b** catalyzed enantioselective Mannich type reaction



### Experimental procedure:

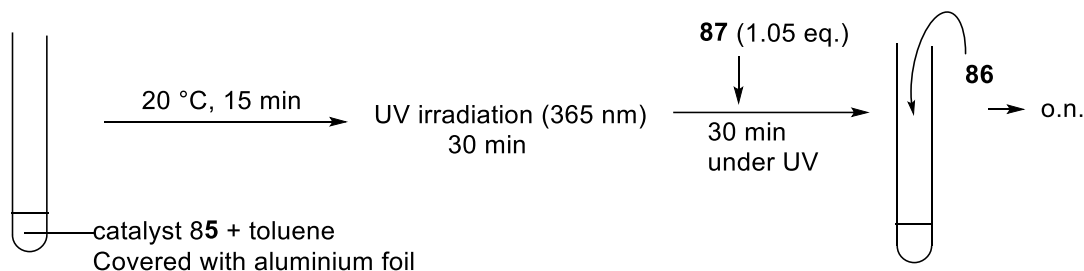
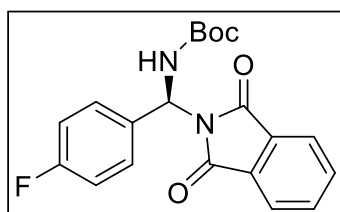




**Figure 23.** Reaction setting with LED (left), apparatus (PER-AMP) (middle), and the color change observed after reaction under dark and UV.

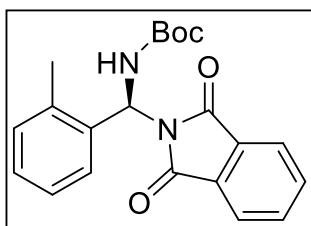
To a flame dried test tube equipped with LED lamp (PER-AMP, Techno Sigma Co., Ltd., 365 nm) maintained at a distance of 0.5 cm away from the reaction tube were added catalyst **85** (0.01 mmol, 10 mol%) and toluene (0.1 M, 1 mL). The solution was stirred at 20 °C for 30 min under photoirradiation. Potassium phthalimide **87** (commercially available) (0.22 mmol, 2.2 eq.) was subsequently added at 20 °C and continued stirring for another 30 min. Then, starting material **86** (0.1 mmol, 1.0 eq.) was added at 20 °C. The reaction mixtures were stirred and expose to UV light during the reaction. After completion of the reaction, water was added to the reaction and the resulting solution was extracted with EtOAc. The combined organic layer was dried over Na<sub>2</sub>SO<sub>4</sub> and concentrated in *vacuo* to give crude mixture. The crude mixture was purified by silica gel column chromatography using hexane-acetone as an eluent (8/1) to provide the desired product **88**. The reaction in dark conditions was carried out following the same procedure without photoirradiation.

#### 2-10-6. NMR and Mass data

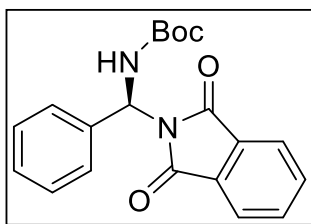


(*S*)-**88a**: White solid, 0.09 mmol, 33 mg, 90% isolated yield, 86% ee under UV; <sup>1</sup>H NMR (400 MHz, CDCl<sub>3</sub>): δ 7.89–7.84 (m, 2H), 7.78–7.72 (m, 2H), 7.46–7.39 (m, 2H), 7.12–7.00 (m, 3H), 6.27 (d, *J* = 7.3 Hz, 1H), 1.45 (s, 9H); HRMS (ESI) *m/z* [M+Na]<sup>+</sup> Calcd for C<sub>20</sub>H<sub>19</sub>FN<sub>2</sub>O<sub>4</sub>Na 393.1221; Found 393.1221; HPLC (OD-H, *n*-hexane/*i*-

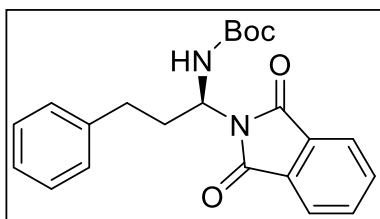
PrOH = 20:1), flow rate = 1.0 mL/min, I = 220 nm), tR = 9.7min (major), tR = 11.2 min (minor). <sup>[42h]</sup>



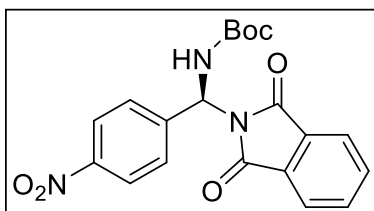
(*S*)-**88b**: White solid, 0.093 mmol, 34 mg, 93% isolated yield, 74% ee under UV;  $^1\text{H}$  NMR (400 MHz,  $\text{CDCl}_3$ ):  $\delta$  1.45 (s, 9H), 2.49 (s, 3H), 6.12 (s, broad, 1H), 7.19–7.21 (m, 4H), 7.54 (d,  $J$  = 7.3 Hz, 1H), 7.70–7.74 (m, 2H), 7.83–7.87 (m, 2H); HRMS (ESI)  $m/z$   $[\text{M}+\text{Na}]^+$  Calcd for  $\text{C}_{21}\text{H}_{22}\text{N}_2\text{O}_4\text{Na}$  389.1472; Found 389.1472; HPLC (OD-H, *n*-hexane/*i*-PrOH = 20:1), flow rate: 1.0 mL/min,  $I$  = 220 nm),  $t_R$  = 14.7 min (major),  $t_R$  = 8.6 min (minor). <sup>[42h]</sup>



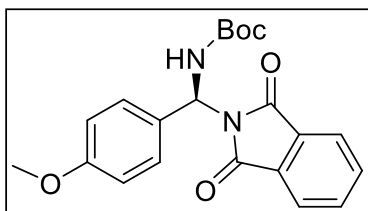
(*S*)-**88c**: White solid, 0.09 mmol, 35 mg, 90% isolated yield, 54% ee under UV;  $^1\text{H}$  NMR (400MHz,  $\text{CDCl}_3$ ):  $\delta$  7.89–7.83 (m, 2H), 7.76–7.70 (m, 2H), 7.43 (d,  $J$  = 7.3 Hz, 2H), 7.39–7.28 (m, 3H), 7.10 (d,  $J$  = 7.3Hz, 1H), 6.26 (s, broad, 1H), 1.45 (s, 9H); HRMS (ESI)  $m/z$   $[\text{M}+\text{Na}]^+$  Calcd for  $\text{C}_{20}\text{H}_{20}\text{N}_2\text{O}_4\text{Na}$  375.1315; Found 375.1319; HPLC (AS-H, *n*-hexane/*i*-PrOH = 9:1, flow rate = 1.0 mL/min,  $I$  = 220 nm),  $t_R$  = 8.6 min (minor). <sup>[42h]</sup>



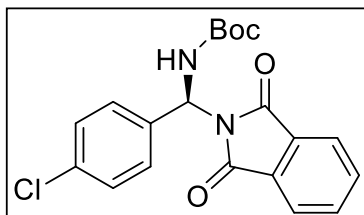
(*S*)-**88d**: White solid, 0.047 mmol, 18 mg, 47% isolated yield, 22% ee under UV;  $^1\text{H}$  NMR (400 MHz,  $\text{CDCl}_3$ ):  $\delta$  7.80 (dd,  $J$  = 5.4, 3.0 Hz, 2H), 7.70 (dd,  $J$  = 5.4, 3.0 Hz, 2H), 7.20 (t,  $J$  = 7.3Hz, 2H), 7.14 (d,  $J$  = 7.3 Hz, 2H), 7.09 (t,  $J$  = 7.3 Hz, 1H), 5.97 (s, 1H), 5.74 (s, 1H), 2.82–2.73 (m, 1H), 2.67–2.57 (m, 1H), 2.43–2.26 (m, 2H), 1.41 (s, 9H); HRMS (ESI)  $m/z$   $[\text{M}+\text{Na}]^+$  Calcd for  $\text{C}_{22}\text{H}_{24}\text{N}_2\text{O}_4\text{Na}$  403.1628; Found 403.1629; HPLC (OD-H, *n*-hexane/*i*-PrOH = 93:7, flow rate = 1.0 mL/min,  $I$  = 230 nm),  $t_R$  = 15.0 min (minor),  $t_R$  = 19.5 min (major). <sup>[42h]</sup>



(*S*)-**88f**: White solid; 0.076 mmol, 30 mg, 76% isolated yield, 21% ee under UV;  $^1\text{H}$ -NMR (400 MHz,  $\text{CDCl}_3$ )  $\delta$  8.22 (d,  $J$  = 8.7 Hz, 2H), 7.86–7.90 (m, 2H), 7.75–7.81 (m, 2H), 7.61 (d,  $J$  = 7.7 Hz, 2H), 7.19 (s, 1H), 6.49–6.18 (1H), 1.47 (s, 9H); HRMS (ESI)  $m/z$   $[\text{M}+\text{Na}]^+$  Calcd for  $\text{C}_{22}\text{H}_{24}\text{N}_2\text{O}_4\text{Na}$  420.1166; Found 420.1158; HPLC (IBN-5, *n*-hexane/*i*-PrOH = 10:1, flow rate = 0.5 mL/min,  $I$  = 230 nm),  $t_R$  = 43.2 min (major),  $t_R$  = 87.7 min (minor).

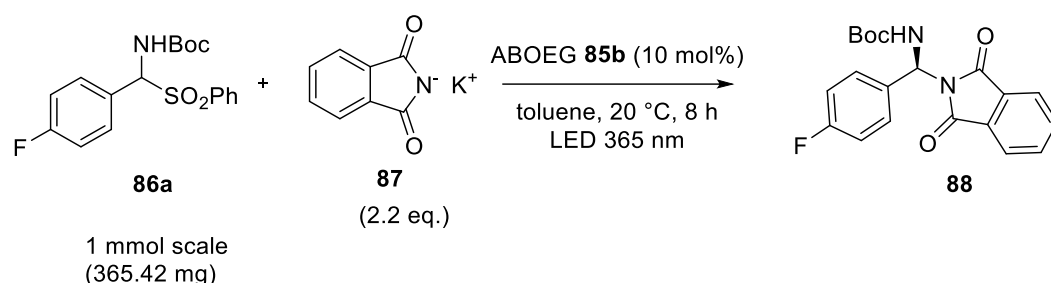


(*S*)-**88g**: White solid; 0.086 mmol, 33 mg, 86% isolated yield, 42% ee under UV;  $^1\text{H}$  NMR (400 MHz,  $\text{CDCl}_3$ ):  $\delta$  7.28 (d,  $J$  = 8.7 Hz, 2H), 6.70–6.88 (m, 5H), 6.15 (s, broad, 1H), 3.78 (s, 3H), 1.45 (s, 9H); HRMS (ESI)  $m/z$   $[\text{M}+\text{Na}]^+$  Calcd for  $\text{C}_{21}\text{H}_{22}\text{N}_2\text{O}_5\text{Na}$  405.1421; Found 405.1418; HPLC (AS-H, *n*-hexane/*i*-PrOH = 10:1, flow rate = 1.0 mL/min,  $I$  = 230 nm),  $t_R$  = 14.3 min (minor),  $t_R$  = 19.1 min (major).



(*S*)-**88h**: White solid; 0.082 mmol, 31 mg, 82% isolated yield, 30% ee under UV  $^1\text{H}$  NMR (400 MHz,  $\text{CDCl}_3$ ):  $\delta$  7.87–7.81 (m, 2H), 7.75–7.69 (m, 2H), 7.35 (d,  $J$  = 8.6 Hz, 2H), 7.29 (d,  $J$  = 7.6 Hz, 2H), 7.04 (d,  $J$  = 9.8 Hz, 1H), 6.24 (s, broad, 1H), 1.43 (s, 9H); HRMS (ESI)  $m/z$   $[\text{M}+\text{Na}]^+$  Calcd for  $\text{C}_{20}\text{H}_{19}\text{ClN}_2\text{O}_4\text{Na}$  409.0926; Found 409.0920; HPLC (AS-H, *n*-hexane/*i*-PrOH = 10:1, flow rate = 1.0 mL/min,  $\lambda$  = 230 nm),  $t_R$  = 13.1 min (major),  $t_R$  = 17.2 min (minor).

**Scheme 30. Representative procedure for enantioselective Mannich type reaction with **86a** (1 mmol) with **8** catalyzed by ABOEG **85b**.**



To a flame dried test tube with a stirrer bar, placed an LED lamp (PER-AMP, Techno Sigma Co., Ltd.) of 365 nm wavelength kept at a distance of 0.5 cm away from the reaction tube were added with catalyst **85** (136.4 mg, 0.1 mmol, 10 mol%) and toluene (0.1 M, 10 mL). The solution was stirred at 20 °C for 30 min under photoirradiation. Potassium phthalimide **87** (commercially available) (407 mg, 2.2 mmol, 2.2 eq.) was subsequently added at 20 °C and continued stirring for another 30 min. Then, starting material **86** (365.4 mg, 1 mmol, 1.0 eq.) was added at 20 °C. The reaction mixtures were stirred and expose to UV light during the reaction. After completion of the reaction, water was added to the reaction and the resulting solution was extracted with EtOAc. The combined organic layer was dried over  $\text{Na}_2\text{SO}_4$  and concentrated in *vacuo* to give crude mixture. The crude mixture was purified by silica gel column chromatography using hexane-acetone as an eluent (8/1) to provide the desired product **88** (320 mg, 0.86 mmol) with 84% isolated yield with 78% ee. The reaction in dark conditions was carried out following the same procedure without photoirradiation provided **88** (145 mg, 0.39 mmol) 39% isolated yield with 34% ee.



## Chapter 3: Photoswitchable dithienylethene based phosphoric acid catalyst: Photocontrol of catalytic activity on enantioselective aza-Friedel Craft reaction

### 3-1. Introduction: Diarylethene photochromic unit

Dithienylethenes (DTEs), more generally diarylethenes (DAE) are a rare class of photochromic molecules, which are able to undergo a  $6\pi$ -photochemical electrocyclization. The main features are that the rapid, reversible, and thermally forbidden characteristics. As a result, they are ideal scaffold for designing catalysts that can be modulated on demand with various impulses of light of different wavelength. Dithienylethenes, a sub classification of DAE were discovered by Irie and co-workers about a quarter-century ago. They explored them in the design of molecular switches.<sup>[44,45]</sup> The dithienylethene skeleton bears two thiophene groups are attached to a cyclopentene moiety at their 3-positions, which can then undergo light induced electrocyclization as shown in Figure 24.<sup>[46]</sup> However, DTEs are classified as P-type molecules which is only able to undergo reverse isomerization in presence of light. This makes them a special moiety setting them apart from the general T-type moieties which are thermally reversible like azobenzene and spiropyran units. But these T-types moieties are spontaneously isomerizing which makes them difficult to control the PSS ratio. By choosing an appropriate wavelength of light, DTE based molecules can be photochemically toggled between an open state and closed state (1c) that can have entirely different steric and electronic properties.<sup>[47]</sup>

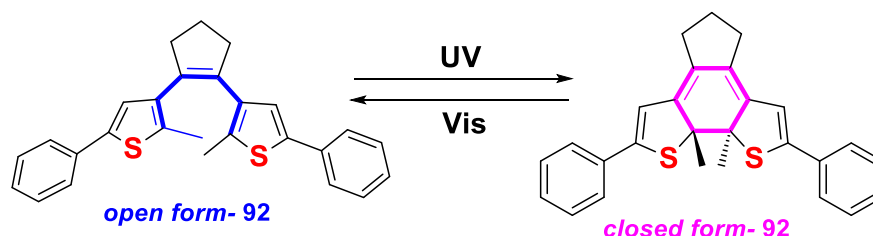


**Figure 24.** Photoisomerization behavior of dithienylethene moiety

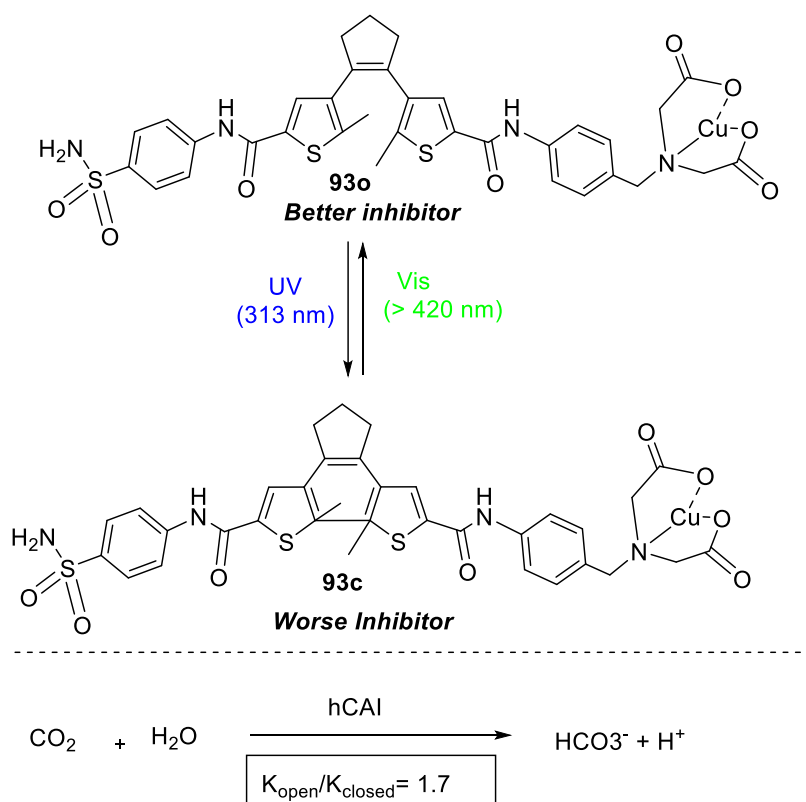
The two thiophenes lacks bond communication between each other in its ring-open form, and are therefore electronically isolated.<sup>[48]</sup> On the other hand, the ring-closed isomer of DTE shows an extensive conjugation, resulting in entirely distinct steric and electronic properties; this provides an excellent opportunity to use this photochromic unit for designing photoswitchable catalytic systems with switch ON/OFF capabilities by deeply affecting the performance of ligands which mainly depends on the electron density at their binding sites.

### 3-2. Dithienylskeleton towards achiral metal catalysis

The design of metal catalyst based on DTE scaffold can be achieved by attachment of metal-coordinating moieties to the 2 and 5 positions of the thiophenes framework. Another way is to attach the chelation sites to the central core of the

molecule to utilize geometric differences between the open and closed isomers to affect chelation and thus providing different catalyst behavior.

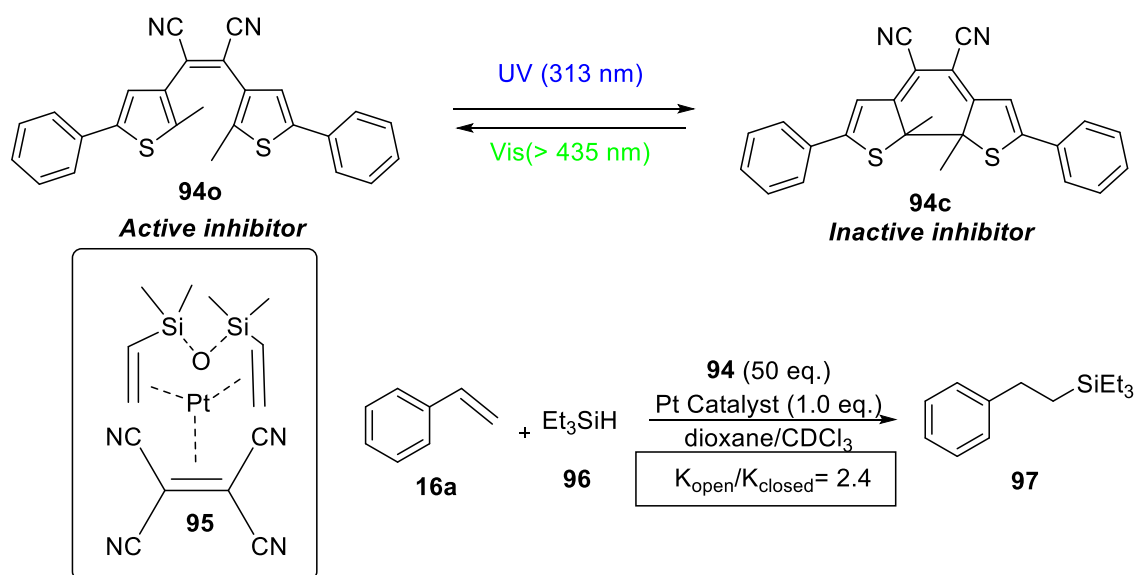
Branda and König groups developed a metal photoswitchable system, in which the DTE based skeleton can inhibit the action of one of the well accelerated homogeneous catalysts like human carbonic anhydrase I (hCAI).<sup>[49]</sup> They have achieved this by incorporating sulfonamide moiety on one end of a DTE skeleton and copper (II) iminodiacetate on the other end (Scheme 31), which aid to develop a reversible molecular switch that can controls hCAI activity. The flexible open isomer **93o** can efficiently deliver both the inhibitory sulfonamide group to the active site, as well as the reversible binding of copper (II) iminodiacetate to histidine residues near the Zn (II) catalytic center happens simultaneously. However, the ring-closed rigid isomer **93c** allows only one of two groups (sulfonamide group and copper (II) iminodiacetate) to bind at a time. As a result, the two moieties stay away from each other and which reduces the inhibition capability. With this DTE skeleton, a PSS ratio of 99% closed isomer **93c** is achieved in just only 34 s with 313 nm wavelength of UV light.



**Scheme 31.** Regulation of hCAI by a DTE-based inhibitor<sup>[49]</sup>

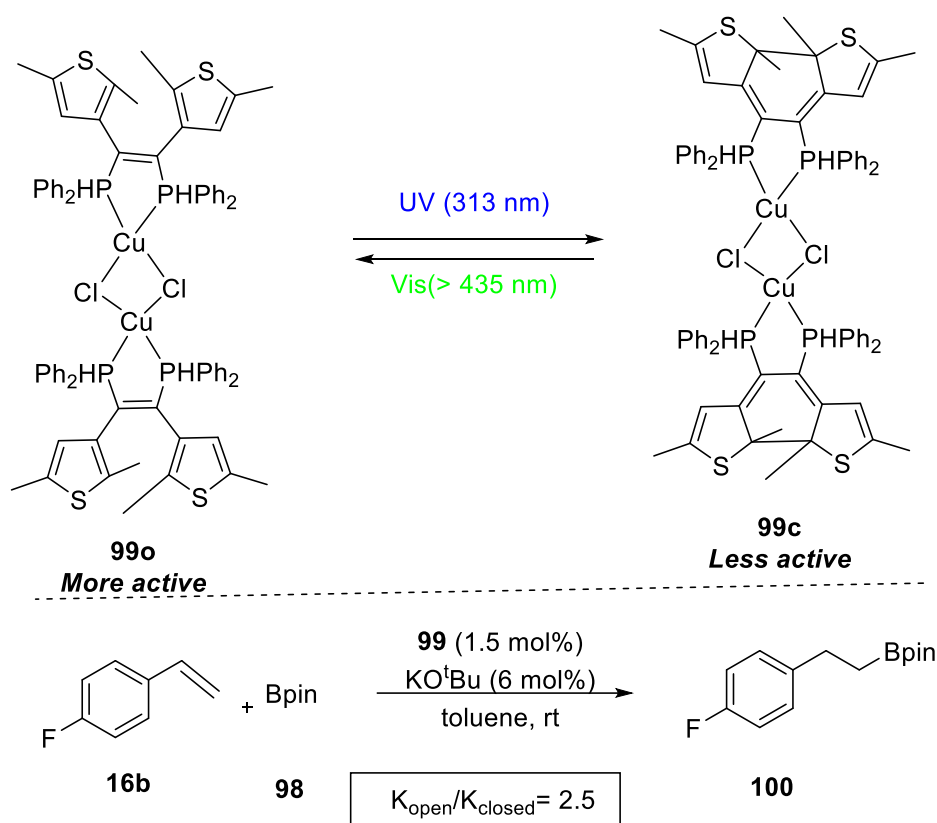
Another similar approach led to the development of another simple unique DTE architecture replacing cyclopentene moiety with alkene cyano groups and utilized that system containing two thiophene junctions for the light modulated inhibition of Karstedt's catalyst (Scheme 32).<sup>[50]</sup> Tetracyanoethelene molecule (TCNE) **95**, an electron poor alkene results in the complex formation with Platinum center as well as

alkene stalling material, thereby interfering the catalysis.<sup>[51,52]</sup> The open form of DTE **94o** having an electron poor alkene group behaved as a Pt inhibitor, while the closed form **94c** did not exhibit inhibition behavior due to distinct electronic structure. A photostationary state ratio of 51% of closed isomer is achieved after 313 nm irradiation for 2 minutes.



**Scheme 32.** Photochromic inhibition of Karstedt's catalyst<sup>[50]</sup>

Wolf and co-workers developed DAE-based phosphine ligands<sup>[53]</sup> which are different from the five membered cyclopentene based skeleton; they capped it by metal centers instead of common five-membered cyclopentene ring system as shown in Scheme 33. The ligand **99o** as the open form for the hydroboration reaction of styrene **16b** with Bpin (pinacolborane) **98** in the presence of K<sup>t</sup>Bu. The reaction rate was 2.5 times faster in comparison with that of the closed form. Probably because the electron density at the metal center which is reduced in the closed isomer due to extended conjugation, slowed down the hydroboration reaction. Although the PSS ratio of this ligand is less than 50%, it can be improved upon varying the substituents, solvents or choosing dynamic range of wavelengths.

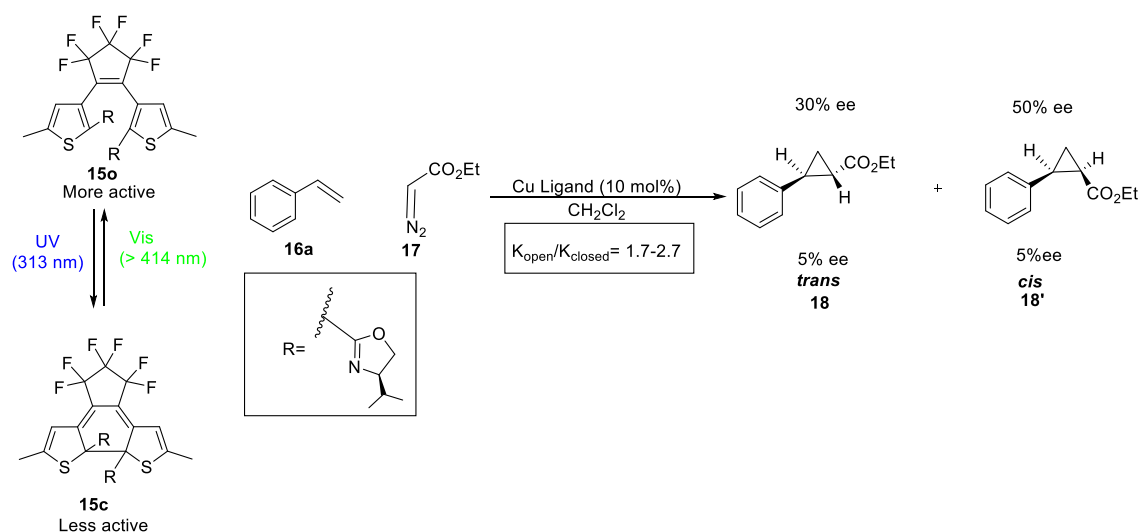


**Scheme 33.** Photoswitchable Hydroboration of **16b** with Pinacolborane<sup>[53]</sup>

Bielawski applied DTE skeleton in development of Ru catalyst with *N*-heterocyclic carbene (NHC) ligand<sup>[54,55]</sup> Their designing photoresponsive second generation Hoveyda–Grubbs catalyst is able to modulate the reactivity of ring-closing metathesis (RCM) and ring-opening metathesis polymerization (ROMP)<sup>[56,57]</sup> in response to 313 nm wavelength of light.

### 3-3. Dithienylskeleton towards chiral metal catalysis

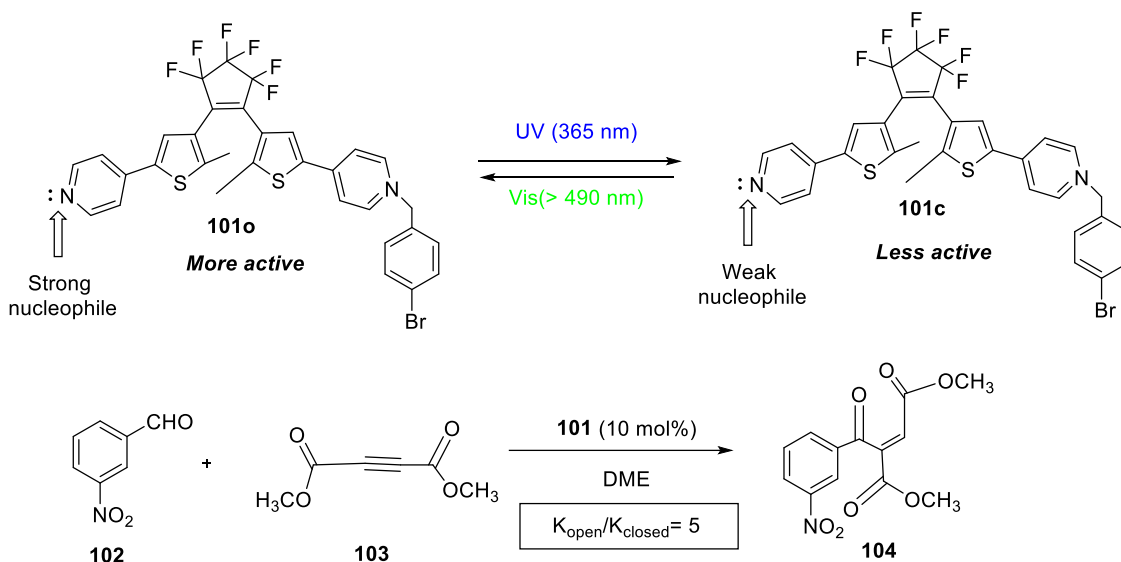
As I mentioned in chapter 1, section 1-5-2, scheme 6, Branda and co-workers reported the first successful example of photoswitchable DTE based catalysis.<sup>[16]</sup> In the flexible ring opening of DTE **15o**, chiral the bis(oxazoline) ligand can much efficiently chelate with the Cu salt, leading to promotion of cyclopropanation of styrene **16a** with diazo ester **17** in stereoselectivity. However, in the ring-closed isomer **15c** obtained with 313 nm light leads to a decrease in the enantiomeric excess (ee) of products from 30% and 50%, to 11% and 37% for the trans- and cis-diastereomers, respectively. Furthermore, chromatographically purified closed-form of catalyst having 97% of closed isomer results in an even more significant reduction in enantioselectivity (Scheme 34). The rigidity of closed isomer might affect chelation of oxazoline with Cu salt, in such a way that the Cu ion is no longer able to make a strong chiral environment.



**Scheme 34.** Cu-DTE-Catalyzed Synthesis of Cyclopropane Derivatives **18**<sup>[16]</sup>

### 3-4. Dithienylskeleton towards achiral organocatalysis

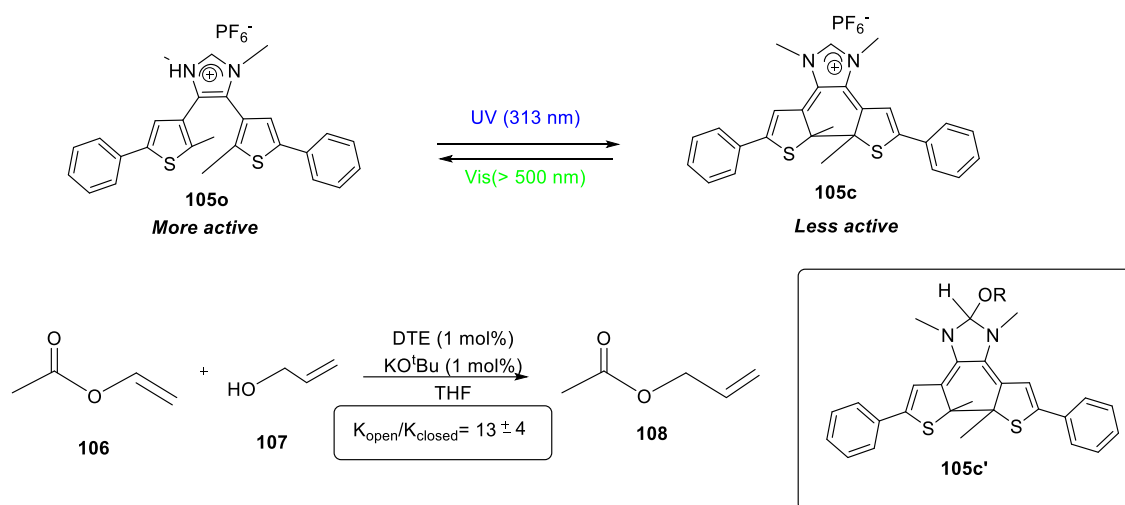
In 2008, Branda and co-workers utilized a pyridine-functionalized 1,2-dithienylcyclopentene skeleton for photomodulating the rate of a nucleophilic addition reaction.<sup>[58]</sup> Their strategy lies on utilizing the extended  $\pi$ -conjugation in the closed isomer **101c** that can reduce the pyridine basicity and nucleophilicity. A PSS ratio of 98% was achieved after irradiation with 365 nm UV light for 10 min, complete reverse isomerization was observed in presence of white light.



**Scheme 35.** Pyridine-functionalized 1,2-dithienylcyclopentene skeleton for photomodulation<sup>[58]</sup>

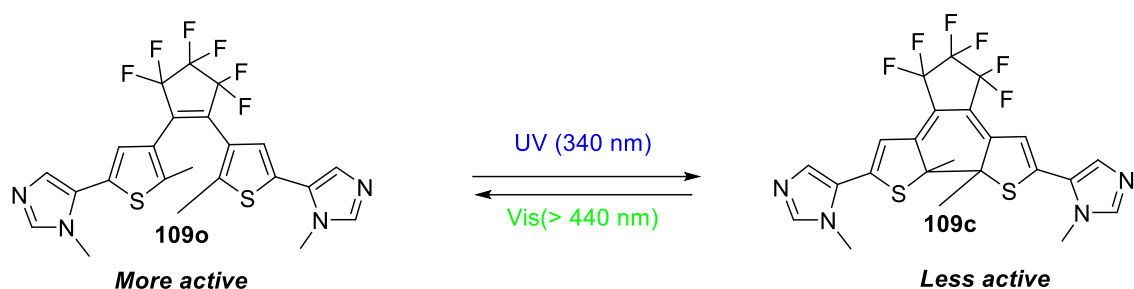
I thought Bielawski's DTE-based NHC catalyst<sup>[54,59]</sup> is the best photoswitchable catalyst reported so far, that can be used for transesterification and amidation.<sup>[60,61]</sup> A PSS ratio of 71% closed isomer **105c** is achieved by exposure to 313 nm light for a

period of 1 h, and subsequent visible light irradiation regenerates 85% of the open isomer. The two thermally stable isomers catalyze transesterification reaction between vinyl acetate **106** and allyl alcohol **107**. The dynamic range was around  $k_{\text{open}}/k_{\text{closed}} = 12.5$ . The important factor is the electron density at the carbenoid center which strongly relies strongly length of conjugated  $\pi$ -system,<sup>[17,20]</sup> which contains the nitrogen lone pairs. They estimated that when there is no sufficient stabilization, the carbene that is generated from closed isomer should be more electrophilic and can form the inactive alcohol adduct with closed ligand. This may be the reason for major rate differences in the amidation reaction between ethyl acetate and 2-aminoethanol ( $k_{\text{open}}/k_{\text{closed}} = 100$ ).

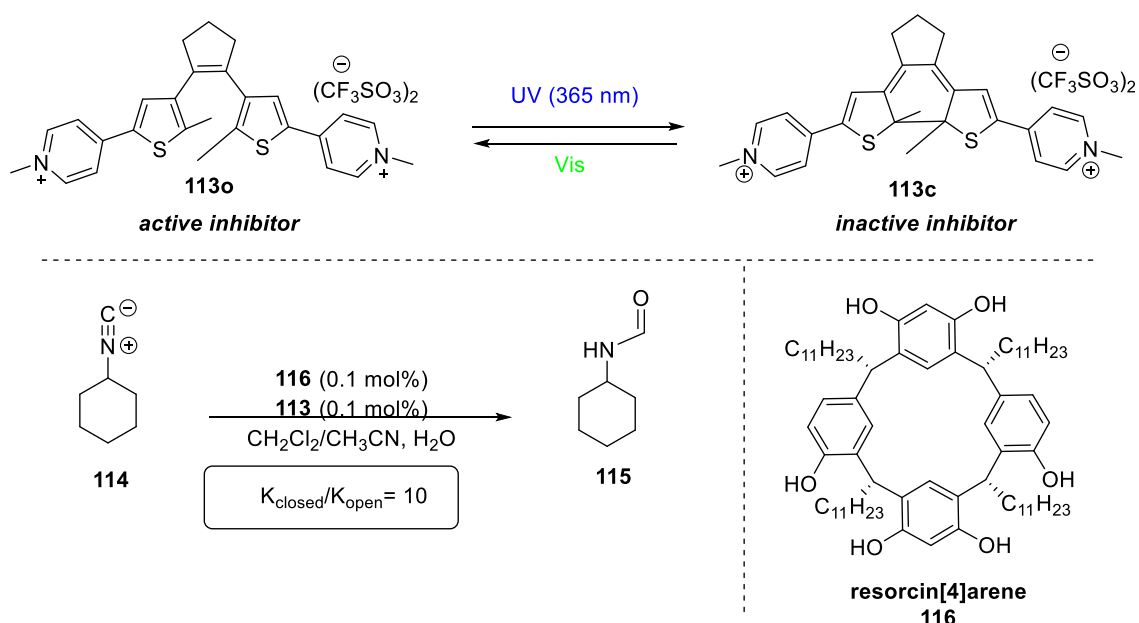


**Scheme 36.** Photochromic DTE Carbene Catalyzing Transesterification <sup>[60]</sup>

Iida and Yashima<sup>[62]</sup> developed a *N*-methyl imidazole based DTE organocatalyst **109**. *N*-methyl imidazole was substituted at the 5 and 5' positions of DTE framework; it resulted in a PSS of 89% of closed isomer **109c** within 8 min under 340 nm UV light irradiation. Complete reverse isomerization was achieved in the presence of visible light for 20 min photoirradiation time. A good dynamic range of  $k_{\text{open}}/k_{\text{closed}} = 13$  was obtained through an elaborate kinetic study of reaction between 2-decanol **110** and acetic anhydride **111**. In the open-form of the catalyst **109o** is active and is able to catalyze the acylation reaction (Scheme 37), whereas in the closed form shows decreasing in their catalyst activity owing to the extended conjugation throughout the whole DTE.



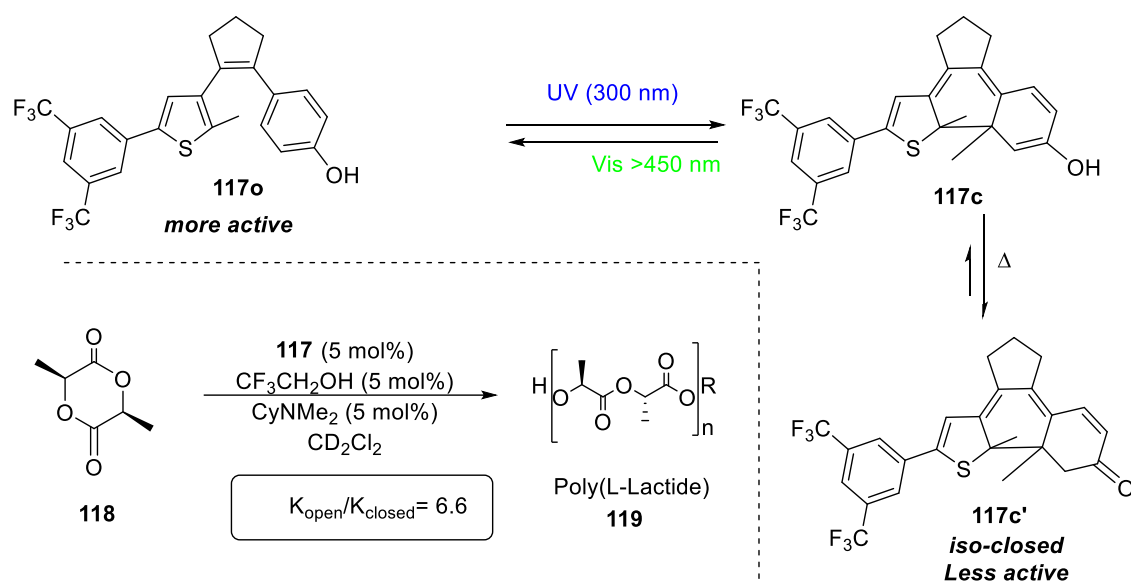
**Scheme 37.** DTE-catalyzed alcohol acylation<sup>[60]</sup>



**Scheme 38.** Photoswitchable Inhibition of Isonitrile Hydration.<sup>[63]</sup>

Scarso and Strukul<sup>[63]</sup> have designed a host guest system (a self-assembled capsule) which can catalyze isonitriles **114** hydration to the corresponding *N*-formamides **115** under mild conditions. Generally, this reaction requires relatively strong acids, which can lead undesirable polymerization reaction. The hexamer of resorcin[4]arene **116** can bind selectively to the bis-pyridyl cation **113**, and after binding, the photogenerated molecule was able to displace the isonitrile substrate **114** to act a competitive inhibitor. However, upon photoirradiation with 365 nm UV light, the flexible open form of catalyst **113o** isomerizes to the more rigid closed isomer **113c**, which is not capable for a suitable fitting in the cavity. As a result of this, a 10-times

faster rate of hydration of isonitrile substrate **114** can be achieved with closed form of catalyst. Further exploring the and overcoming the boundaries of DTE based organocatalysis, Hecht and co-workers developed another photoswitchable moiety replaces one of the thiophene ring on traditional dithienylethene to phenyl ring (Scheme 39).<sup>[64]</sup> The closed form of the catalyst **117c** underwent a keto enol tautomerism to the corresponding iso-closed form **117c'**. The generated iso-closed form **117c'** can be returned back by irradiating with ambient wavelength of light.<sup>[65]</sup> With 300 nm wavelength of light for just 3 minutes changed the PSS ratio to 98 % closed isomer. This can be applied towards ring-opening polymerization reaction. Only the phenol moiety in ring opened form can activate the C=O group of L-lactide through hydrogen bonding. There is background reaction taking place even though iso closed form lacks hydrogen bonding interactions, resulting in  $K_o/K_c = 6.6$ .



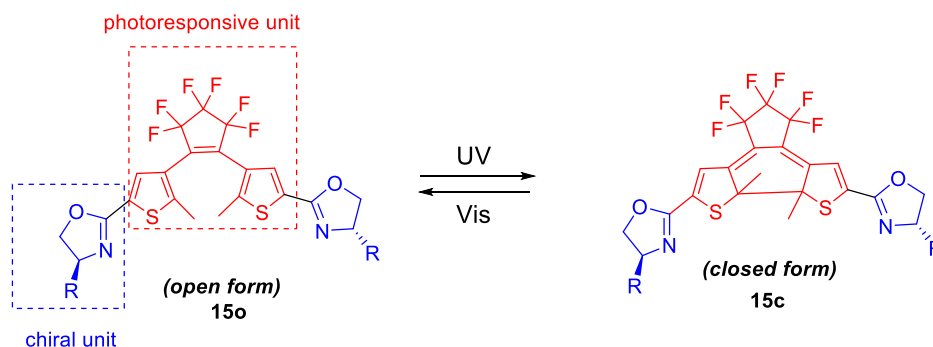
**Scheme 39.** Photoswitchable polymerization of *L*-lactide<sup>[64]</sup>

### 3-5. This Work: Development of Photoswitchable Dithienylethene Based Chiral Phosphoric Acid Catalyst.

Even though DTE catalyzed reaction reached far milestone, there has been no report to use DTE to control the stereochemical outcome, with the exception of the first and only successful report by Branda and coworkers in 2005.<sup>[16]</sup> So in this work, I have developed a novel photoswitchable chiral organocatalyst utilizing DTE photochromic unit for asymmetric transformations. As I mentioned in the chapter 1, the light responsive regulation in catalyst function was achieved by Branda and coworkers<sup>[16]</sup> by integrating the light responsive DTE framework to chiral oxazoline skeletons. Their studies on light responsive DTEs, encouraged us to envision the possibility to explore dithienyl photochromic skeletons towards asymmetric organocatalysis (Figure 25b).



**a) Branda and coworkers: photo-regulation in chiral metal catalysis**



**b) Our Work: photo-regulation in chiral organocatalysis**

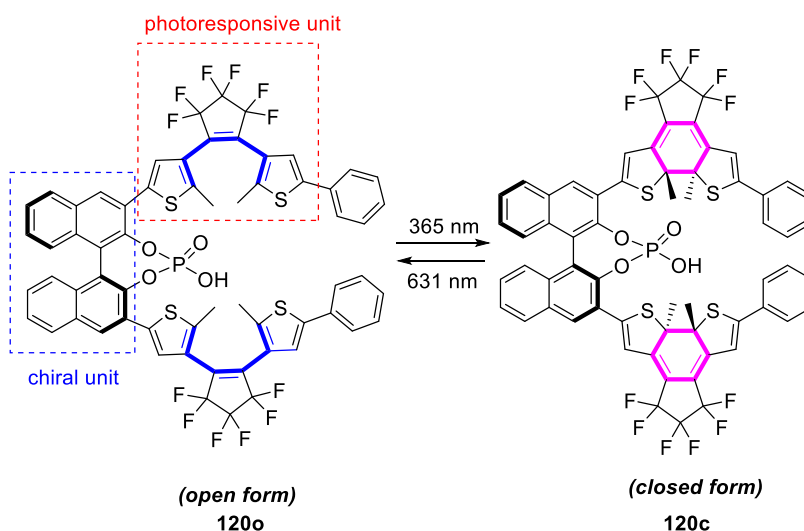


**Figure 25.** (a) Previous reports by Branda and coworkers: chiral oxazoline-DTE based metal catalyst, (b) this work: BINOL based dithienylethene phosphoric acid catalyst as a photoswitchable chiral organocatalyst **120o**

To open a new pathway towards asymmetric Brønsted acid catalysis, our research focused on the design of photoswitchable chiral phosphoric acid. The unique structural and chemical features of Akiyama and Terada's phosphoric acid catalyst prompted us to use this concept towards the development of photoresponsive designs.

Features of Akiyama and Terada type phosphoric acid catalyst

- 1) ability for acid/base dual function
- 2) conformational flexibility of the chiral backbone can be restricted effectively by introducing ring system
- 3) steric and electronic influence with substitution to promote efficient enantioselective transformations<sup>[66-69]</sup>

Generally, for phosphoric acid catalysed reactions, substituents at the 3,3' position on the binaphthol ring are crucial for bringing enantioselectivity and the steric bulk at these positions influences selectivity to a greater extent. However, catalyst bearing too large substituents can sometimes hinder the reaction progress,<sup>[70]</sup> and bulky catalysts leads to reversal in stereoinductions.<sup>[71]</sup> The strategic design of photoresponsive catalyst for modulation become more challenging.

### My hypothesis:

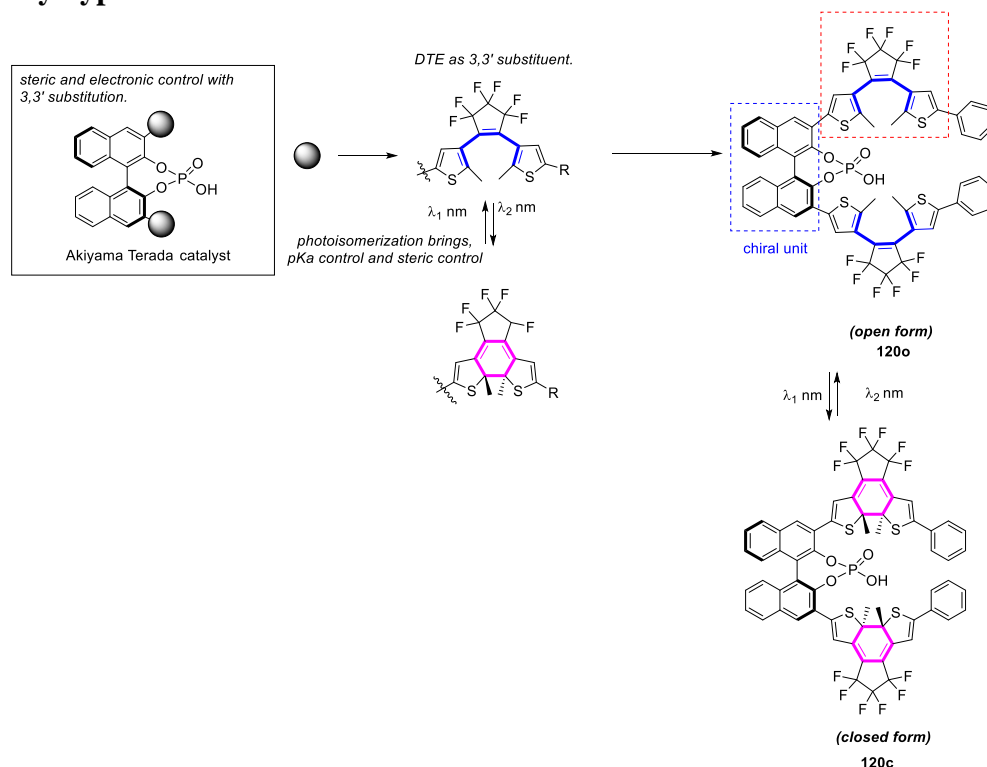
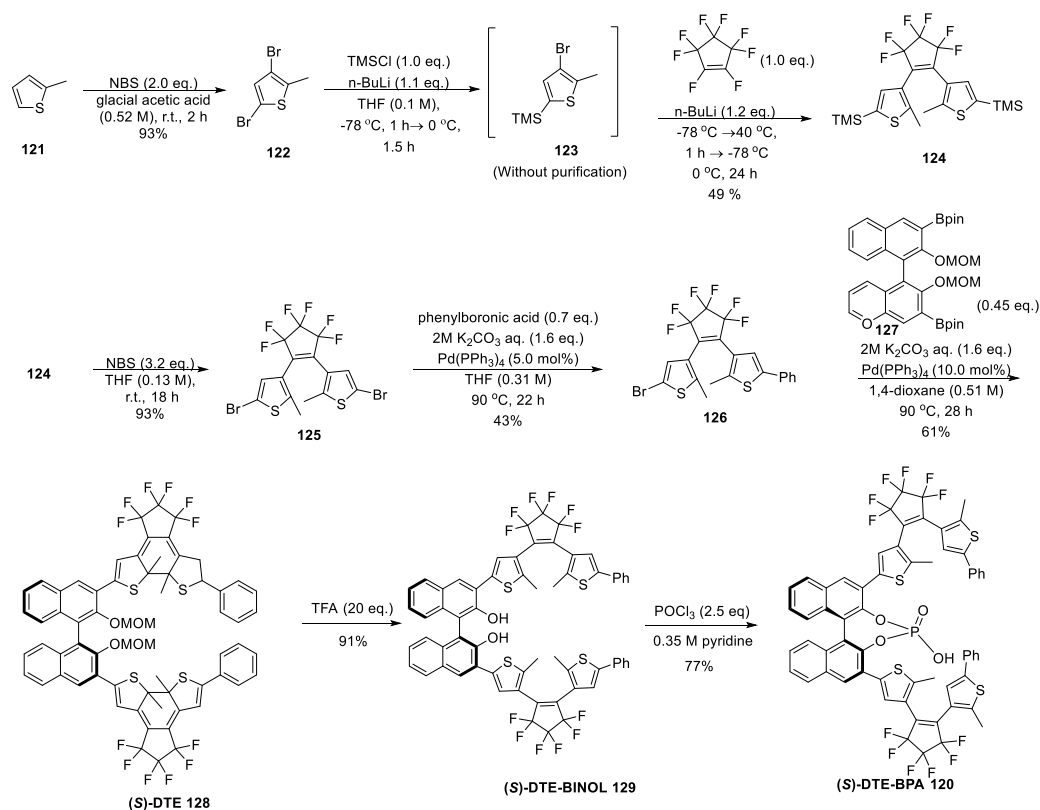


**Figure 25.** Our initial hypothesis for utilizing DTE towards phosphoric acid catalyst **120** designing

Chiral induction ability of Akiya-Terada catalyst mainly relies on the 3,3' position of BINOL backbone. If a photochromic unit DTE is able to introduce at the 3,3' position of BINOL backbone, we can control the catalyst function based on the isomerization between the thermally stable open and closed forms of DTEs. The reactivity change may be influenced by the different  $pK_a$  values as well as the distinct steric environment originated from ring closing. Herein, I report the synthesis of photoswitchable phosphoric acid catalyst by combining photochromic dithienylethene moiety with chiral BINOL backbone for modulating the catalyst functions. My approach includes utilizing the advantage of electronic differences between the two photoisomers (open and closed forms) of DTE to influence the outcome of  $pK_a$  for phosphoric acid-catalyzed reaction. In this report, the synthesis of photoresponsive chiral **DTE-BPA-120** and their interesting photoisomerization properties as well as the ability to modulate asymmetric reactions were described.

### 3-6. General procedure for preparation of DTE-BPA- 120

I started synthesizing the desired **DTE-BPA-120** depicted in Scheme 40 and was established in 8 steps.



**Scheme 40.** General synthesis route for the dithienyl BINOL based photoswitchable phosphoric acid catalyst (DTE-BPAs)

Following a similar procedure reported by Li and his co-workers<sup>[29]</sup> for the synthesis of dithienylethene based photoswitch for the photocontrol of the fluorescence of conjugated polymers, I synthesized the photoswitchable DTEs **125** and **126** starting from 2-methylthiophene (**121**) in 5 steps. Finally, the desired catalyst **(S)-DTE-BPA-120** was synthesized from **126** in further 3 steps involving, (i) Suzuki -Miyura cross-coupling, (ii) TFA deprotection, and (iii) phosphoric acid formation. After synthesizing the desired catalyst **120**, I carried out the photoisomerization experiments to understand the photostationary ratio of the catalyst.

### 3-7. Photoisomerization experiments

#### 3-7-1. Isomerization studies of DTE-BPA- 120 using NMR spectroscopy

The photo-chemical isomerization's between thermally stable isomers of **(S)-DTE-120** were studied using <sup>1</sup>H NMR spectroscopies. (Figures 26a and 26b). Both **(S)-**

**DTE-BINOL-128** and **(S)-DTE-BPA-120** undergoes electrocyclic ring closing isomerization upon exposure to photoirradiation. However, when comparing our newly designed DTE catalyst **(S)-DTE-BPA-120 [open]** with the previously reported ones, the complexity after photoirradiation is much higher due to the formation of five possible conformers (Figure 26a). UV irradiation of **(S)-DTE-BPA-120** solution in CDCl<sub>3</sub> under 365 nm LED light for 12 h brought a maximum ratio of **(S)-DTE-BPA-120o** / **(S)-DTE-BPA-120c**.

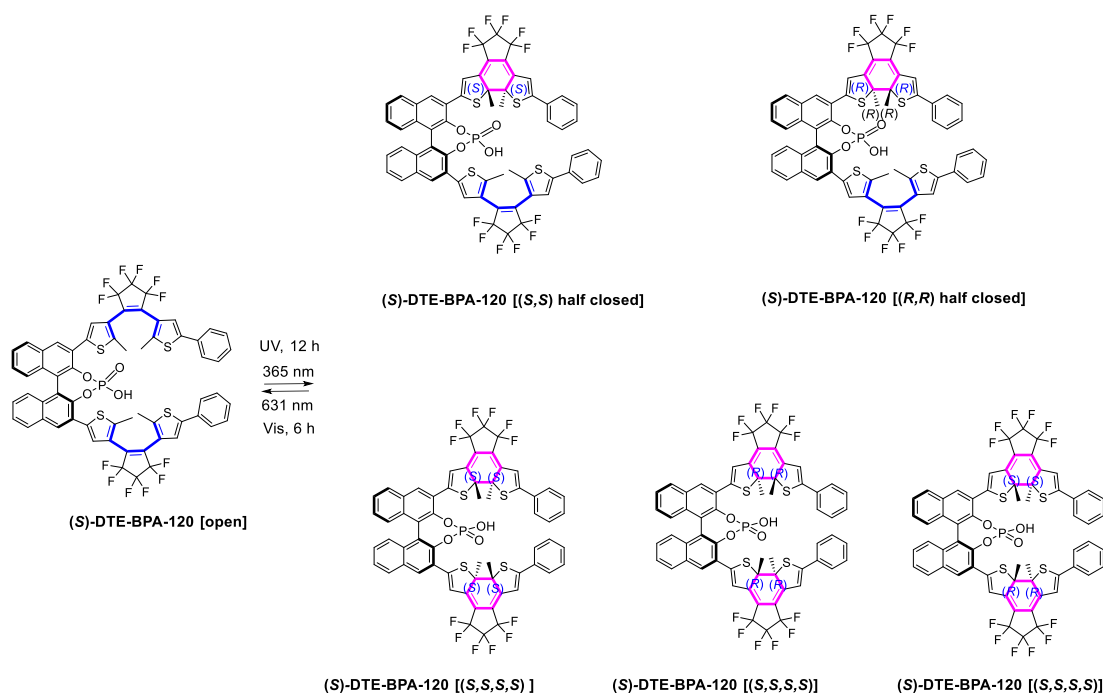


**Figure 26a.** Schematic representation of all the possible conformers of **(S)-DTE-BPA-120** after photoirradiation (365 nm, 12h)

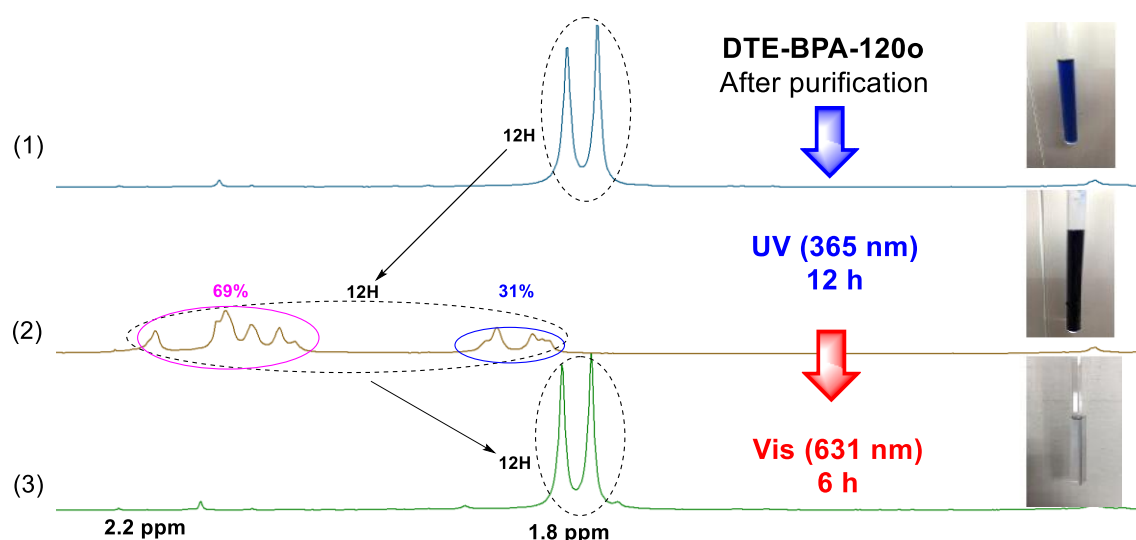


**Figure 26b.** Photoisomerization experiments of **DTE-BPA-120** using <sup>1</sup>H NMR (in CDCl<sub>3</sub>)

When 365 nm UV light was irradiated to the  $\text{CDCl}_3$  solution of (*S*)-**DTE-BPA-120o** for 12 h, a PSS ratio of 69% **120o** was obtained with dark solution (Figure 26b-2). Further irradiation of visible light (631 nm) provided a complete conversion of **120c** to **120o**. The  $^1\text{H}$  (Figure 27) and  $^{31}\text{P}$  NMR also suggest that the reverse isomerization is achieved with 100% efficiency without any decomposition of catalyst. On the  $^{31}\text{P}$  NMR studies, the open isomer **120o** showed a singlet around 5.0 ppm. After UV irradiation of the sample with 365 nm for 12 h led to the appearance of peaks corresponds to closed isomer of catalyst **120c**. Initial  $^{31}\text{P}$  NMR were restored by irradiating the sample with 631 nm for another 6 h.

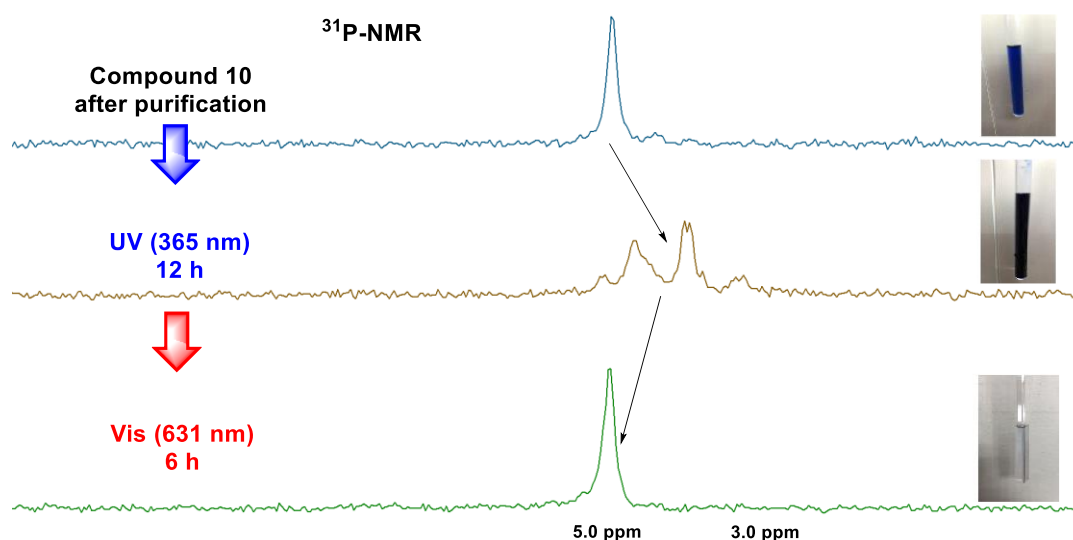


**Figure 27.** Photoisomerization experiments of **DTE-BPA-120** using  $^{31}\text{P}$  NMR (in  $\text{CDCl}_3$ ).

### 3-7-2. Isomerization studies of **DTE-BPA-120** using UV-vis spectroscopy

In the UV-visible spectra, the open form of (*S*)-**DTE-BPA-120o** (20  $\mu\text{M}$  in  $\text{CDCl}_3$ ) showed an intense absorption bands at 285 nm, which corresponds to the  $\pi \rightarrow \pi^*$  transition in the dithienylethene thiophene-cyclopentene junctions (Figure 28a). Concomitantly, the intensity of absorption band corresponds to the generated extended  $\pi$  conjugated system (electrocyclic conrotatory ring closure) of (*S*)-**DTE-BPA-120c** after UV irradiation (365 nm, 12 h) decrease the band that correspond to 285 nm and two new bands appeared in the UV-Vis spectra at 370 and 600 nm.<sup>[72]</sup> The stoichiometric product formation is confirmed with the isobestic point observed at 315 nm which suggest that the photoisomerization of (*S*)-**DTE-BPA-120** proceeds without significant byproduct formation.<sup>[73]</sup> Initial UV/Vis spectra were restored by subsequent photoirradiation of the solutions containing (*S*)-**DTE-BPA-120** with visible light of 631 nm wavelength for 6 h resulted in quantitative conversion.

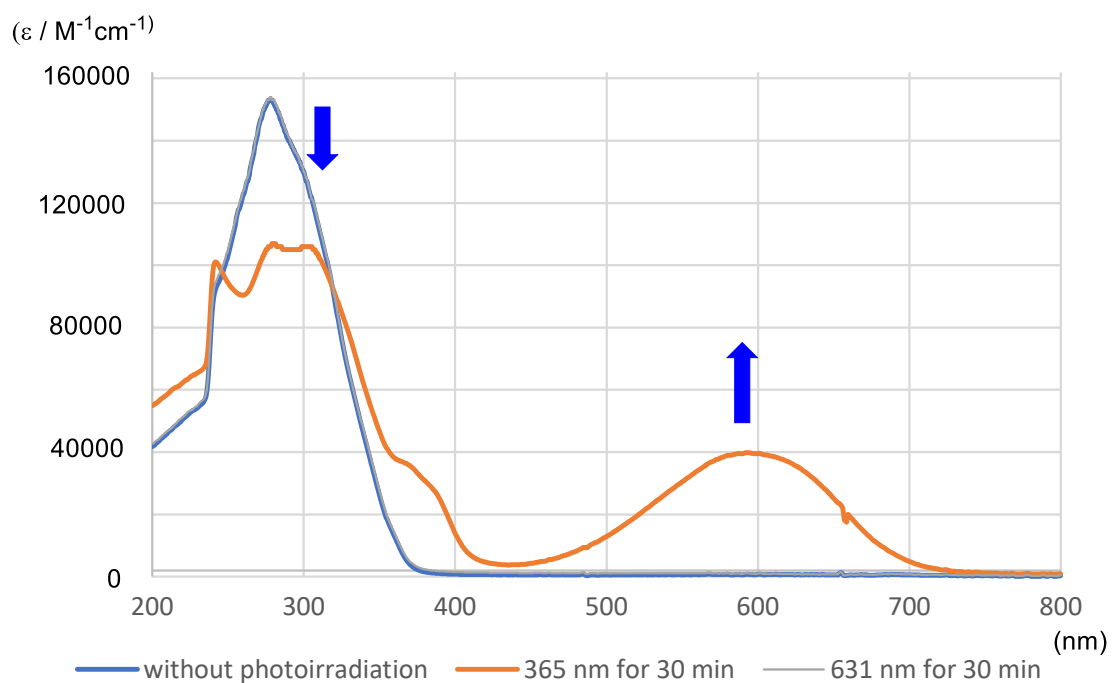
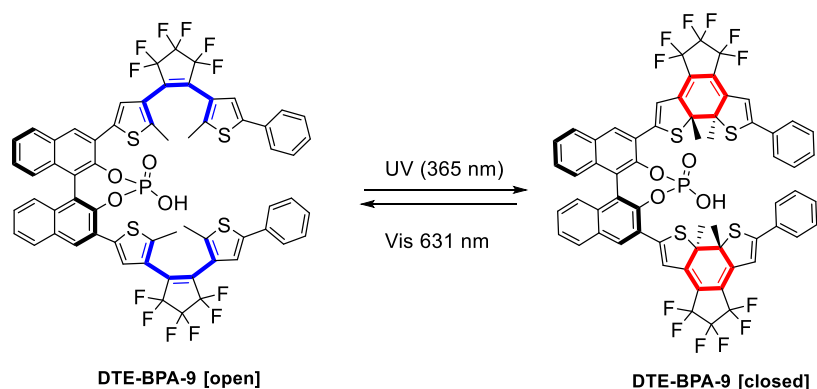


**Figure 28a.** Changes in the UV-vis spectra of (*S*)-**DTE-BPA-120** (in  $\text{CHCl}_3$ , 20  $\mu\text{M}$ )

Similarly, I also analysed the photoisomerization behavior of (*S*)-**DTE-BINOL-129**. A similar trend in the absorption was observed for (*S*)-**DTE-BINOL-129** (Figure 28b).

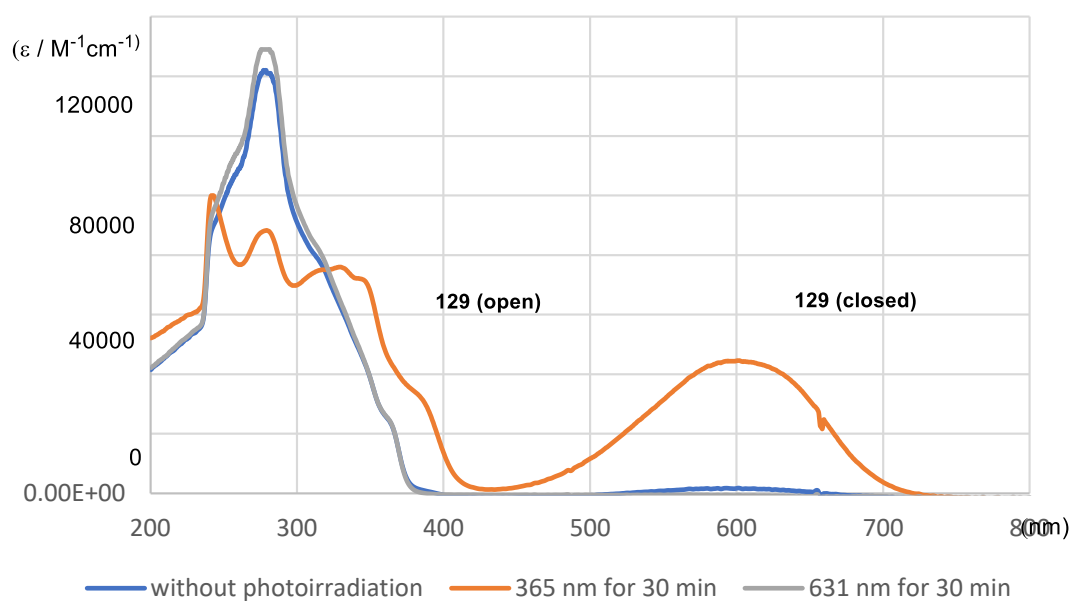
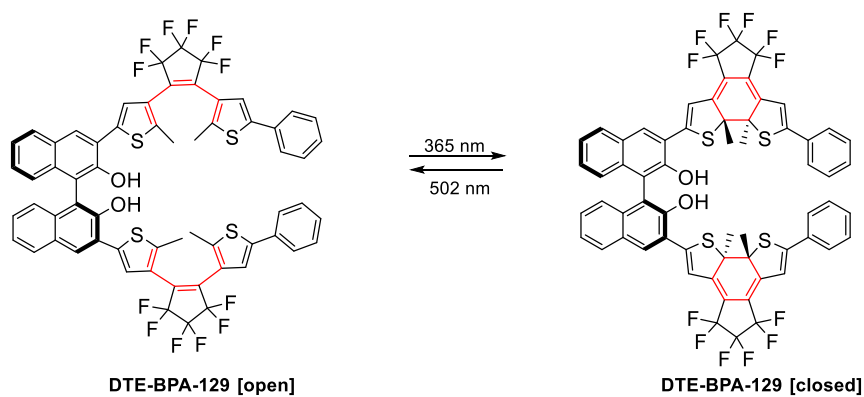


**Figure 28b.** Changes in the UV-vis spectra of (*S*)-DTE-BINOL-129 (in CHCl<sub>3</sub>, 20 μM)

Then I compared the photoisomerization isomerization ratios between (*S*)-DTE-BPA-120, (*S*)-DTE-BINOL-129, and (*S*)-DTE-MOMBINOL-128 as shown in Figure 29.

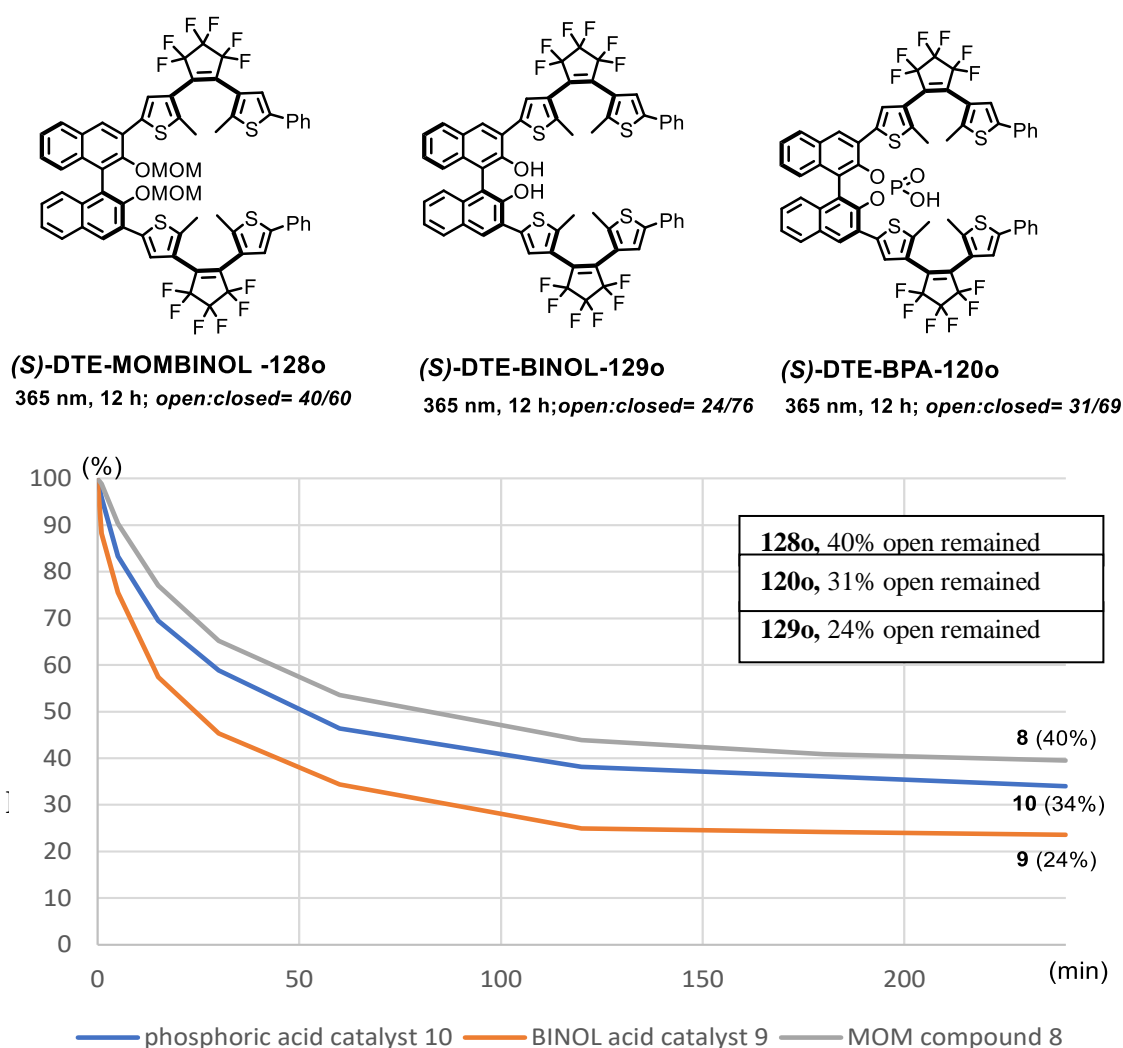


**Figure 29.** Comparison of photoisomerization ratio of BINOL based DTE derivatives.

The Figure 29 clearly indicated that MOM protected BINOL based DTE has lower isomerization rate. Although the diol (*S*)-DTE-BINOL-129 improved the photoisomerization rate, the phosphoric acid moiety (*S*)-DTE-BPA-120 again decreased the isomerization ability under UV light.

The descending order of photoisomerization ability:

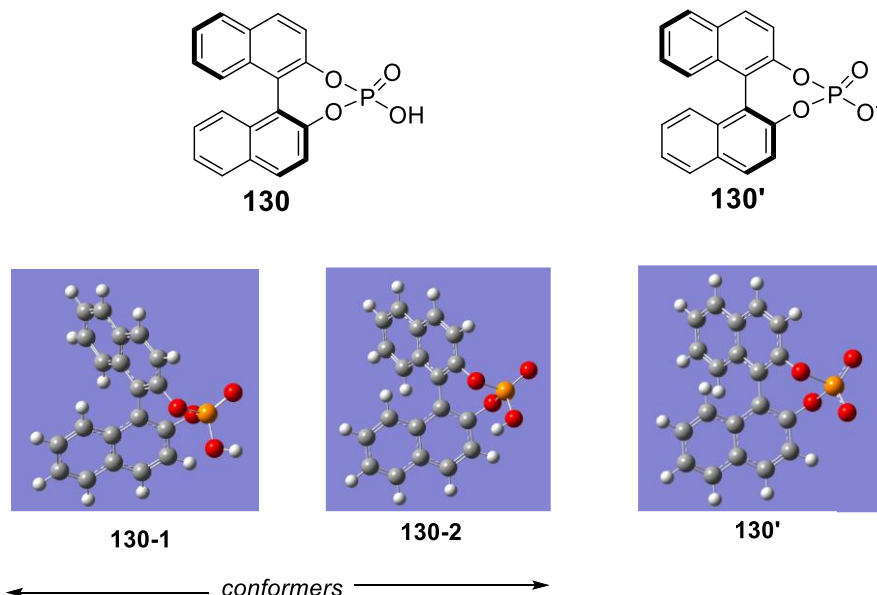
**(S)-DTE-BINOL-129 > (S)-DTE-BPA-120 > (S)-DTE-MOMBINOL-128**

To gain further information about the influence of photochemical isomerization on the  $pK_a$  values of these two isomers, however, experimental calculation using UV-vis spectroscopy with internal standards was failed due to a mixture of isomers after photoirradiation. Therefore, the DFT studies were performed to estimate the  $pK_a$  values of these each isomer.



## Determination of pK<sub>a</sub> value for (S)-DTE-BPA-120 using DFT studies

To elucidate the influence of the photocyclization of BINOL-DTEs on the pK<sub>a</sub> values, DFT calculations were performed for both isomeric forms using SMD/B3LYP/6-31+G(d) method. The free energy of acid dissociation in DMSO can be obtained using eq 1.



$$\Delta G^*_{\text{soln}} = \Delta G^*_{\text{gas}} + \Delta G^*_{\text{solv}}(\text{A}^-) + \Delta G^*_{\text{solv,DMSO}}(\text{H}^+) - \Delta G^*_{\text{solv}}(\text{HA}) \quad \text{eq 1.}$$

$$\text{pK}_a = \Delta G^*_{\text{soln}} / RT \ln(10) \quad \text{eq 2.}$$

where \* denotes the standard state of 1 mol/L in any phase.

However, by considering other parameters like solvation free energy of proton (values range from -252.89 to -273.3 kcal/mol) as well as the number of charged species that are not conserved across the reaction, proton-exchange method is utilized to afford reliable pK<sub>a</sub> values with respect to the experiment value of reference acid **130**. pK<sub>a</sub> value (3.37) of **130** is already reported in DMSO solvent; the exchange free energy in DMSO can be described by the equation.

$$\Delta G^*_{\text{exchange}} = \Delta G^*_{\text{gas,exchange}} + \Delta G^*_{\text{solv}}(\text{A}^-) + \Delta G^*_{\text{solv}}(\text{H}_{\text{Ref}}) - \Delta G^*_{\text{solv}}(\text{HA}) - \Delta G^*_{\text{solv}}(\text{Ref}^-) \quad \text{eq 3.}$$

$$\text{pK}_a = (\Delta G^*_{\text{exchange}} / RT \ln(10)) + \text{pK}_a(\text{H}_{\text{Ref}}) \quad \text{eq 4.}$$

The obtained BINOL phosphoric acids have the two possible conformers **130-1** and **130-2**. The DFT calculations were performed for geometry optimization using the B3LYP/6-31+G(d) methods in gas-phase. Frequency calculations at the same level of theory was employed to understand the nature of the stationary points and thermal corrections to Gibbs free energy (ZPG). SMD calculation (B3LYP/6-31+G(d)) with the gas-phase optimized geometries were employed with thermal corrections to the Gibbs



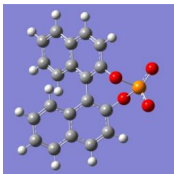
free energies (green color) to obtain the energies in solution phase (blue color). It should be noted that no consideration of any conformers with higher energy in the following analogues.

**Individual free energy value for each optimized structure of BPA-10 in gas and solvent phase**

**N.B.-** Values in green color indicate gas phase free energy values. Whereas, values in blue color indicate solvent phase free energy values.

Level of theory associated with free energy (G) values in gas and solvent phase [Unit of G is in Hatree. ( $1E_h = 627.50$  Kcal/mol)]

Sl.No                      Model                      B3LYP/6-31+ G(d)    B3LYP/6-31+ G(d)

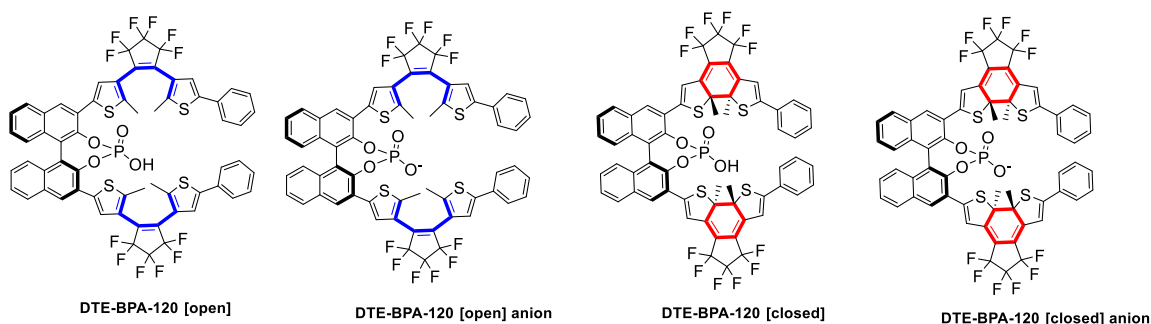
1	 10-1	ZPG= 0.237223 -1412.110478 ZPG=0.236479 -1412.138437 Diff.= 17.54 Kcal/mol
2	 10-2	ZPG= 0.237325 -1412.108709 ZPG=0.236459 -1412.137549 Diff.= 18.09 Kcal/mol
3	 10'	ZPG= 0.224946 -1411.615492 ZPG=0.226023 -1411.707525 Diff.= 57.75 Kcal/mol

**Table 11.** Free energy change of solvation for phosphoric acid catalyst **130**.

Using DFT calculations, it was found that the change in Gibbs energy of solvation for phosphoric acid catalyst **130-1** is 17.54 kcal/mol and the corresponding conformer **130-2** showed a little higher energy change in solvation (18.09 kcal/mol). (Table 11). The solvation energy corresponds to the anion **130'** after deprotonation is 57.75 kcal/mol. Since the **130-2** have higher energy compared to **130-1**, it was neglected for further calculation.

## Major Conformers of (S)-DTE-BPA-[open]-120 and (S)-DTE-BPA-[closed]-120 Preliminary lowest energy calculations

The geometry optimization was performed using the B3LYP/6-31+G(d) methods in gas-phase. Frequency calculations at the same level of theory was employed to understand the nature of the stationary points and thermal corrections to Gibbs free energy (ZPG). Due to the higher flexibility of (S)-DTE-BPAs, conformational screening was performed to obtain the most stable conformer for preliminary lowest energy calculations. Among the 291 possible conformers for open isomer of DTE, 9 conformers of (S)-DTE-BPA-[open] with lowest energy were selected for further calculation. It should be noted that no consideration of any conformers with higher energy in the following analogues.



## Gas phase calculation for most stable conformers of (S)-DTE-BPA-[open]

Initially the gas phase calculation for the most stable 9 conformers of DTEs were performed using B3LYP/6-31+G(d) methods. Frequency calculations at the same level of theory was employed to understand the nature of the stationary points and thermal corrections to Gibbs free energy (ZPG); zero-point correction, sum of electronic and zero-point energies, sum of electronic and thermal energies (U), enthalpies (H), Gibbs free energies (E) were determined. The values correspond to each of these are summarized below.

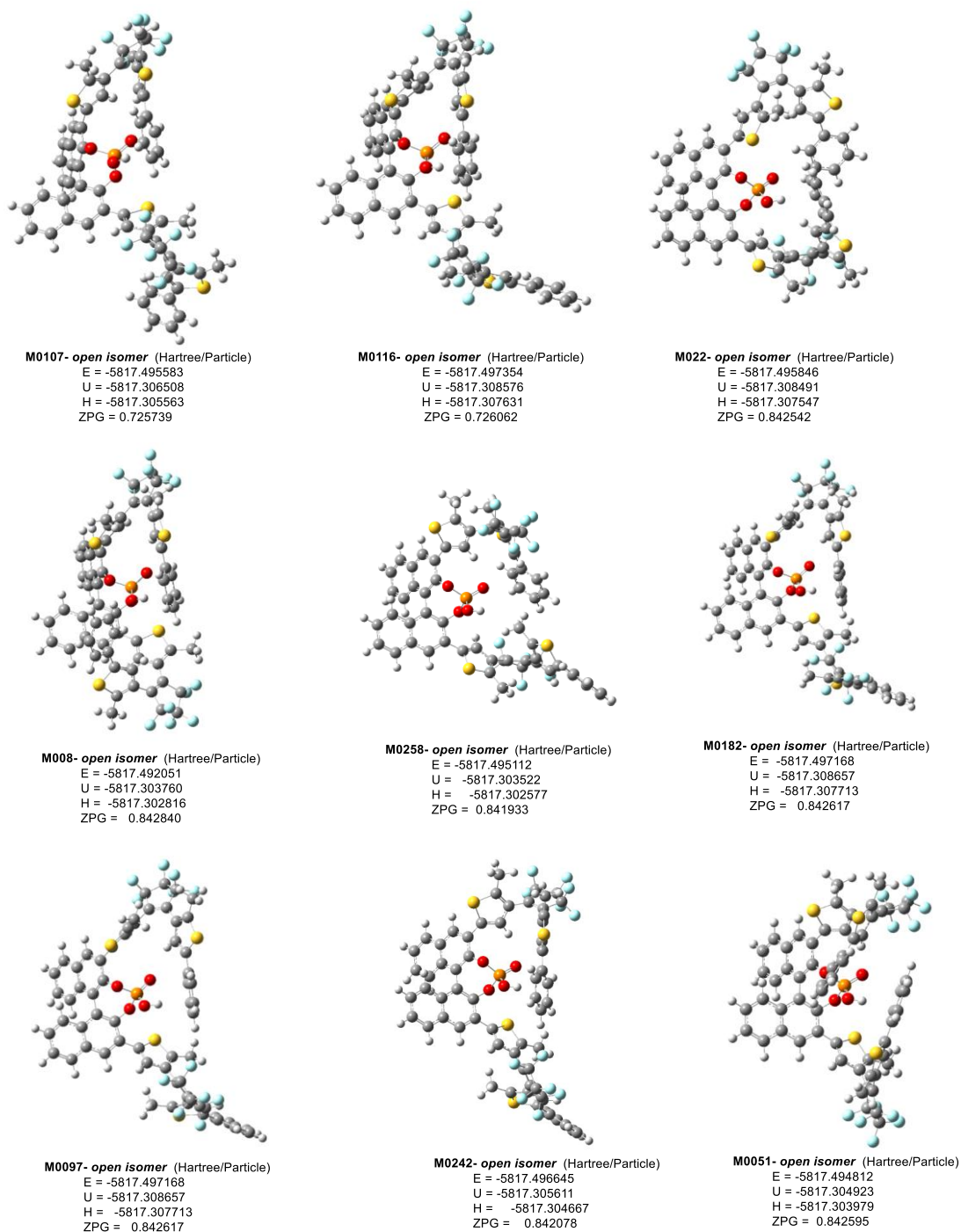


**Figure 30.** Gas phase calculation for most stable conformers of (S)-DTE-BPA-[open].

**Energy difference between most stable conformer with other lowest energy conformers in gas phase**

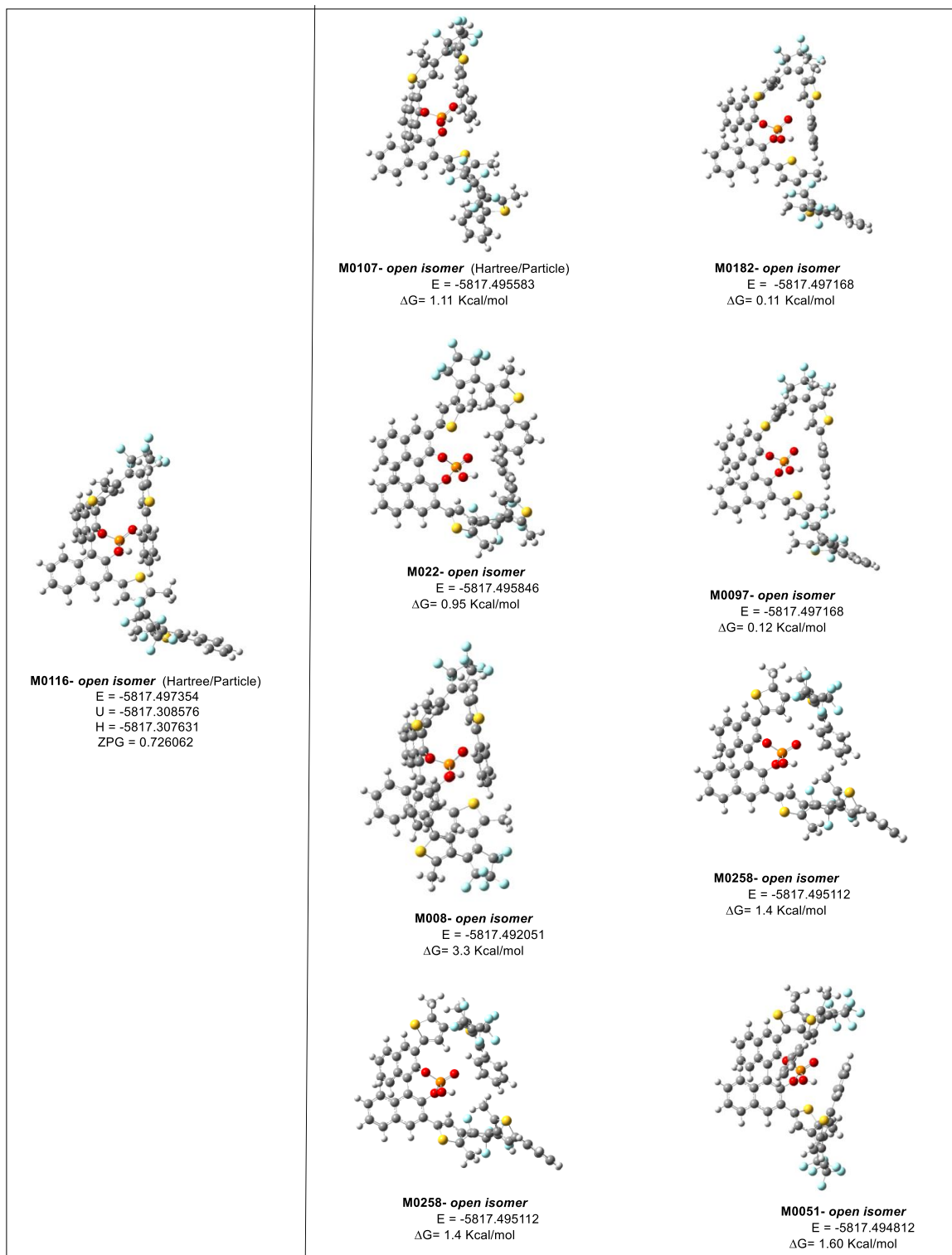


**Figure 31.** Gibbs free energy in gas phase for the most stable conformer with other lowest energy conformers.

## Solvation phase calculation (DMSO) for the most stable conformers of (S)-DTE-BPA-[open]

The solvation phase calculation for the most stable 9 conformers of DTEs were performed using SMD/B3LYP/6-31+G(d) methods. Frequency calculations at the same level of theory was employed to understand the nature of the stationary points and thermal corrections to Gibbs free energy (ZPG); zero-point correction, sum of electronic and zero-point energies, sum of electronic and thermal energies (U), enthalpies (H), Gibbs free energies (E) were determined. The values correspond to each of these are summarized below.

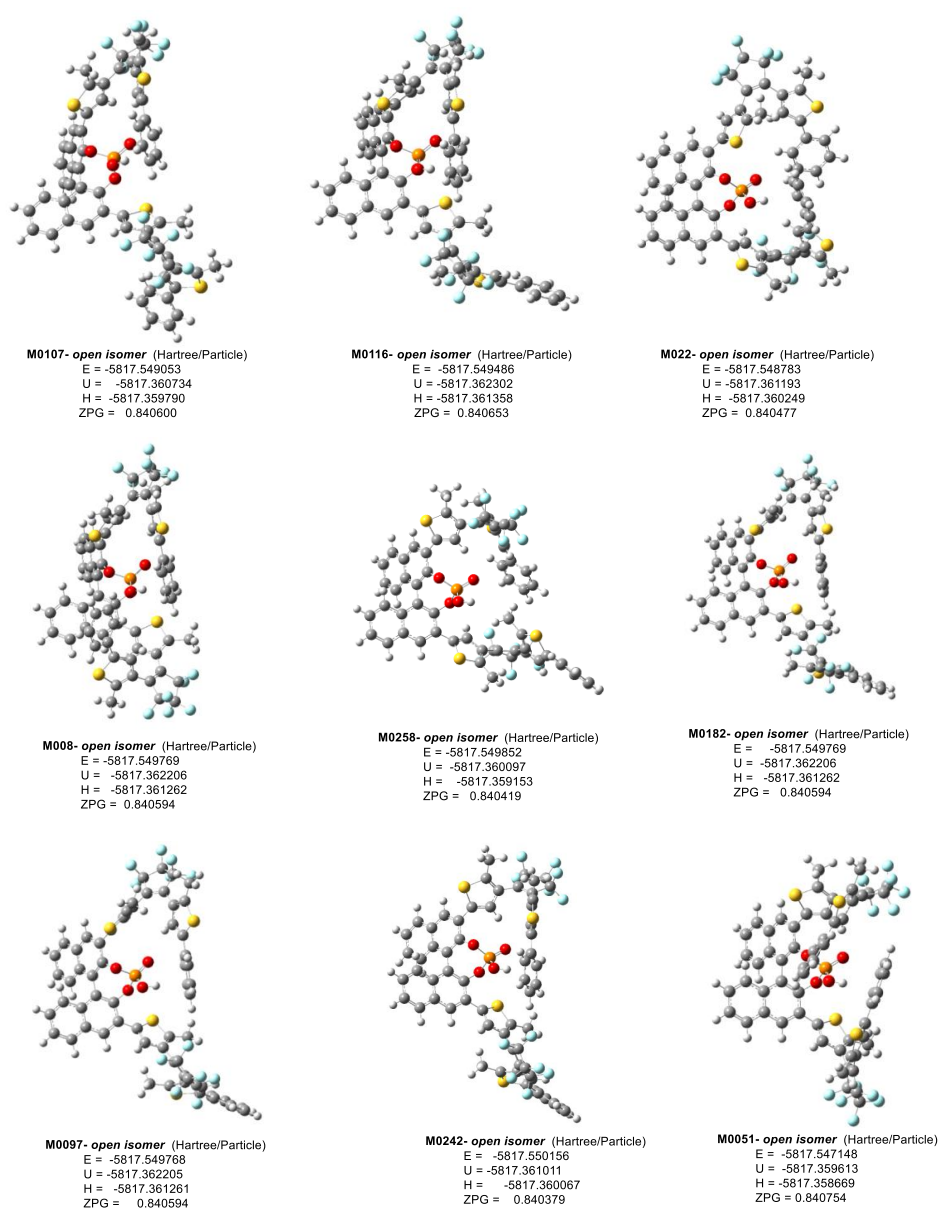


**Figure 32.** Solvation phase calculation for most stable conformers of (S)-DTE-BPA-[open] 120.



## Free Energy Value for Each Optimized structure of DTE-BPA-9 [open] in Gas and Solvent Phase.

**N.B.-**Values in **green** color indicate gas phase free energy values. Whereas, values in **blue** color indicate solvent phase free energy values.

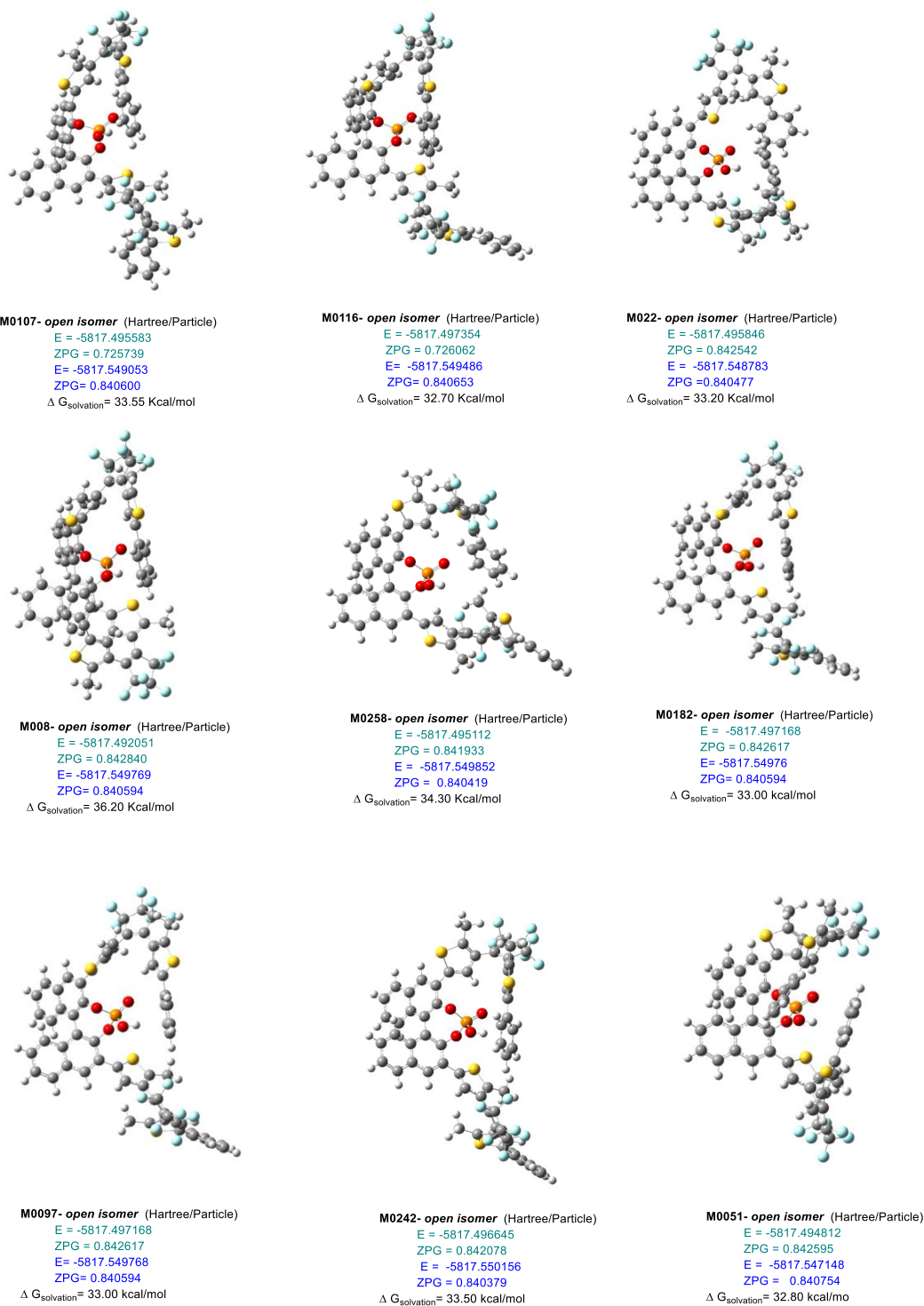


**Figure 33.** Free energy change of solvation for phosphoric acid catalyst (*S*)-DTE-BPA-[open] **120**.

### Gas phase calculation for most 10 stable conformers of (S)-DTE-BPA-[open]anion

Similar gas phase calculation was performed for all the corresponding DTE-BPA-anions using B3LYP/6-31+G(d) methods. Frequency calculations at the same level of theory was employed to understand the nature of the stationary points and thermal corrections to Gibbs free energy (ZPG). The values correspond to zero-point correction, internal energies, enthalpy as well as Gibbs free energies are summarized below.

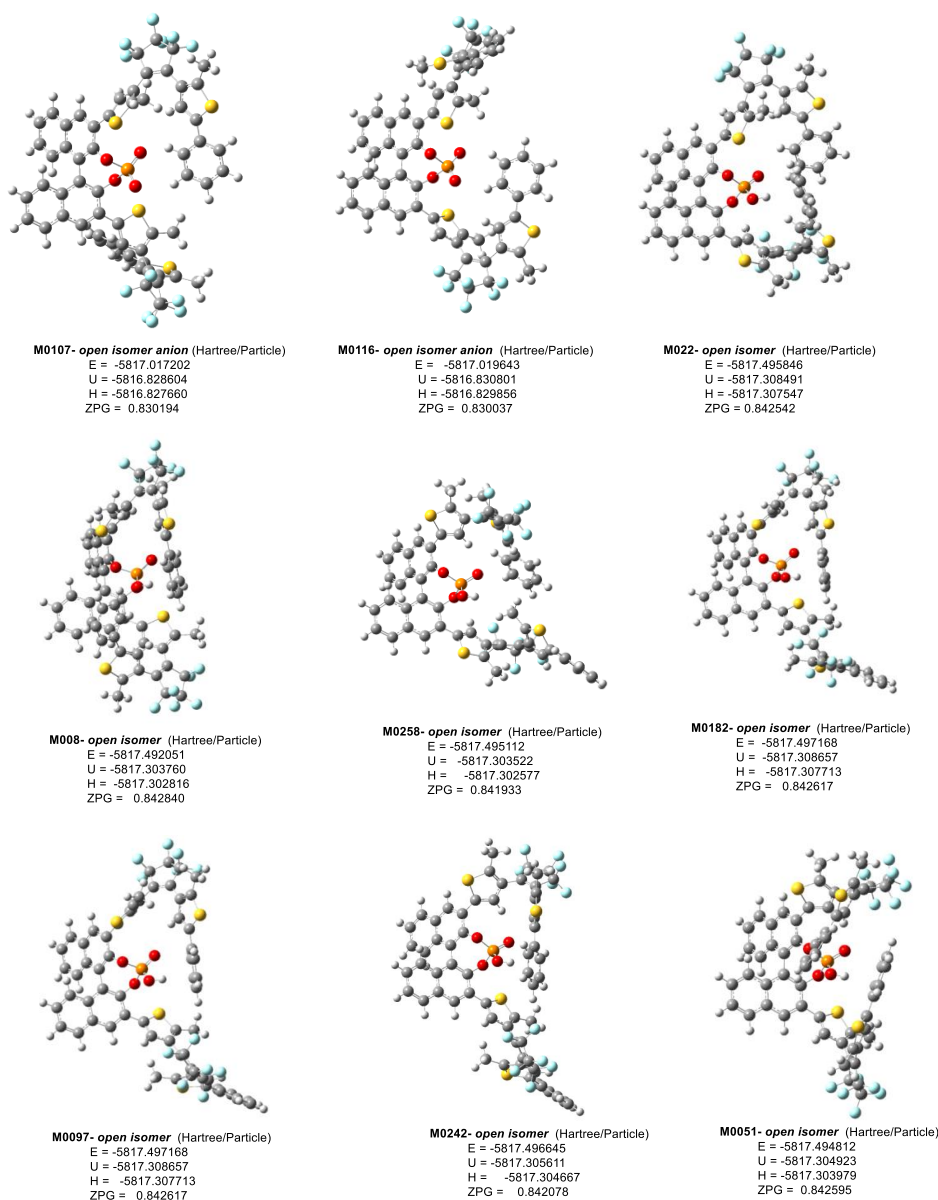


**Figure 33.** Gas phase calculation for most 9 stable conformers of (S)-DTE-BPA-[open]anion



## Solvation phase calculation for most 9 stable conformers of (S)-DTE-BPA-[open]anion

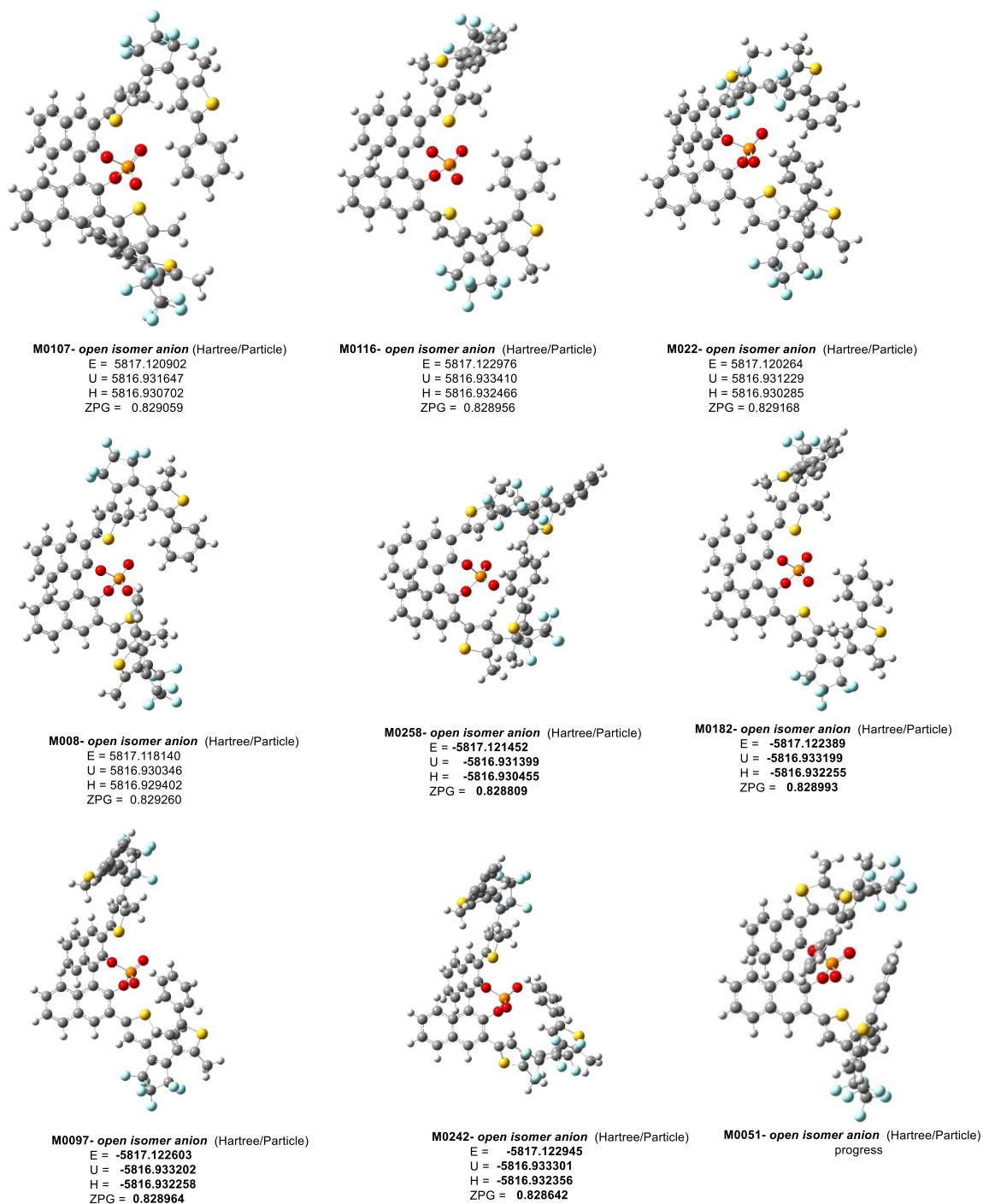


**Figure 34.** Solvation phase calculation for conformers of (S)-DTE-BPA-[open]anion

## Change in Gibbs free energy calculation for most stable conformers of (S)-DTE-BPA-[open] anion

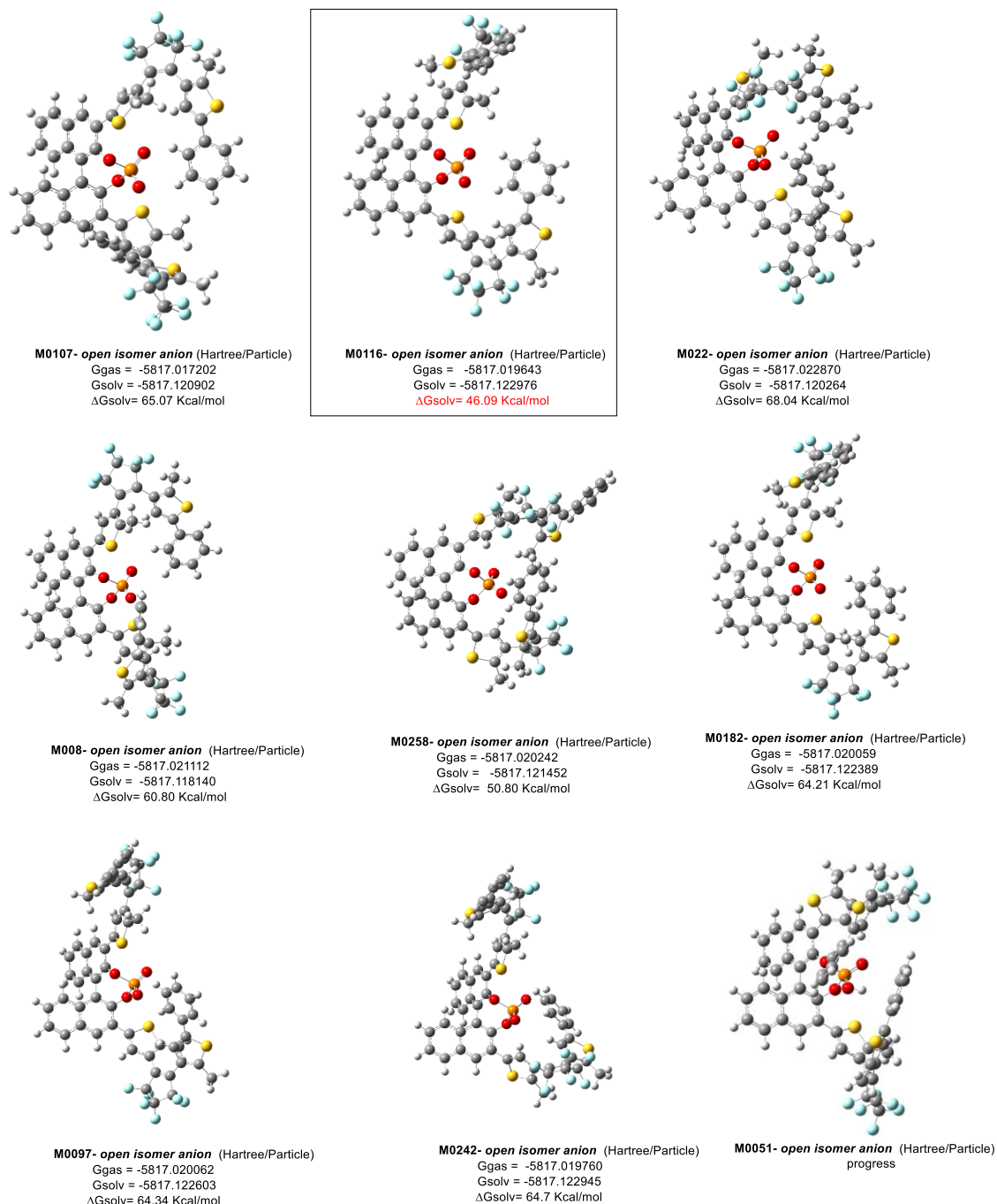


**Figure 35.** Free energy change of solvation for phosphoric acid catalyst (S)-DTE-BPA-[open] anion **120o'**.

Among all the conformers of (S)-DTE-BPA-[open] anion, M0116 seem to be the most stable conformer with a free energy solvation energy of 46.09 Kcal/mol. Based on the calculated values for (S)-DTE-BPA-[open] isomer, I have determined the pKa value of the phosphoric acid catalyst **120o** (Table 12).

#### Determination of pKa value for (S)-DTE-BPA-[open] conformers

$$\Delta G^*_{\text{exchange}} = \Delta G^*_{\text{gas,exchange}} + \Delta G^*_{\text{solv}(A^-)} + \Delta G^*_{\text{solv}(H_{\text{Ref}})} - \Delta G^*_{\text{solv}(HA)} - \Delta G^*_{\text{solv}(Ref^+)};$$

$$pK_a = (\Delta G^*_{\text{exchange}}/RT\ln(10)) + pK_a(H_{\text{Ref}})$$

**Table 12.** Determination of pKa value for (S)-DTE-BPA-[open] **120o** conformers.

	$\Delta G^*_{\text{gas,exchange}}$ (Kcal/mol)	$\Delta G^*_{\text{solv}(S)\text{-DTE-BPA-[open] anion}}$ (Kcal/mol)	$\Delta G^*_{\text{solv}(H_{\text{Ref}})}$ (Kcal/mol)	$\Delta G^*_{\text{solv}(S)\text{-DTE-BPA-[open]}}$ (Kcal/mol)	$\Delta G^*_{\text{solv}(Ref^+)}$ (Kcal/mol)	$\Delta G^*_{\text{exchange}}$ (Kcal/mol)	$\Delta G^*_{\text{exchange}}/RT\ln(10)$	pKa
<b>M0107</b>	300.18	65.07	17.54	33.55	57.75	291.49	0.21	3.58
<b>M0116</b>	299.76	46.09	17.54	32.70	57.75	272.94	0.20	3.57
<b>M022</b>	296.79	68.04	17.54	33.20	57.75	291.42	0.21	3.58
<b>M008</b>	295.51	60.80	17.54	36.20	57.75	279.90	0.21	3.58
<b>M0258</b>	297.98	50.80	17.54	34.30	57.75	274.27	0.20	3.57
<b>M0182</b>	299.38	64.21	17.54	33.00	57.75	290.38	0.21	3.58
<b>M0097</b>	299.38	64.34	17.54	33.00	57.75	290.51	0.21	3.58
<b>M0242</b>	299.24	64.70	17.54	33.50	57.75	290.23	0.21	3.58

The pKa value of (S)-DTE-BPA-[open]-**120o** is determined to be 3.58.

Similar calculation was performed for the closed isomer (S)-DTE-BPA-[open]-**120c**.

Details of calculations are summarized below.

#### Gas phase calculation for most 10 stable conformers of (S)-DTE-BPA-[closed]

In case of closed isomer of **DTE-120**, the rigidity of the isomer leads to a decrease in the number of possible conformations. That is, 291 conformers were possible for open isomer **120o** whereas 23 conformers were only possible for closed isomer **120c**. From that the most stable 10 isomers were selected for further preliminary energy calculations.

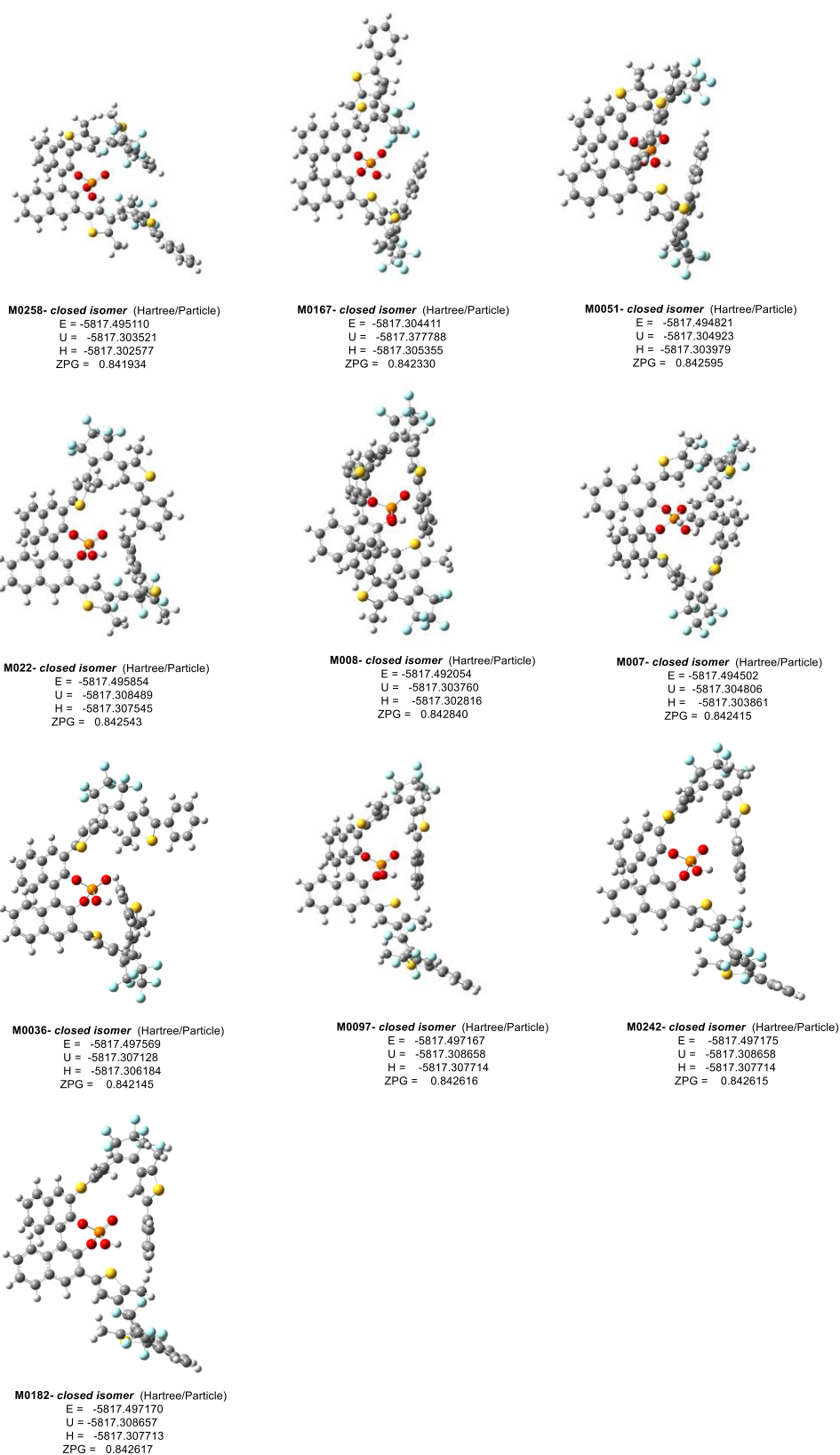


**Figure 36.** Gas phase calculation for most 10 stable conformers of (S)-DTE-BPA-[closed]

## Energy difference between most stable conformer with other lowest energy conformers in gas phase

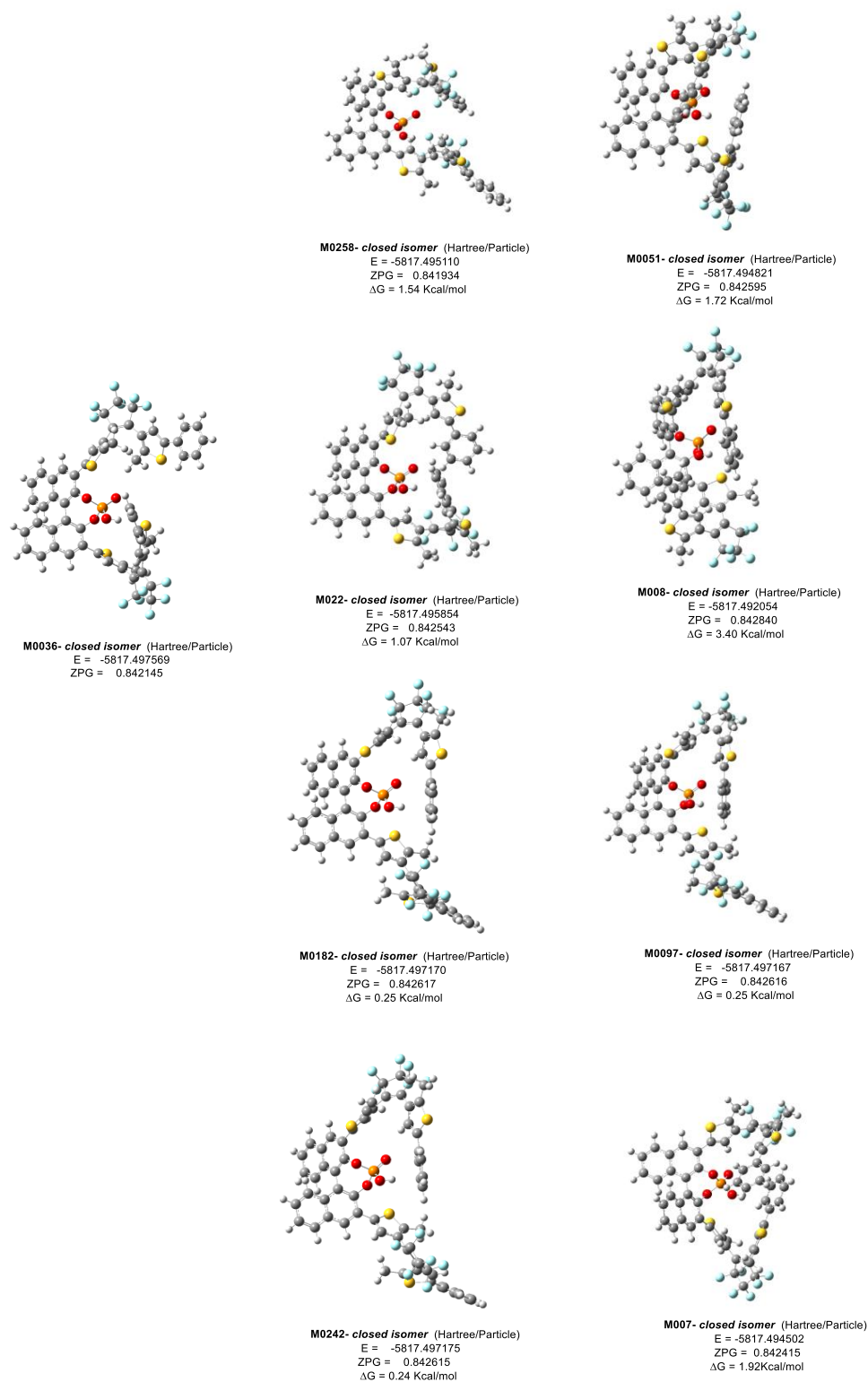


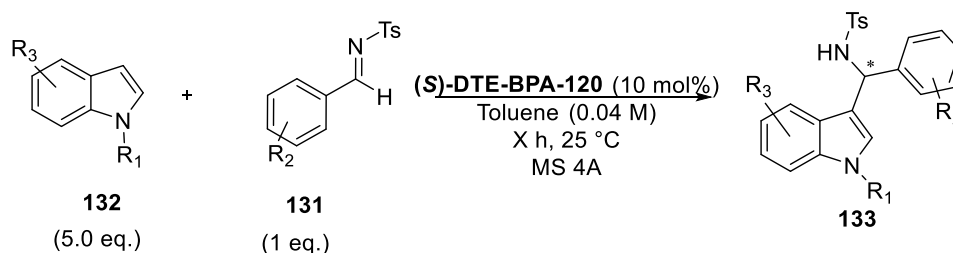
**Figure 37.** Gibbs free energy in gas phase for the most stable conformer with other lowest energy conformers of (S)-DTE-BPA-[closed]120c.

I expect that, the increased conjugation in the cyclopentene thiophene junction can significantly affect the pK<sub>a</sub> value of (*S*)-DTE-BPA catalyst upon photochemical ring closing.

### 3-9. Application of DTE-BPA-120 towards enantioselective aza-Friedel-Craft reaction

The photoisomerization ability and pK<sub>a</sub> modular ability through photochemical isomerization of our newly designed photoresponsive Brønsted acid catalyst (*S*)-DTE-BPA **120** prompted us to further examine their modulation behavior in catalytic activity as well as asymmetric induction ability with and without photoirradiation. I investigated modulation ability of (*S*)-DTE-BPA **120** to aza-Friedel crafts reaction of indoles (**130 a**) with aldimine (**131a**) (Table 13).

**Table 13.** Preliminary results for enantioselective aza-Friedal craft reaction



entry	<b>132</b>	<b>131</b>	time (h)	catalyst	yield <b>133</b> (%)	ee (%)
1	<b>132a</b>	<b>131a</b>	2	<b>120o</b>	30	40
2	(R <sup>1</sup> = H)	(R <sup>2</sup> = H)	2	<b>120c</b>	35 $\nearrow$ +5%	62 $\nearrow$ +22%
3	<b>132a</b>	<b>131b</b>	4	<b>120o</b>	42	18
4	(R <sup>1</sup> = H)	(R <sup>2</sup> = Cl)	4	<b>120c</b>	70 $\nearrow$ +28%	50 $\nearrow$ +32%
5	<b>132b</b>	<b>131c</b>	1.5	<b>120o</b>	37	38
6	(R <sup>1</sup> = Me)	(R <sup>2</sup> = Me)	1.5	<b>120c</b>	71 $\nearrow$ 34%	69 $\nearrow$ +31%

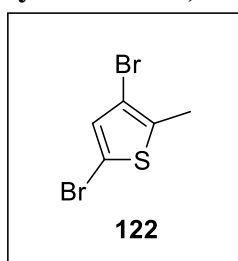
An initial catalyst loading of 10 mol% of DTE-BPA-**120** was applied to the enantioselective aza-Friedel-Craft reaction of indole **132a** with tosylimine **131a**, no remarkable different reactivity was observed with (entry 2, 35% yield) and without photoirradiation (entry 1, 30% yield). However, the enantioselectivity of product **133a** was enhanced in presence of 365 nm light irradiation (40 vs 62% ee). Also when I applied much reactive *p*-Cl-tosylimine **131b**, both the yield (42% vs 70%) and ee (18% vs 50%) of product significantly improved under UV light of 365 nm. Next, I tested Me-

protected 1-H indole **132 b** with **131b**, resulted in a much higher modulation in yield (37% vs 71%) and enantioselectivity (38% vs 69%) of the product. These preliminary results suggest that the catalyst is able to modulate the enantioselective aza-Friedel-Craft reaction in response to the light. The ring closed isomeric form can provide a better chiral environment than ring open isomer of **120**.

### 3-10. Experimental section

#### Synthesis procedure for the Dithienyl BINOL based photoswitchable catalysts DTE-BINOL-129 and DTE-BPA-120

##### Synthesis of 3,5-dibromo-2-methylthiophene (**122**)

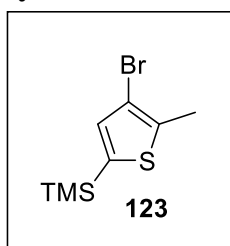


To a solution of 1.00 g (10.19 mmol) of 2-methylthiophene in glacial acetic acid (20 mL), 3.63 g (20.37 mmol) of NBS was added in portion. Then, the reaction mixture was stirred at room temperature for 48 h. After that the crude mixture was extracted with DCM and the organic phase was washed with 1 M aqueous NaOH (200 mL). The organic phase was collected, dried over Na<sub>2</sub>SO<sub>4</sub> and the solvent was removed *in vacuo* to afford the product **2** in 99 % yield (2.59 g) as yellow liquid. If trace amount of impurities is there, column chromatography can be performed with hexane as eluent. Spectroscopic data agree with those reported in the literature.<sup>[74,75]</sup>

<sup>1</sup>H NMR (400 MHz, CDCl<sub>3</sub>): δ 6.86 (s, 1 H), 2.34 (s, 3 H).

##### Stepwise synthesis from **122** to **124**

##### Synthesis of 3-bromo-2-methyl-5-trimethylsilylthiophene (**123**)

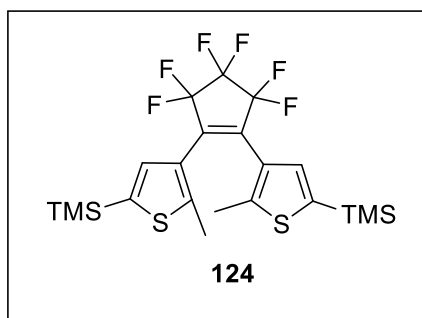


A dry THF solution (13.0 mL) of **122** (3.2 mmol, 0.770 g) in a flame-dried two-neck round bottom flask with a magnetic stirrer bar was degassed with nitrogen for 5 minutes and kept under nitrogen atmosphere at -78 °C. *n*-BuLi (1.60 mol/L in *n*-hexane, 3.33 mmol) was added dropwise *via* nitrogen flushed needle and the solution turned yellow. The mixture was then stirred for 1.5 hours at -78 °C, followed by slow addition of trimethylsilyl chloride (7.56 mmol, 0.97 mL) *via* syringe. After further 2.5 hours of stirring at -78 °C, the solution was allowed to cool to 22 °C. The reaction mixture was quenched by adding aqueous saturated solution of NH<sub>4</sub>Cl and then poured into water, and the organic layer was separated and extracted with chloroform (3 × 10.0 mL). The organic layer was dried over Na<sub>2</sub>SO<sub>4</sub> and concentrated under vacuum. The crude mixture was separated using silica gel column chromatography with *n*-hexane as the eluent to afford **123** as a colorless clear liquid (0.590 g, 79%). Spectroscopic data agree with those reported in the literature.<sup>[75]</sup>

<sup>1</sup>H NMR (400 MHz, CDCl<sub>3</sub>): δ 7.02 (s, 1 H), 2.42 (s, 3 H), 0.29 (s, 9 H).



### Synthesis of 1,2-bis(2'-methyl-5'-trimethylsilylthien-3'-yl)hexafluorocyclopent-1-ene (**124**).

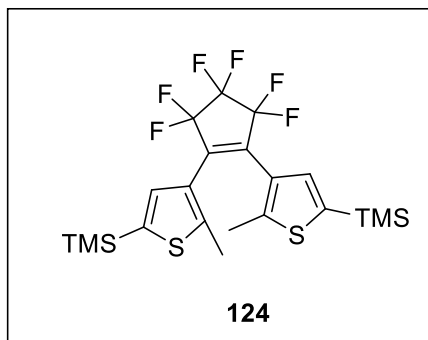


A dry THF solution (22.0 mL) of **123** (2.45 mmol, 0.610 g) in a flame-dried two-neck round bottom flask with a magnetic stirrer bar was degassed with nitrogen for 5 minutes and kept under nitrogen atmosphere at 78 °C. The mixture was stirred and added *n*-BuLi (0.160 mol/L in *n*-hexane, 2.69 mmol) dropwise *via* syringe under nitrogen atmosphere. The mixture was then stirred at -78°C for 2 h. Next octafluorocyclopentene (1.10 mmol, 0.15 mL) in

THF (1.0 mL) was added at -78°C slowly *via* syringe. After addition of octafluorocyclopentene, the reaction mixture turned to a red-brownish color. The solution was then stirred at -78°C for 4 h and the solution was stirred for another 24 h at room temperature. Then, the reaction was quenched with aqueous saturated solution of NH<sub>4</sub>Cl and then poured into water, and the organic layer was separated and extracted with chloroform (3 × 10.0 mL). The organic layer was dried using Na<sub>2</sub>SO<sub>4</sub> and concentrated under vacuum. And the crude mixture residue was purified using silica gel column chromatography with *n*-hexane as the eluent to afford **124** as a white solid (0.4210 g, 65%). Spectroscopic data agree with those reported in the literature.<sup>[76]</sup>

<sup>1</sup>H NMR (400 MHz, CDCl<sub>3</sub>): δ 7.05 (s, 2 H), 1.91 (s, 6 H), 0.27 (s, 18 H).

### One pot synthesis from **122** to **124**



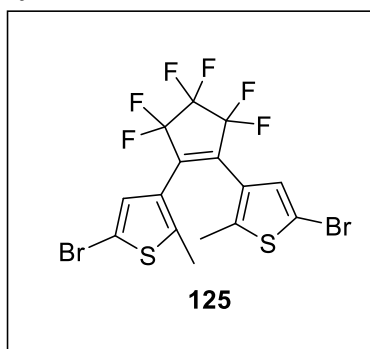
To a solution of 1.00 g (3.91 mmol) of 3,5-dibromo-2-methylthiophene (**122**) in a flame dried round bottom flask under inert atmosphere, added 4 mL of THF at kept at -78 °C. Then added *n*-BuLi (2.34 mL, 4.69 mmol, 2 M in *n*-hexane) dropwise over 10 minutes and allowed to stir for 1 h. Next TMSCl (425 mg, 3.91 mmol) was added and allowed to stir at 0 °C for another 1 h. The solution was again brought to -78 °C and another 2.34 mL of *n*-BuLi

was added and keep the reaction at -40 °C for 1.5 h. Again, the temperature is dropped to -78 °C followed by fast addition of perfluorocyclopent-1-ene (414 mg, 0.262 mL, 1.95 mmol) and the reaction is kept overnight at 0 °C. After the completion of reaction, the crude solution was quenched with water and was extracted with EtOAc and the organic phase was collected dried over Na<sub>2</sub>SO<sub>4</sub> and the solvent was removed *in vacuo* and purified by silica gel column chromatography with *n*-hexane as eluent to afford the product **124** in 49% yield.<sup>[77]</sup>

<sup>1</sup>H NMR (400 MHz, CDCl<sub>3</sub>): δ 7.05 (s, 2 H), 1.91 (s, 6 H), 0.27 (s, 18 H).



### Synthesis of **125**



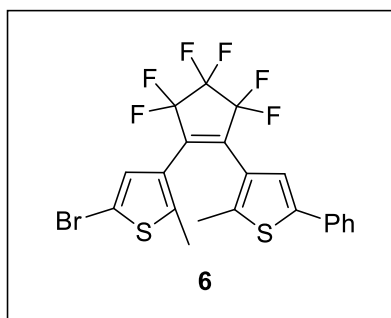
A solution of **124** (1.05 g, 2.05 mmol) and NBS (0.802 g, 4.50 mmol) in THF (16 mL) were placed in a flame dried round-bottom flask with a magnetic stirrer bar. The mixture was covered with aluminium foil and stirred for 3 h in an ice-water bath under nitrogen atmosphere. Then, the reaction was stirred overnight at room temperature and quenched with acetone (1.2 mL). After evaporation of the solvent, the mixture was washed with brine and extracted with chloroform. The organic layer was then

dried over anhydrous  $\text{Na}_2\text{SO}_4$  and the solvent was removed *in vacuo* and the crude product was purified by column chromatography on silica gel with petroleum ether or hexane as an eluent to afford a pale-pink powder (0.991 g, 92 %). Spectroscopic data agree with those reported in the literature.<sup>[77]</sup>

$^1\text{H}$ -NMR (400 MHz,  $\text{CDCl}_3$ )  $\delta$  7.01 (s, 2H), 1.89 (s, 6H).

$^{13}\text{C}$ -NMR (100 MHz,  $\text{CDCl}_3$ )  $\delta$  143.4, 129.1, 125.3, 110.1, 14.5.

### Synthesis of 1,2-bis(2-methyl-5-phenyl-3-thienyl)perfluorocyclopentene (**126**)

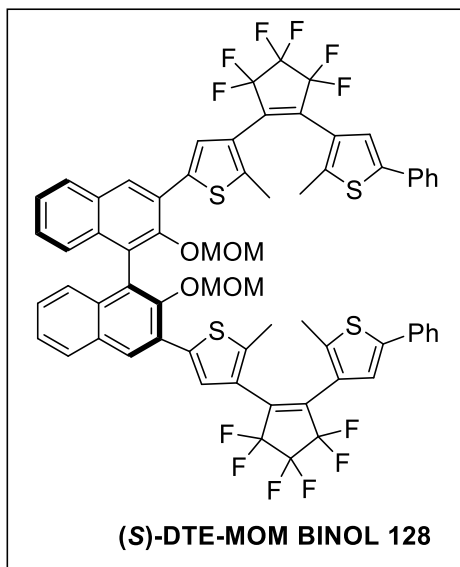


Compound **125** (2.00 g, 3.80 mmol) and phenylboronic acid (1.02 g, 8.36 mmol) were placed into a 100 mL two-necked round-bottom flask under nitrogen atmosphere. A solution of toluene (40 mL) and  $\text{K}_2\text{CO}_3$  aqueous solution (10 mL, 2.0 M) were added to the flask and the solution was degassed with nitrogen for 10 min, followed by addition of  $\text{Pd}(\text{PPh}_3)_4$  (0.22 g, 0.19 mmol). The reaction mixture was covered with aluminium foil and stirred at 85 °C for 48 h under a

nitrogen atmosphere. After warming to room temperature, the toluene was evaporated under reduced pressure and the remaining crude mixture was extracted with DCM and washed with brine. The organic layer was dried over  $\text{Na}_2\text{SO}_4$  and the solvent was evaporated under *vacuo*. The crude product was purified by column chromatography on silica gel with hexane as an eluent to afford a pale-blue powder (1.44 g, 73 %). Spectroscopic data agree with those reported in the literature.<sup>[77]</sup>

$^1\text{H}$ -NMR (400 MHz,  $\text{CDCl}_3$ )  $\delta$  7.52-7.54 (d, 2H), 7.37-7.40 (t, 2H), 7.31 (t,  $J = 7.1$ , 1.1 Hz, 1H), 7.24 (s, 1H), 7.06 (s, 1H), 1.96 (s, 3H), 1.88 (s,  $J = 0.9$  Hz, 3H).

## Synthesis of (S)-DTE-MOM BINOL 128



To a solution of compound **126** (270 mg, 0.52 mmol, 1.0 eq.) in 1,4-dioxane (0.37 M, 1.4 mL) kept under nitrogen atmosphere in a round bottom flask with a magnetic stirrer bar was added with boronic acid ester **127** (147 mg, 0.24 mmol, 0.46 eq.),  $K_2CO_3$  aq (2 M, 0.2 mL). The solution was then degassed under nitrogen for 10 minutes. Next  $(PPh_3)_4$  (27.0 mg, 0.02 mmol, 10 mol%) was added to the solution and stirred for 28 h at 90 °C. After the starting material consumption from TLC, sat.  $NH_4Cl$  aq (2.0 mL) was poured into the flask and extraction was performed by EtOAc. The collected organic layer was dried over  $Na_2SO_4$ . After filtration, concentrated residue was purified using column chromatography (*n*-hexane as

eluent system) to afford the desired product **(S)-DTE 128** (243 mg, 81% yield) as blue solid as blue solid.

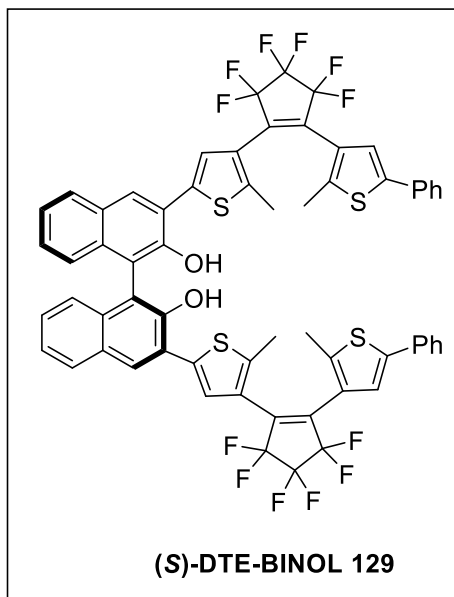
$^1H$ -NMR (400 MHz,  $CDCl_3$ )  $\delta$  8.12 (s, 2H), 7.88 (d,  $J$  = 8.2 Hz, 2H), 7.61 (s, 2H), 7.54 (d,  $J$  = 7.8 Hz, 4H), 7.45-7.22 (m, 14H), 4.54 (dd,  $J$  = 53.8, 5.3 Hz, 4H), 2.45 (s, 6H), 2.04 (d,  $J$  = 5.5 Hz, 12H).

$^{13}C$ -NMR (125 MHz,  $CDCl_3$ )  $\delta$  151.1, 150.3, 149.7, 148.4, 143.0, 142.6, 142.5, 141.5, 141.3, 138.1, 137.7, 137.6, 137.1, 136.5 (t,  $^2J_{CF}$  = 19.12 Hz,  $CF_2C=CCF_2$ ), 136.4 (t,  $^2J_{CF}$  = 19.12 Hz,  $CF_2C=CCF_2$ ), 133.8, 133.4, 132.7, 130.9, 129.5, 129.4, 129.2, 128.7, 128.1, 127.4, 127.0, 126.8, 126.6, 126.4, 126.1, 125.9, 125.7, 125.5, 125.1, 124.1, 122.7, 116.4 (t,  $^1J_{CF}$  = 211.8 Hz, t,  $^2J_{CF}$  = 19.25 Hz,  $CF_2CF_2CF_2$ , and  $CF_2CF_2CF_2$ ), 117.5, 111.3 (t,  $^1J_{CF}$  = 225.0 Hz, quint,  $^2J_{CF}$  = 21.5 Hz,  $CF_2CF_2CF_2$ ), 112.0, 111.6, 111.5, 111.3, 111.1, 111.0, 109.8, 109.7, 109.5, 109.4, 109.2, 98.6 (OCH<sub>2</sub>OMe), 60.3, 56.1 (OMe), 20.7, 14.7, 14.6, 14.5, 14.3.

HRMS (APCI) calcd for  $C_{66}H_{46}F_{12}O_4S_4$ :  $m/z$  ( $[M+H]^+$ ) 1258.21, found 1256.21

IR (KBr) 3064, 2961, 2924, 1737, 1601, 1551, 1499, 1440, 1336, 1272, 1190, 1055, 987, 901, 753  $cm^{-1}$

### 3-10-2-7. Synthesis of (S)-DTE 129



To a solution of compound **128** (243 mg, 0.19 mmol, 1.0 eq.) in a round bottom flask kept under nitrogen atmosphere in dry dichloromethane (0.01M, 17 mL), trifluoroacetic acid (TFA) (433 mg, 3.8 mmol, 20 eq.) was slowly added at 0 °C and brought to rt. The solution was continued stirring for 18 h at rt. After evaporation of solvent, water was added and the organic phase was collected after separation, dried over Na<sub>2</sub>SO<sub>4</sub> and the residue was purified by column chromatography (hexane/DCM = 7:3) to afford the product **(S)-DTE 129** (203 mg, 91% yield) as blue solid.

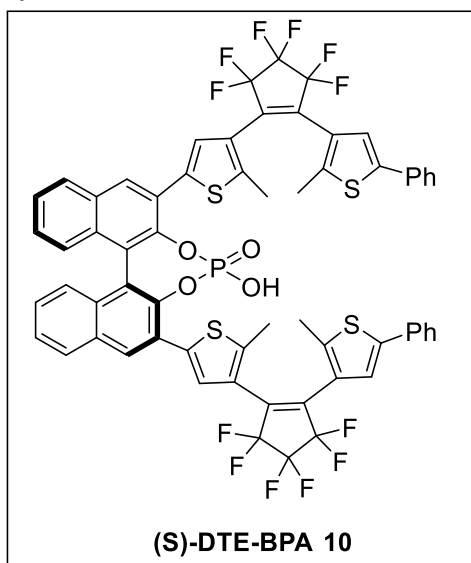
<sup>1</sup>H-NMR (400 MHz, CDCl<sub>3</sub>) δ 8.22 (s, 2H), 7.90 (d, J = 7.8 Hz, 2H), 7.71 (s, 2H), 7.53 (d, J = 7.3 Hz, 4H), 7.42-7.28 (m, 12H), 7.12 (d, J = 8.2 Hz, 2H), 5.55 (s, 2H), 2.00 (d, J = 2.3 Hz, 12H).

<sup>13</sup>C-NMR (125 MHz, CDCl<sub>3</sub>) δ 149.6, 142.6, 142.4, 141.5, 137.0, 136.5 (t, <sup>2</sup>J<sub>CF</sub> = 20.25 Hz, CF<sub>2</sub>C=CCF<sub>2</sub>), 136.3 (t, <sup>2</sup>J<sub>CF</sub> = 19.12 Hz, CF<sub>2</sub>C=CCF<sub>2</sub>), 133.5, 132.6, 129.5, 129.3, 129.2, 128.7, 128.1, 126.7, 126.0, 125.7, 125.5, 125.1, 124.1, 122.6, 122.6, 116.4 (t, <sup>1</sup>J<sub>CF</sub> = 211.8 Hz, t, <sup>2</sup>J<sub>CF</sub> = 20.25 Hz, CF<sub>2</sub>CF<sub>2</sub>CF<sub>2</sub>, and CF<sub>2</sub>CF<sub>2</sub>CF<sub>2</sub>), 111.9, 111.3 (t, <sup>1</sup>J<sub>CF</sub> = 225.0 Hz, quint, <sup>2</sup>J<sub>CF</sub> = 20.4 Hz, CF<sub>2</sub>CF<sub>2</sub>CF<sub>2</sub>), 31.8, 29.9, 22.8, 14.8, 14.5, 14.2.

HRMS (APCI) calcd for C<sub>62</sub>H<sub>38</sub>F<sub>12</sub>O<sub>2</sub>S<sub>4</sub>: m/z ([M+H]<sup>+</sup>) 1171.1720, found 1171.1636

IR (KBr) 3500, 3060, 2920, 2852, 1722, 1598, 1502, 1433, 1358, 1337, 1272, 1192, 1138, 1118, 1054, 986, 891, 750 cm<sup>-1</sup>.

### Synthesis of (S)-DTE-BPA 120



To a solution of compound **129** (203 mg, 0.17 mmol, 1.0 eq.) in pyridine (0.5 mL) was slowly added POCl<sub>3</sub> (65.9 mg, 0.43 mmol, 2.5 eq.) at rt. The solution was stirred for 12 h at 95 °C. Next water (1.0 mL) was added to the solution and stirred for another 6 h at 95 °C. Then, HCl aq (1M, 2 mL) was poured into the flask and extracted with EtOAc. The collected organic layer was dried over Na<sub>2</sub>SO<sub>4</sub>. After filtration, concentrated residue was purified over column chromatography (hexane/EtOAc = 3/1) to give the product **(S)-DTE 120** (161 mg, 77% yield) as blue solid.

<sup>1</sup>H-NMR (400 MHz, CDCl<sub>3</sub>) δ 8.26 (s, 2H), 7.95 (d, J = 8.2 Hz, 2H), 7.55 (s, 2H), 7.51-7.46 (m,

2H), 7.36 (d,  $J = 7.6$  Hz, 2H), 7.19 (s, 12H), 7.14 (s, 2H), 5.76 (br, 1H), 1.72 (d,  $J = 11.4$  Hz, 12H).

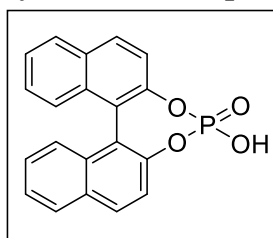
$^{13}\text{C}$ -NMR (125 MHz,  $\text{CDCl}_3$ )  $\delta$  145.6, 145.5, 144.3, 142.8, 142.2, 141.9, 141.6, 137.2, 136.1 (t,  $^2J_{\text{CF}} = 18.0$  Hz,  $\text{CF}_2\text{C}=\text{CCF}_2$  and  $\text{CF}_2\text{C}=\text{CCF}_2$ ), 133.4, 132.2, 131.0, 129.1, 128.4, 128.0, 126.9, 126.7, 126.5, 126.3, 126.1, 125.8, 125.7, 125.6, 125.0, 123.6, 122.2, 116.34 (t,  $^1J_{\text{CF}} = 211.8$  Hz, t,  $^2J_{\text{CF}} = 19.12$  Hz,  $\text{CF}_2\text{CF}_2\text{CF}_2$ ), 116.26 (t,  $^1J_{\text{CF}} = 211.9$  Hz, t,  $^2J_{\text{CF}} = 19.12$  Hz,  $\text{CF}_2\text{CF}_2\text{CF}_2$ ), 111.2 (t,  $^1J_{\text{CF}} = 223.8$  Hz, quint,  $^2J_{\text{CF}} = 20.3$  Hz,  $\text{CF}_2\text{CF}_2\text{CF}_2$ ), 60.5, 29.8, 21.1, 14.7, 14.3.

$^{31}\text{P}$ -NMR (189 MHz,  $\text{CDCl}_3$ )  $\delta$  4.61.

HRMS (APCI) calcd for  $\text{C}_{62}\text{H}_{37}\text{F}_{12}\text{O}_4\text{PS}_4$ :  $m/z$  ( $[\text{M}+\text{H}]^+$ ) 1233.1193, found 1233.1198.

IR (KBr) 3064, 2957, 2922, 2853, 2364, 2345, 1335, 1269, 1189, 1115, 1048, 1021, 985, 952, 894, 751  $\text{cm}^{-1}$ .

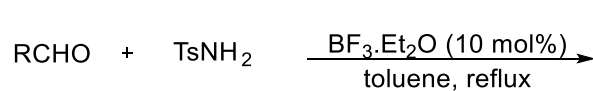
### Synthesis of *rac*-phosphoric acid catalyst 130



To a solution of *rac*-BINOL (286 mg, 1 mmol, 1.0 eq.) in pyridine (2.9 mL) was slowly added  $\text{POCl}_3$  (329 mg, 0.43 mmol, 2.5 eq.) at rt. The solution was stirred for 12 h at 95 °C. Next water (6.0 mL) was added to the solution and stirred for another 6 h at 95 °C. Then, HCl aq (1M, 1 mL) was poured into the flask and extracted with EtOAc. The collected organic layer was dried over  $\text{Na}_2\text{SO}_4$ . After filtration, concentrated residue was purified

over column chromatography (*n*-hexane/EtOAc = 3:1) to give the *rac*-phosphoric acid catalyst (161 mg, 77% yield) as white solid. <sup>[79]</sup>

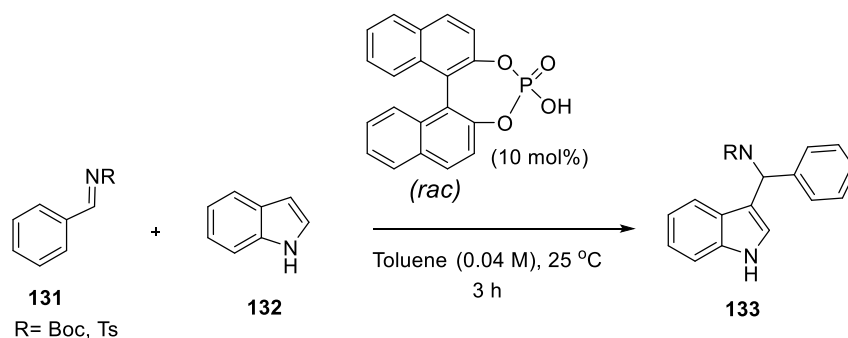
### General procedure for the preparation of aldimines<sup>[78]</sup>



To a 100 mL screw-top pressure reaction tube with a magnetic stirring bar were

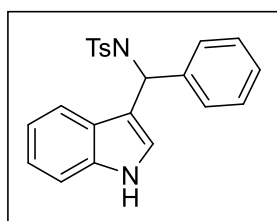
added aldehyde (1.1 equiv), *p*-toluenesulfonamide (1.0 equiv), boron trifluoride etherate (10 mol%) and toluene under nitrogen atmosphere. The reaction mixture was heated at 120 °C (an oil bath) for 12 h. After cooling to room temperature, it was concentrated under reduced pressure, purified by recrystallization using *n*-hexane/DCM.

### General procedure for the racemic aza-Friedel-Craft reaction



Reaction setup

A well flame dried round bottom flask with a magnetic stirrer bar was kept under vacuum followed by 3 times flushing under nitrogen atmosphere. 4A molecular sieves were added to the tube and maintained the flask under nitrogen atmosphere. Then, corresponding imine **131** was added (1 mmol, 1.0 eq.) followed by 25 mL (0.04 M) toluene at 25 °C. Next 1H-indole **132** (5 mmol, 5.0 eq.) and catalyst (10 mol%, 0.1 eq.) was added to the flask and allowed to stir for 3 h. The reaction was quenched with NaHCO<sub>3</sub> and extracted with EtOAc (1 mL x 3 times) and organic phase was collected and dried over Na<sub>2</sub>SO<sub>4</sub>, followed by concentration under reduced pressure to afford desired product. <sup>[78]</sup>



White solid; <sup>1</sup>H-NMR (400 MHz, CDCl<sub>3</sub>)  $\delta$  7.98 (s, 1H), 7.57 (d,  $J$  = 8.2 Hz, 2H), 7.31 (d,  $J$  = 7.8 Hz, 1H), 7.22 (m,  $J$  = 9.6, 3.7 Hz, 6H), 7.12 (d,  $J$  = 8.2 Hz, 2H), 7.00 (s, 1H), 6.69 (d,  $J$  = 2.3 Hz, 1H), 5.86 (d,  $J$  = 6.4 Hz, 1H), 5.02 (s, 1H), 2.37 (s, 3H); HPLC (Chiracel OD-H, iPrOH/hexane = 30/70, 0.6 mL/min, 254 nm)  $t_1$  = 17.5 min (minor),  $t_2$  = 30.3 min (major).

## Chapter 4. Summary

In the chapter 2, I report the development of a novel asymmetric cation binding catalysis using azobenzene decorated BINOL-based oligoethylene glycols. Photo-responsiveness of the catalyst was demonstrated by employing towards the enantioselective synthesis of hemi-aminal products from amidosulfone and nitrogen nucleophiles. I observed high yields and good enantioselectivity of desired products upon exposure to a 365nm light source affording the *Z*-isomer of the azobenzene unit. In contrast, the *E*-isomer of catalyst hinders the reaction progress. Modified catalysts were prepared to investigate the role of functional groups on the catalyst backbone and it is evident that the directional effects on the azobenzene linker and chain length of catalyst were found to be important for asymmetric induction. Moreover, the terminal hydrogen bonding donor (phenols) were critical to obtain high yield and enantioselectivity due to the extra stabilization of the substrate inside the chiral cation cage.

In the chapter 3, dithienyl hexafluorocyclopentene was used as the photoresponsive site and a BINOL derived photoresponsive phosphoric acid were synthesized for asymmetric catalysis. This novel catalyst possesses two dithienyl hexafluorocyclopenteneframework at the 3,3'-position of BINOL backbone which creates a reaction field surrounded by them and acts as an acid catalyst. I was able to efficiently synthesize BINOL derived photoresponsive phosphoric acid catalysts. The newly developed ligand attained a PSS of 69% after 365 nm photoirradiation which can be completely isomerized back to the *E* form with 631 nm visible light without any decomposition. The photoisomerization process was confirmed by NMR as well UV-vis spectroscopy.

It was also confirmed by the spectrum that the ring closure was a mixture of multiple isomers. The open isomer showed absorption in the ultraviolet and the closed body showed absorption in the visible region. These features have realized reversible photoisomerization of catalyst. Moreover, photoswitchable catalyst is able to photomodulate the enantioselective aza-Friedel-Craft reaction. The ring-closed isomer showed high yield and enantioselectivity in contrast to open isomer of catalyst. This is because, the asymmetric reaction field in the ring closure undergoes an efficient steric effect due to the two dithienyl hexafluorocyclopentenenes, and the high acidity of the ring closure causes stronger intermolecular interactions. Furthermore, the fact that relatively high enantioselectivity was obtained in the Me -substituted indole on N in the Aza Friedel-Crafts reaction was a very interesting result, demonstrating the usefulness of the asymmetric reaction field of this new catalyst.

## Chapter 5. References

1. For reviews on molecular machines see: (a) Watson, M. A.; Cockcroft, S. L. *Chem. Soc. Rev.* **2016**, *45*, 6118–6129. (b) Kassem, S.; Leeuwen, T. V.; Lubbe, A. S.; Wilson, M. R.; Feringa, B. L.; Leigh, D. A. *Chem. Soc. Rev.* **2017**, *46*, 2592–2621. (c) Aprahamian, I. *ACS Cent. Sci.* **2020**, *6*, 347–358.
2. For reviews and selected publications on directed evolution of enzyme and their non-natural reactivities, see: (a) Strohmeier, G. A.; Pichler, H.; May, O.; Gruber-Khadjawi, M. *Chem. Rev.* **2011**, *111*, 4141–4164. (b) Reetz, M. T. *Angew. Chem. Int. Ed.* **2011**, *50*, 138–174. (c) Hyster, T. K.; Farwell, C. C.; Buller, A. R.; McIntosh, J. A.; Arnold, F. H. *J. Am. Chem. Soc.* **2014**, *136*, 15505–15508. (d) Hyster, T. K.; Ward, T. R. *Angew. Chem. Int. Ed.* **2016**, *55*, 7344–7357. (e) Zhang, R. K.; Chen, K.; Huang, X.; Wohlschlager, L.; Renata, H.; Arnold, F.H. *Nature*, **2019**, *565*, 67–72.
3. For reviews and selected publications on ppm level loading catalyst, see: (a) Park, S. Y.; Lee, J. W.; Song, C. E. *Nat. Commun.* **2015**, *6*, 7512. (b) Roy, D.; Uozumi, Y. *Adv. Synth. Catal.* **2018**, *360*, 602–625. (c) Bae, H. Y.; Hofler, D.; Kaib, P. S. J.; Butchers, P.; De, C.K.; Döhring, A.; Lee, S.; Kaupmees, K.; Leito, I.; List, B. *Nat. Chem.* **2018**, *10*, 888–894. (c) Zhang, Y.; Takale, B. S.; Gallou, F.; Reilly, J.; Lipshutz, B. H. *Chem. Sci.* **2019**, *10*, 10556–10561.
4. (a) Dioumaev, V. K.; Bullock, R. M. *Nature* **2003**, *424*, 530–532 (b) Benaglia, M. *New J. Chem.* **2006**, *30*, 1525–1533. (c) Molnár, A.; Papp, A. *Coord. Chem. Rev.* **2017**, *349*, 1–65.
5. For reviews and selected publications on enantiodivergent catalysts, see: (a) Macharia, J.; Wambua, V.; Hong, Y.; Harris, L.; Hirschi, J. S.; Evans, G. B.; Vetticatt, M. J. A. *Angew. Chem. Int. Ed.* **2017**, *56*, 8756–8760. (b) Beletskaya, I. P.; Najera, C.; Yus, M. *Chem. Rev.* **2018**, *118*, 5080–5200. (c) Dai, J.; Wang, Z.; Deng, Y.; Zhu, I.; Peng, F.; Lan, Y.; Shao, Z. *Nat. Commun.* **2019**, *10*, 5182.
6. For reviews on immobilized catalysts in flow system, see: (a) Yamada, Y. M. A. *Chem. Pharm. Bull.* **2017**, *65*, 805–821.
7. Cacciapaglia, R.; Di Stefano, S.; Mandolini, L. *J. Am. Chem. Soc.* **2003**, *125*, 2224–2227.
8. Shinkai, S.; Ishikawa, Y.; Shinkai, H.; Tsuno, T.; Makishima, H.; Ueda, K.; Manabe, O. *J. Am. Chem. Soc.* **1984**, *106*, 1801–1808.
9. Blanco, V.; Leigh, D. A.; Marcos, V.; Morales-Serna, J. A.; Nussbaumer, A. L. *J. Am. Chem. Soc.* **2014**, *136*, 4905.
10. Beswick, J.; Blanco, V.; De Bo, G.; Leigh, D. A.; Lewandowska, U.; Lewandowski, B.; Mishiro, K. *Chem. Sci.* **2015**, *6*, 140–143.
11. (a) Birnbaum, P. P.; Linford, J. H.; Style, D. W. G. *Trans. Faraday. Soc.* **1953**, *49*, 735–744. (b) Gegiou, D.; Muszkat, K. A.; Fischer, E. *J. Am. Chem. Soc.* **1968**, *90*, 3907–3918. (c) Waldeck, D. H. *Chem. Rev.* **1991**, *91*, 415–436. (d) Bandara, H. M. D.; Burdette, S. C. *Chem. Soc. Rev.* **2012**, *41*, 1809–1825.
12. Sugimoto, H.; Kimura, T.; Inoue, S. *J. Am. Chem. Soc.*, **1999**, *121*, 2325.
13. Kean, Z. S.; Akbulatov, S.; Tian, Y.; Widenhoefer, R. A.; Boulatov, R.; Craig, S. L. *Angew. Chem. Int. Ed.* **2014**, *53*, 14508–14511.
14. Koumura, N.; Zijlstra, R. W. J.; Van Delden, R. A.; Harada, N.; Feringa, B. L. *Nature* **1999**, *401*, 152–155.
15. (a) Irie, M.; Mohri, M. *J. Org. Chem.* **1988**, *53*, 803–808. (b) Nakamura, S.; Irie, M. *J. Org. Chem.* **1988**, *53*, 6136–6138. (b) Nakamura, S.; Irie, M. *J. Org. Chem.* **1988**,

- 53, 6136–6138. (c) Irie, M.; Fukaminato, T.; Matsuda, K.; Kobatake, S. *Chem. Rev.* **2014**, *114*, 12174–12277.
16. Sud, D.; Norsten, T. B.; Branda, N. R. *Angew. Chem. Int.* **2005**, *44*, 2019–2021.
17. Neilson, B. M.; Bielawski, C. W. *J. Am. Chem. Soc.* **2012**, *134*, 12693–12699.
18. Iida, H.; Umebayashi, N.; Yashima, E. *Tetrahedron* **2013**, *69*, 11064–11069.
19. Würthner, F.; Rebek, J. *Angew. Chem., Int. Ed. Engl.* **1995**, *34*, 446.
20. Samanta, M.; Krishna, V. S. R.; Bandyopadhyay, S. *Chem. Commun.* **2014**, *50*, 10577.
21. Arif, T.; Cazorla, C.; Bogliotti, N.; Saleh, N.; Blanchard, F.; Gandon, V.; Métivier, R.; Xie, J.; Voituriez, A.; Marinetti, A. *Catal. Sci. Technol.* **2018**, *8*, 710.
22. Osorio-Planes, L.; Rodríguez-Esrich, C.; Pericàs, M. A. *Org. Lett.* **2014**, *16*, 1704.
23. Dai, Z.; Cui, Y.; Chen, C.; Wu, J. *Chem. Commun.*, **2016**, *52*, 8826.
24. (a) Peters, M. V.; Stoll, R. S.; Kühn, A.; Hecht, S. *Angew. Chem., Int. Ed.* **2008**, *47*, 5968. (b) Stoll, R. S.; Peters, M. V.; Kühn, A.; Heiles, S.; Goddard, R.; Bühl, M.; Thiele, C. M.; Hecht, S. *J. Am. Chem. Soc.* **2009**, *131*, 357.
25. Fu, W.; Pi, Y.; Gao, M.; Wang, W.; Li, C.; Tan, R.; Yin, D. *Chem. Commun.* **2020**, *56*, 5993–5996.
26. Kondo, M.; Nakamura, K.; Krishnan, C. G.; Takizawa, S.; Abe, T.; Sasai, H. *ACS Catal.* **2021**, *11*, 1863–1867.
27. Nakamura, K.; Kondo, M.; Krishnan, C. G.; Takizawa, S.; Sasai, H. *Chem. Commun.* **2021**, *57*, 7414.
28. (a) Lehn, J.-M. *Chem. – Eur. J.* **2006**, *12*, 5910. (b) Greb, L.; Lehn, J.-M. *J. Am. Chem. Soc.* **2014**, *136*, 13114. (c) Greb, L.; Eichhöfer, A.; Lehn, J.-M. *Angew. Chem., Int. Ed.* **2015**, *54*, 14345.
29. Aprahamian, I. *Chem. Commun.* **2017**, *53*, 6674.
30. de Bo, G.; Leigh, D. A.; McTernan, C. R.; Wang, S. *Chem. Sci.* **2017**, *8*, 7077.
31. Pedersen, C. J. *Angew. Chem. Int. Ed.* **1988**, *27*, 1021–1027.
32. (a) Paik, M.-J.; Kang, J. S.; Huang, B.-S.; Carey, J. R.; Lee, W. *J. Chromatogr. A* **2013**, *1274*, 1–5. (b) Lim, L. W.; Tokunaga, K.; Takeuchi, T. *Chromatography* **2014**, *35*, 95–101.
33. (a) Shiga, M.; Takagi, M.; Ueno, K. *Chem. Lett.* **1980**, *9*, 1021–1022. (B) Shinkai, S.; Minami, T.; Kusano, Y.; Manabe, O. *J. Am. Chem. Soc.* **1983**, *105*, 1851–1856.
34. Shinkai, S.; Nakaji, T.; Ogawa, T.; Shigematsu, K.; Manabe, O. *J. Am. Chem. Soc.* **1981**, *103*, 1851–1856.
35. Cacciapaglia, R.; Di Stefano, S.; Mandolini, L. *J. Am. Chem. Soc.* **2003**, *125*, 2224–2227.
36. Dolling, U.-H.; Davis, P.; Grabowski, E. J. J. *J. Am. Chem. Soc.* **1984**, *106*, 446–447.
37. Suzuki, H.; Sato, I.; Yamashita, Y.; Kobayashi, S. *J. Am. Chem. Soc.* **2015**, *137*, 4336–4339.
38. Yonezawa, K.; Patil, M. L.; Sasai, H.; Takizawa, S. *Heterocycles* **2005**, *66*, 639–644.
39. Brak, K.; Jacobsen, E. N. *Angew. Chem., Int. Ed.* **2013**, *52*, 534–561.
40. Bakó, P.; Vizvárdi, K.; Bajor, Z.; Tőke, L. *Chem. Commun.* **1998**, 1193–1194.
41. Bakó, T.; Bakó, P.; Keglevich, G.; Bombicz, P.; Kubinyi, M.; Pál, K.; Bodor, S.; Makó, A.; Tőke, L. *Tetrahedron; Asymmetry*. **2004**, *15*, 1589–1595.
42. (a) Lee, J.-W.; Yan, H.; Jang, H. B.; Kim, H. K.; Park, S.-W.; Lee, S.; Chi, D. Y.; Song, C. E. *Angew. Chem., Int. Ed.* **2009**, *48*, 7683–7686. (b) Paladhi, S.; Liu, Y.; Kumar, B. S.; Jung, M.-J.; Park, S. Y.; Yan, H.; Song, C. E. *Org. Lett.* **2017**, *19*,



- 3279–3282. (c) Park, S. Y.; Lee, J.-W.; Song, C. E. *Nat. Commun.* **2015**, *6*, 7512.
- (d) Li, L.; Liu, Y.; Peng, Y.; Yu, L.; Wu, X.; Yan, H. *Angew. Chem., Int. Ed.* **2016**, *55*, 331–335. (e) Tan, Y.; Luo, S.; Li, D.; Zhang, N.; Jia, S.; Liu, Y.; Qin, W.; Song, C. E.; Yan, H. *J. Am. Chem. Soc.* **2017**, *139*, 6431–6436. (f) Yan, H.; Jang, H. B.; Lee, J.-W.; Kim, H. K.; Lee, S. W.; Yang, J. W.; Song, C. E. *Angew. Chem. Int. Ed.* **2010**, *49*, 8915–8917. (g) Kweon, Y. K.; Jeong, Y. B.; Duan, M.; Tan, Y.; Lee, J.-W.; Yan, H.; Song, C. E. *Chem. -Eur. J.* **2018**, *24*, 1020–1025. (h) Park, S. Y.; Liu, Y.; Oh, J. S.; Kweon, Y. K.; Jeong, Y. B.; Duan, M.; Tan, Y.; Lee, J.-W.; Yan, H.; Song, C. E. *Chem. Eur. J.* **2018**, *24*, 1020–1025.
43. Krishnan, C. G.; Kondo, M.; Nakamura, K.; Sasai, H.; Takizawa, S. *Org. Lett.* **2022**, *24*, 2670.
44. Irie, M.; Mohri, M. *J. Org. Chem.* **1988**, *53*, 803–808.
45. Nakamura, S.; Irie, M. *J. Org. Chem.* **1988**, *53*, 6136–6138.
46. Irie, M.; Fukaminato, T.; Matsuda, K.; Kobatake, S. *Chem. Rev.* **2014**, *114*, 12174–12277.
47. Tian, H.; Wang, S. *Chem. Commun.* **2007**, 781–792.
48. Wilson, D.; Branda, N. R. *Angew. Chem., Int. Ed.* **2012**, *51*, 5431–5434.
49. Vomasta, D.; Högner, C.; Branda, N. R.; König, B. *Angew. Chem., Int. Ed.* **2008**, *47*, 7644–7647.
50. Kaur, B.; Raza, R.; Stashick, M. J.; Branda, N. R. *Org. Chem. Front.* **2019**, *6*, 1253–1256.
51. Faglioni, F.; Blanco, M.; Goddard, W. A.; Saunders, D. *J. Phys. Chem. B.* **2002**, *106*, 1714–1721.
52. Lewis, L. N.; Stein, J.; Colborn, R. E.; Gao, Y.; Dong, J. *J. Organomet. Chem.* **1996**, *521*, 221–227.
53. Xu, Z.; Cao, Y.; Patrick, B. O.; Wolf, M. O. *Chem. - Eur. J.* **2018**, *24*, 10315–10319.
54. Neilson, B. M.; Lynch, V. M.; Bielawski, C. W. *Angew. Chem., Int. Ed.* **2011**, *50*, 10322–10326.
55. Peris, E. *Chem. Rev.* **2018**, *118*, 9988–10031.
56. Vougioukalakis, G. C.; Grubbs, R. H. *Chem. Rev.* **2010**, *110*, 1746–1787.
57. Sutthasupa, S.; Shiotsuki, M.; Sanda, F. *Polym. J.* **2010**, *42*, 905–915.
58. Samachetty, H. D.; Lemieux, V.; Branda, N. R. *Tetrahedron.* **2008**, *64*, 8292–8300.
59. Neilson, B. M.; Bielawski, C. W. *J. Am. Chem. Soc.* **2012**, *134*, 12693–12699.
60. Grasa, G. A.; Kissling, R. M.; Nolan, S. P. *Org. Lett.* **2002**, *4*, 3583–3586.
61. Movassaghi, M.; Schmidt, M. A. *Org. Lett.* **2005**, *7*, 2453–2456.
62. Iida, H.; Umebayashi, N.; Yashima, E. *Tetrahedron.* **2013**, *69*, 11064–11069.
63. Bianchini, G.; Sorella, G. L.; Canever, N.; Scarso, A.; Strukul, G. *Chem. Commun.* **2013**, *49*, 5322–5324.
64. Eisenreich, F.; Kathan, M.; Dallmann, A.; Ihrig, S. P.; Schwaar, T.; Schmidt, B. M.; Hecht, S. *Nat. Catal.* **2018**, *1*, 516–522.
65. Yamaguchi, T.; Kamihashi, Y.; Ozeki, T.; Uyama, A.; Kitai, J.-i.; Kasuno, M.; Sumaru, K.; Kimura, Y.; Yokojima, S.; Nakamura, S.; Morimoto, M.; Uchida, K. *Bull. Chem. Soc. Jpn.* **2014**, *87*, 528–538.
66. Terada, M. *Bull. Chem. Soc. Jpn.* **2010**, *2*, 101–119.
67. Akiyama, T. *Chem. Rev.* **2007**, *107*, 5744.
68. Terada, M. *Synthesis* **2010**, 1929.
69. Parmar, D.; Sugiono, E.; Raja, S.; Rueping, M. *Chem. Rev.* **2014**, *114*, 9047.

70. For examples where no reaction is observed for structurally bulky catalysts see: (a) Saha, S.; Schneider, C. *Chem. Eur. J.* **2015**, *21*, 2348. (b) Lu, M.; Lu, Y.; Zhu, D.; Zeng, X.; Li, X.; Zhong, G. *Angew. Chem. Int. Ed.* **2010**, *49*, 8588; *Angew. Chem.* **2010**, *122*, 8770. (c) Wen, W.; Zheng, Y.; Li-Yu, P.; Li-Na, F.; Qi-Xang, G. *Org. Lett.* **2015**, *17*, 3922.
71. For examples where, large catalysts proceed with reversal in stereoinduction see: (a) Yu, X.; Wang, Y.; Wu, G.; Song, H.; Zhou, Z.; Tang, C. *Eur. J. Org. Chem.* **2011**, 3060. (b) Kang, Q.; Zhao, Z.-A.; You, S.-L. *Org. Lett.* **2008**, *10*, 2031. (c) Gu, Q.; Rong, Z.-Q.; Zheng, C.; You, S.-L. *J. Am. Chem. Soc.* **2010**, *132*, 4056. (d) Liao, S.; Coric, I.; Wang, Q.; List, B. *J. Am. Chem. Soc.* **2012**, *134*, 10765. (e) Feng, J.; Yan, W.; Wang, D.; Li, P.; Sun, Q.; Wang, R. *Chem. Commun.* **2012**, 48, 8003.
72. Akita, M. *Organometallics* **2011**, *30*, 43.
73. Mauser, H. Z. *Naturforsch. B.* **1968**, *23*, 1021.
74. S. Friederich, A. Bonassera, V. Valderrey, S. Hecht, *J. Am. Chem. Soc.* **2018**, *140*, 20, 6432–6440.
75. Nana Sun, Chiming Wang, Hailong Wang, Xuewang Gao, Jianzhuang Jiang *ACS Appl. Mater. Interfaces* **2020**, *12*, 50, 56491–56498.
76. Liu, Ronghua; Yang, Yu; Cui, Qianling; Xu, Wenqiang; Peng, Rui; Li, Lidong., *Chem. Eur. J.* **2018**, *24*, 17756–17766
77. Stark, D. G.; O'Riordan, T. J.; Smith, A. D. *Org. Lett.* **2014**, *16*, 6496-6499.
78. Hrdina, Radim. *Organometallics*. **2013**, *32*, 473-479.

## **Acknowledgments**

I would like to express my sincere gratitude to Professor Hiroaki Sasai and Professor Takayoshi Suzuki at Sanken (the Institute of Scientific and Industrial Research), Osaka University, for their kind guidance and encouragement in conducting this research. I would like to express my sincere gratitude to Dr. Shinobu Takizawa, Associate Professor, at Sanken (the Institute of Scientific and Industrial Research), Osaka University, and Dr. Masaru Kondo, Assistant Professor, Faculty of Engineering, Ibaraki University, for their direct guidance through this research. I am deeply grateful to Kento Nakamura, Assistant Professor, Graduate School of Pharmaceutical Sciences, Hokkaido University, who provided useful advice and guidance in advancing this research.

I would like to express my deep gratitude to Dr. Khalid Md Imrul, Dr. Kumar Ankit, Dr. HDP Wathsala, Dr. Akimasa Sugizaki, Ms. Aye Tin Zar, Mr. Mohamed SHS, Mr. Ganesh KT, Mr. Ahmed Sabri, Ms. Fan Duona, Ms. Meghna Sasi at Sanken (the Institute of Scientific and Industrial Research), Osaka University for their help in experiments and everyday life, and for having a pleasant research life. I would like to thank Ms. Kaya Yoshino for taking care of us in our daily office work and miscellaneous tasks. I would like to thank everyone at Sanken (the Institute of Scientific and Industrial Research) as well as Dr Takayuki Suzuki and staffs in the comprehensive analysis center, Osaka University for their cooperation in instrumental analysis. Finally, I would like to express my deep gratitude to all my friends and acquaintances who supported me in various ways and to my family who kindly supported my long student life.

Chandu G Krishnan

2022